

รายงานวิจัยฉบับสมบูรณ์

โปรติโอมิกส์ของกุ้งเพื่อการศึกษาโรคไวรัส Proteomics of Shrimps and Viral Interaction

รศ. ดร. ชาติชาย กฤตนัย

รายงานวิจัยฉบับสมบูรณ์

โปรติโอมิกส์ของกุ้งเพื่อการศึกษาโรคไวรัส Proteomics of Shrimps and Viral Interaction

ผู้วิจัย

นายชาติชาย กฤตนัย

สถาบันชีววิทยาศาสตร์โมเลกุล มหาวิทยาลัยมหิดล

สนับสนุนโดยสำนักงานกองทุนสนับสนุนการวิจัย
(ความเห็นในรายงานนี้เป็นของผู้วิจัย สกว.ไม่จำเป็นต้องเห็นด้วยเสมอไป)

สารบัญ

กิตติกรรมประกาศ	1
บทคัดย่อภาษาอังกฤษ	2
บทคัดย่อภาษาไทย	3
เนื้อหางานวิจัย	
Introduction	5
Materials and Methods	15
Results and Discussion	35
Concluding Summary	61
Output จากการวิจัย	63
ภาคผนวก	66

Acknowledgement

โครงการวิจัยนี้ได้รับทุนสนับสนุนจากสำนักงานกองทุนสนับสนุนการวิจัย (สกว.) ตามโครงการทุนวิจัย แบบมุ่งเป้า "การผลิตสัตว์น้ำเศรษฐกิจ " สัญญาเลขที่ DBG5180008 โดยได้รับการสนับสนุนด้านเครื่องมือและห้องปฏิบัติการจากสถาบันชีววิทยาศาสตร์โมเลกุล มหาวิทยาลัยมหิดล

Abstract

Project Code DBG5180008

Project Title Proteomics of Shrimps and Viral Interaction

Investigators Chartchai Krittanai

Institute of Molecular Biosciences, Mahidol University

Email: chartchai.krit@mahidol.ac.th

Project Period May 2008 - January 2013

We have utilized proteomic workflow and protein identification technology to investigate total protein expression in shrimp cells and tissues. In this project, we focused on the hemocytes that play a crucial role in shrimp defense mechanism. Circulating hemocytes separated from hemolymph of the black tiger shrimp (P. monodon) were classified into three types based on their granularity. They are hyaline (HC), granular (GC) and semi-granular cells (SGC). Each individual cell types were successfully isolated by Percoll gradient centrifugation and were investigated by proteomic analysis using 1D and 2D electrophoresis. These cell types demonstrated different pattern of protein expression suggesting distinctive functionality. LC/MS/MS protein identification of granular-containing cells uncovered many proteins involving in shrimp immune system. In yellow head virus (YHV) infected shrimp, we have demonstrated and confirmed that only GC and SGC can be infected by the virus. The study also investigated post translational phosphorylation of the proteins in GC during YHV infection. The results revealed several proteins with differential phosphorylation in post viral infection. Some of these proteins, myosin regulartory light chain (MRLC) and caspase were further examined for their functional roles in response to YHV infection. An increase of MRLC phophorylation was found to involve with defensive phagocytosis mechanism and rearrangement of actin polymerization. Inhibition of the MRLC phosphorylation in YHV infected cells showed a reduction of phagocytosis activity and increase in shrimp mortality. Moreover an increased phosphorylation of caspase was found to play roles in defensive apoptosis in the viral infected hemocytes. These results demonstrated that proteomic and phosphoproteomic changes in shrimp hemocytes are the responses of immunity against viral infection. The responsive changes in expression and phosphorylation of proteins such as MRLC and caspase could play the vital roles for shrimp survival. These research findings can provide a deep understanding of the molecular event that can be led to an effective control or treatment of the viral diseases in penaeid shrimps.

Keywords: Proteomics, phosphoproteomics, penaeid shrimp, viral infection, immune response

บทคัดย่อ

รหัสโครงการ DBG5180008

โครงการ โปรติโอมิกส์ของกุ้งเพื่อการศึกษาโรคไวรัส

ผู้วิจัย รองศาสตราจารย์ชาติชาย กฤตนับ

สถาบันชีววิทยาศาสตร์โมเลกุล มหาวิทยาลัยมหิดล

E-mail chartchai.kri@mahidol.ac.th

ระยะเวลาโครงการ พฤษภาคม 2551 - มกราคม 2556

โครงการวิจัยนี้เป็นการประยุกต์ใช้เทคโนโลยีทางด้านโปรติโอมิกส์และแมสสเปคโตรเมตรีในการศึกษา โปรตีนต่างๆที่มีการแสดงออกภายในเซลล์ของกุ้งกุลาดำ ซึ่งได้มุ่งเน้นที่เซลล์เม็ดเลือดของกุ้งที่มีบทบาท สำคัญเกี่ยวข้องกับขบวนการสร้างภูมิคุ้มกันต่อโรคต่างๆ โดยเซลล์เม็ดเลือดของกุ้งที่ถูกแยกออกจากน้ำ เลือดแล้วได้ถูกคัดแยกออกเป็นเม็ดเลือดชนิดต่างๆ ด้วยเทคนิคการแยกในสารละลาย Percoll จนได้เซลล์ เม็ดเลือดจำนวน 3 ชนิด ได้แก่ hyaline (HC) granular (GC) และ semi-granular (SGC) เซลล์เม็ดเลือด ชนิดต่างๆเหล่าได้ถูกนำมาสกัดและวิเคราะห์โปรตีนด้วยเทคนิคของโปรติโอมิกส์ พบว่าเซลล์เม็ดเลือดแต่ ละชนิดมีรูปแบบการแสดงออกของโปรตีนที่แตกต่างกันอย่างชัดเจน ซึ่งอาจหมายถึงการมีบทบาทหน้าที่ที่ แตกต่างกันด้วย เมื่อทำการระบุชนิดของโปรตีนเหล่านี้ พบว่าเซลล์เม็ดเลือดกลุ่มที่มีแกรนูล มีการ แสดงออกของโปรตีนหลายชนิดที่มีความเกี่ยวข้องกับขบวนการสร้างภูมิคุ้มกันของกุ้ง อีกทั้งเมื่อทำการ ทดลองฉีดเชื้อไวรัสหัวเหลือง เซลล์เม็ดเลือดกลุ่มนี้ยังเป็นเซลล์ที่เกิดการติดเชื้อไวรัสอีกด้วย นอกจาก การศึกษาเกี่ยวกับโปรตีนที่แสดงออกในเซลล์เม็ดเลือดเหล่านี้แล้ว โครงการนี้ยังได้ศึกษาถึงขบวนการเติม หมู่ฟอสเฟตของโปรตีนในเซลล์เม็ดเลือดกุ้งอีกด้วย โดยผลการวิเคราะห์พบว่ามีโปรตีนหลายชนิดที่มีเกิด การเติมหมู่ฟอสเฟตเพิ่มมากขึ้นอย่างชัดเจนเมื่อเซลล์เม็ดเลือดเกิดการติดเชื้อไวรัส เช่น regulartory light chain (MRLC) และ caspase จากการทดลองพบว่าการเติมหมู่ฟอสเฟตของโปรตีน MRLC มีความเกี่ยวข้องกับการเกิด phagocytosis ซึ่งหากยับยั้งการเติมหมู่ฟอสเฟตของ MRLC ในเซลล์ เม็ดเลือดชนิด GC ที่มีการติดเชื้อไวรัสหัวเหลือง จะพบการลดลงของการเกิด phagocytosis และทำให้ เกิดการตายของกุ้งเพิ่มขึ้นมาก ในส่วนของโปรตีน caspase นั้น พบว่าการเติมหมู่ฟอสเฟตที่เพิ่มขึ้นใน caspase ได้ชักนำไปสู่การเกิดการทำลายเซลล์แบบ apoptosis ที่เพิ่มมากขึ้นอีกด้วย ผลจากการทดลอง ้ต่างๆในโครงการนี้ ได้แสดงให้เห็นว่า การเปลี่ยนแปลงทั้งในด้านปริมาณการแสดงออกและการเติมหมู่ ฟอสเฟตของโปรตีนชนิดต่างๆในเซลล์เม็ดเลือดของกุ้ง เป็นการตอบสนองต่อการติดเชื้อไวรัส ซึ่งการ เปลี่ยนแปลงเหล่านี้ ได้ส่งผลให้เกิดการทำหน้าที่ของโปรตีนต่างๆ ที่มีความสำคัญต่อการต่อต้านไวรัสและ รักษาสถาวะการอยู่รอดของเซลล์ โดยความรู้ความเข้าใจในเชิงลึกถึงปรากฏการณ์ที่เกิดขึ้นในระดับ โมเลกุลดังกล่าวนี้ อาจนำไปสู่การพัฒนาและประยุกต์ใช้เพื่อการรักษาหรือควบคุมการเกิดโรคไวรัสในกุ้ง ได้ต่อไป

คำหลัก: โปรติโอมิกส์ ฟอสโฟโปรติโอมิกส์ กุ้ง การติดเชื้อไวรัส การตอบสนองด้านภูมิคุ้มกัน

สรุปเนื้อหาของงานวิจัย

INTRODUCTION

Research Background

Shrimp farming is one of the major aquaculture industries of Thailand. It generates a significant economic impact for the country and involves with a great number of local farmers, brood stock breeder, traders, exporters as well as customers. To maintain Thai shrimp farming, effort is needed to promote for more research and development for the future sustainability. One of the important researches is involved with detection, prevention, and treatment of shrimp diseases. Many approaches in cell biology and genomic research have been applied to study important pathogens, especially those from viral origin, aiming to understand the mechanism of pathogen infection, host responses, and pathogenesis of shrimp diseases in various tissues at the cellular and molecular levels. However those genomic approaches do not provide enough information on the molecular structure, abundance, and functional roles of proteins which are the main active molecules of most biological processes. This research project aims to investigate the total proteins which are expressed from the genome (proteome) of shrimp cells. The technology of proteomic analysis can be used to monitor the dynamic changes of shrimp proteome under selected controlled factor and condition, making it an attractive approach for an investigation of the molecular response and pathogenesis viral-host in shrimp systems. An understanding of molecular events and model of viral infection in shrimp could help us moving forward to the effective measures for the disease control and treatment.

Shrimp hemocyte and its role in immune defense mechanism

There are two major sources of crustacean immune responses. They were mostly described as humoral and cellular (or cell mediated) immunity. However, both types of immune function are reciprocally related. For cell mediated immunity, shrimp responses controls by blood cell, called hemocytes. Several characteristics of hemocyte mediated immune function have been reported. Phagocytosis, encapsulation, nodule formation, and degranulation (releasing of immune effective molecules) are processed by hemocytes. Moreover, many effective mechanisms involved in defense responses are also regulated by

hemocytes i.e. prophenoloxidase activating system, antimicrobial peptides synthesis, and clottable protein production. The mechanism of hemocyte mediated responses against major foreign pathogen such as bacteria, fungi, and virus have been described. These defense response mechanisms are similar to insect such as Drosophila sp. Distinct types of hemocyte populations were found regulated different immune function. In drosophila system, plasmatocyte plays major role in phogocytosis, meanwhile, encapsulation, nodule formation and melanization are regulated by lamellocyte and crystal cell, respectively. Comparison with shrimp hemocyte responses, hyaline cell (HC) has been reported to play phagocytic activity whereas granular containing hemocytes (SGC and GC) are involved in encapsulation, nodule formation, AMPs production, and melanization. The pattern hemocyte recognizes pathogens have been reported. In crustacean, synthesis of foreign material binding proteins or called pattern recognition proteins (PRPs) was existed in hemocyte. The major pathogen surface molecules such as lipopolysaccharide (LPS), beta-glucan (BG), peptidoglycan (PG), glycoproteins (GP) are called pathogen associated molecular patterns (PAMs). They were recognized by immune responses and signaling pathways are activated in hemocytes.

For shrimp virus infection, the role of hemocytes specific immune responses is not well known. Lacking of adaptive immune system is mainly described. However, the evidence of memory against virus infection was proposed. Major important mechanisms of hemocyte antiviral activity remain associated with general innate immune functions such as phagocytosis, antimicrobial peptides production, apoptosis induction, and prophenoloxidase (ProPO) activating system. The pattern of shrimp response to virus pathogen is uncommonly found to those in vertebrates. Persistent infected shrimp is normally presented and multiple infection of virus in one shrimp also detected. The viral accommodation with infected host and other pathogenic viruses was also hypothesized.

Taura syndrome virus (TSV)

Taura syndrome virus (TSV) is an important pathogen in penaeid shrimps. It causes serious morbidity in the infected shrimps with a mortality rate of up to 95% in *P. vannamei* [13]. Shrimp epithelial cells are normally the virus target as viral particles can replicate and accumulate in the cytoplasm of the infected epithelial cells. Electron micrograph of purified

TSV illustrates a non-enveloped virion with icosahedral shape and size of approximately 31–32 nm in diameter [14]. TSV has recently been classified into a new genus namely "Cricket paralysis-like viruses" based on its nucleotide sequences [15]. The viral genome contains a positive single-stranded RNA of approximately 10 kb with two distinct ORFs. ORF1 and ORF2 encode for nonstructural and structural proteins, respectively. Separation of TSV structural proteins by SDS-PAGE shows three major bands with molecular masses of 24, 40, and 55 kDa, and one minor band at 58 kDa [15]. Recently, our group performed a preliminary study to evaluate alterations in *P. vannamei* hemocytic proteome during TSV infection [3]. Differential proteomics analysis by two-dimensional electrophoresis (2-DE) revealed several altered hemocytic proteins upon TSV infection [3]. Interestingly, we observed significant changes in levels of several fragments of hemocyanin. Some fragments were up-regulated, whereas some other fragments were down-regulated. Molecular mechanisms underlying these disparate results remained unclear. In the present study, we therefore extended our previous expression proteomics study and then further characterized functional significance of hemocyanin fragments during TSV infection.

Yellow head disease (YHD)

YHV infection in cultured shrimp in Thailand has been reported since 1991. It causes a massive mortality loss of shrimp farming especially in Black Tiger shrimp culture within 3-5 days after appearance of clinical signs. Yellow head disease outbreaks have been reported specifically in *Penaeus monodon* and Pacific shrimp (*Litopenaeus vannamei*). However, a natural infection in others prawns have been also investigated. The name of this virus derived from gross signs of yellow head disease which are yellowish of cephalothorax part and pale yellow coloration of moribund infected shrimp.

Yellow head virus was characterized in Thailand since 1993. Yellow head virus (YHV) is a rod shape with tri-laminar enveloped virus, an approximately 40-50 nm in diameter and 150-170 nm in length. Study on virology of this virus revealed that YHV was composed of positive single-stranded RNA as a genome structure and 26,662 nucleotides in length. This virus has been classified as Gill-associated virus in the genus Okavirus, family Roniviridae, and order Nidovirales. Structural investigation yellow head virus indicated three major viral

structural proteins. Glycoprotein gp116 and gp 64 are deposited in viral envelope and a nucleoprotein, p20, was in the nucleocapsid of the virus particle. Until now, YHV can be classified into 6 genotypes worldwide. YHV genotype 1 (YHV-1) is known to cause yellow head disease in penaeid shrimp. Genotype 2 (YHV-2), named as Gill-associated virus (GAV), was widely spread in shrimp in Australia. YHV genotype 2 and another four genotypes were also reported in healthy shrimp but they are not reported to cause yellow head disease outbreak. Recent report indicated that YHV1 is genetically mutated. YHV1a, a reference strain of YHV which found in Chachoengsao province/1998 in Thailand and YHV1b (Ratchaburi province/2006, Thailand) showed deletion of 54 amino acid in the ORF3 gene, resulting in the loss of six conserved cysteine residues and two predicted N-glycosylation sites. Testing of the virulence in both types of YHV showed high mortality in penaeid shrimps.

YHV pathogenesis

Detection of YHV distribution in shrimp revealed that gill and lymphoid organ is the major replication target. In addition, several tissues can be infected by YHV including muscle, hepatopancreas, heart, nerve cord, and eye stalk. The gross sign of yellow head disease in shrimp is not specific. The common sign is pale yellowish of shrimp head derived from hepatopancreas. The common gross of YHV infected cell is nuclear pyknosis and karyorrhexis. The number of cytoplasmic inclusion was also investigated. The spheroid in lymphoid organ affected by YHV infection is observed.

Until now, the detailed mechanism of YHV infection in host cell has not been reported. However, many studies have been described to investigate of YHV infection mechanism especially in shrimp. Some viral structural protein is found to involve in virus and host interaction, leading to disease progression. Glycoprotein, gp116 is a major viral protein reported to interact with host and facilitate virus infection. Inhibition of YHV interaction by antigp116 antibody revealed significant inhibition of viral-host interaction resulting in more surviving of shrimp. Recently, it has been reported that mutated changing of amino acid in gp116 polypeptide has resulted in higher virulence than wild type. However, a non virulent type of YHV genotype particle can be associated with some feature linked to ORF1b rather than the deletion in the gp116 gene at ORF3 of viral genome. In susceptible shrimp host,

previous studies showed that lymphoid organ (LO) is a first selective tissue of YHV and several cellular proteins from host can be interact with this virus. For instance, investigation of specific YHV receptor in LO indicated a 64 kDa protein that can interact with YHV particle. Another study in hemocyte, yeast two hybrid system revealed shrimp serine protease homologue interacted with YHV. Moreover, RNAi technology was used to suppress specific gene, *Pm*Rab7. The suppression of *Pm*Rab7 protein expression affected YHV multiplication in host. Many cellular proteins from shrimp host were investigated in term of specific pathway involved in virus and host interaction. Virus entry to host cell have not been proposed and need to be investigated further.

Shrimp defense against YHV infection

The mechanism of shrimp defense responses to YHV is not known precisely. Evaluation of both transcriptional and translation level of YHV-targeted tissue were demonstrated. YHV causes several immune and non-immune associated gene and protein alteration. Several antimicrobial peptides (AMPs) such as anti-lipopolysaccharide factor (ALF) and crustins were identified in YHV-infected hemocyte by using suppression subtractive hybridization (SSH). Apoptosis regulating genes are one of the major groups which were highly modulated upon virus infection. However, the relationship of apoptosis gene associated with shrimp defense mechanism is not known. In vertebrates, antiviral process through apoptosis induction in viral-infected cell is one of the mechanisms that have been reported. In shrimp, induction of YHV-targeted cell apoptosis was found in both primary targeted tissue (lymphoid organ) and shrimp immune cell (hemocyte). In white spot syndrome virus (WSSV) infected shrimp, induction of host cell apoptosis is inhibited by specific viral protein in early infection. Therefore, it was suggested that activation of host cell apoptosis is an evolutionary conserved mechanism of antiviral defense among different animals. However, upon YHV infection, an increase of apoptotic rate is a major cause of shrimp mortality rather than the positive result in YHV elimination. Experimental study of RNAi mechanism against YHV infection was also investigated. Inhibition of YHV protease gene using dsDNA could prevent high mortality of shrimp post YHV infection. It was suggested that antiviral immunity through RNAi mechanism is general innate immunity containing in this organism.

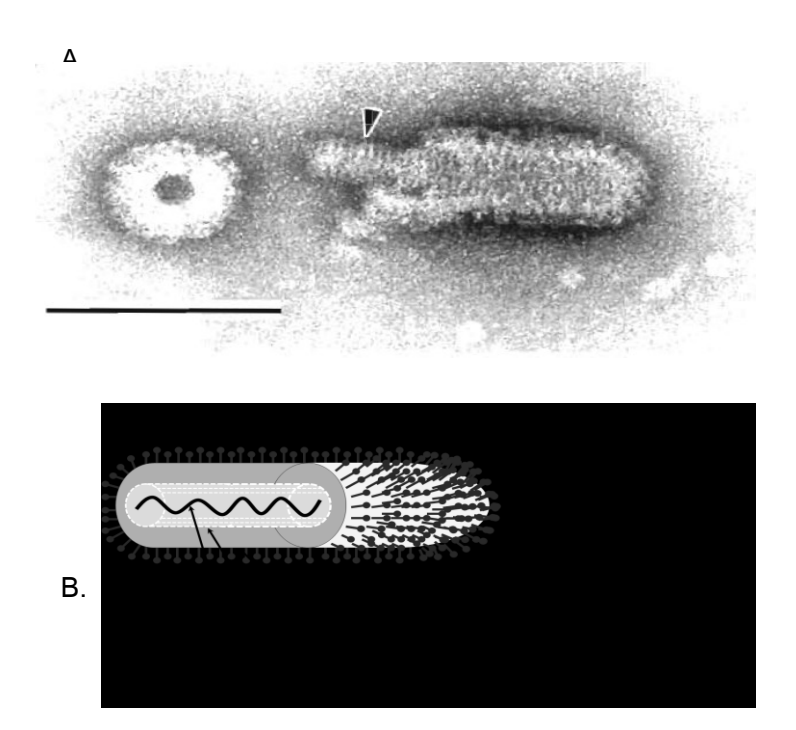


Figure 1. Electron micrograph revealed bullet shape of YHV particle. The picture showed the nucleocapsid structure inside covering by viral envelope (arrow head).

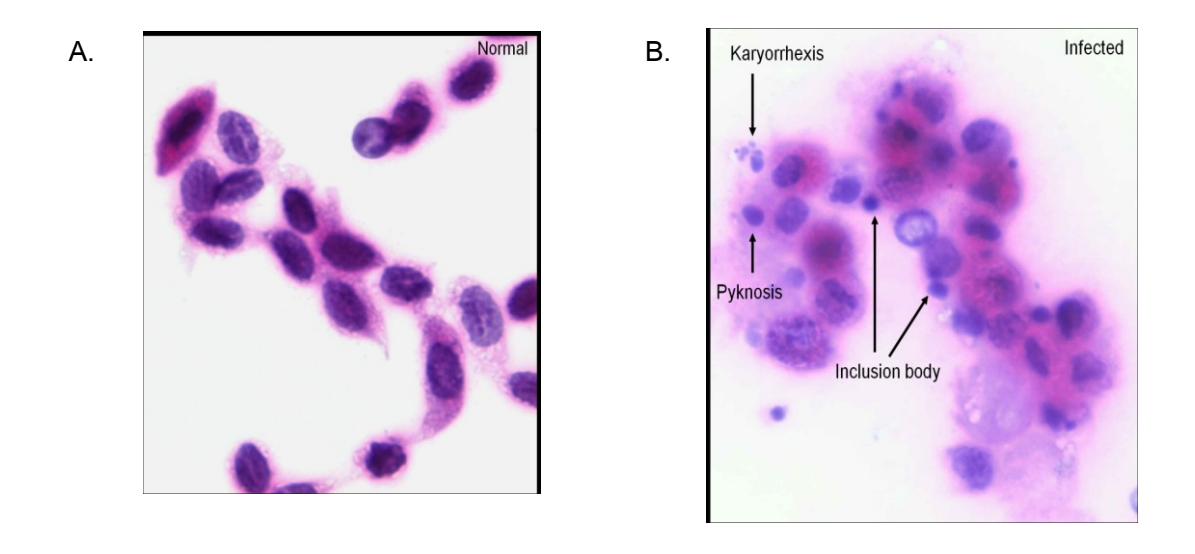


Figure 2. Microscopic examination indicated normal shrimp hemocyte morphology (A). The common gross of YHV infected cell is necrosis. The nuclear karyorrhexis, pyknosis, and inclusion body were indicated (B).

Protein phosphorylation and phosphoprotein detection

Post translational protein modification is important for protein function regulation. For instance, reversible protein phosphorylation plays crucial role in many biological processes and pathways such as cell growth and development, program cell death, immune response, and metabolism. In eukaryotes, more than thousand of potential phosphorylation sites are known, with three types of protein phosphorylation sites; pSer, pThr, and pTyr, with ratio 1000:100:1. Two types of enzymes are generally known to posses protein phosphorylation regulation i.e. protein kinases (phosphorylated) and protein phosphatases (dephosphorylated). Both types of enzymes can affect the function of protein by the mechanisms to increase or reduce activity of protein, stabilize or break down of protein, facilitate or inhibit movement of protein, and induce or disrupt of protein – protein interaction.

Protein phosphorylation and it roles in eukaryotic system

One of the most phosphoprotein functional characterizations is immune related phosphoprotein. In eukaryotes, several phosphoproteins regulate immune function. For example, IL-1R-associated kinase (IRAK), extracellular signal-regulated kinase (ERK), and c-Jun N-terminal kinase (JNK) are crucially involved in innate immune responses and inflammatory response. Similar to vertebrates, study of invertebrates phosphoprotein involving in immune system indicates evolutionally conserved of phosphoprotein function. However, the information of invertebrate phosphoprotein remains poor. In case of crustacean, study on the role of phosphoprotein in immune response is also lacking. A few phosphoproteins have been reported to play critical function in defense responses such as PI-3 kinase, protein kinase C (PKC), ERK, STAT and Hemocyanin. Those identified proteins are regulated by phosphorylation and associated with immune function.

Phosphoprotein detection

At present, study of protein phosphorylation and their role in biological system is widely established. Various methods of phosphoprotein characterization including protein

phosphorylation state, phosphorylation types, and phosphorylation sites of several proteins were described. Mass spectrometry is a powerful tool for phosphoprotein study. The methods used for phosphorylated protein characterization are based on research aims and their facility. Most of the phosphoproteins presenting in cell has very little expression, therefore, the method of phosphoprotein enrichment is often coupled with phosphoprotein study. Nowadays, development of effective separation of protein mixture by two – dimensional electrophoresis (2-DE) coupled with less toxic and high sensitive phosphoprotein detection methods (such as fluorescence detection rather than radioisotope labeling) provide an advantage for phosphoprotein separation and detection. The workflow of phosphoproteomics study is normally include sample preparation, protein digestion and enrichment, phosphopeptides enrichment and mass spectrometry, database searching and analysis, analysis of phosphoprotein network and functional analysis of phosphoprotein targets.

Gel based phosphoproteome analysis.

Protein separation using both one dimensional (1D) and two dimensional (2D) electrophoresis coupled with several techniques of phosphoprotein visualization is widely established for phosphoprotein detection in cell. For example, 2-DE and multiplex protein detection by fluorescence dyes detection could distinguish between phosphoprotein and nonphosphorylated protein based on selective property of fluorescence dye. This technique can be applied for quantitative phosphoproteomics similar to conventional 2-DE. However, cross detection of fluorescence dye in negatively charged containing proteins is also reported. Immunodetection of type specific phosphoprotein is one of the most widely used. This technique allows detection of phosphoprotein on transferred membrane using specific antibody which recognize one type of phosphoprtein such as pSer, pThr, or pTyr. The limitation of this tool is based on several factors such as targeted cell, mass spectrometry, and databases. Most of phosphoproteins in cell which plays crucial roles in biological processes exist in a very little expression level. Therefore, identification of phosphoprotein based on gel can miss a large numbers of protein targets. However, development of phosphoprotein enrichment before separation is one of the techniques which could resolve this problem.

Mass spectrometry based phosphorproteome analysis.

Mass spectrometry based phosphoproteome is a powerful tool of phosphoprotein research. Based on high sensitivity and high throughput of protein identification, this technique can resolve the problem of phosphoprotein identification in cell with very low abundant of phosphoprotein targets. Development of both isotope and non-isotope phosphoprotein labeling couple with mass spectrometry detection is described for quantitative phosphoproteomics. Phosphopeptides enrichment is generally include in mass spectrometry based phosphoproteomics workflow. Several methods have been described such as IMAC (Immobilized metal affinity chromatography), TiO₂, and SIMAC (sequential elution from IMAC). One important part is the mapping of phosphorylation site in the phosphopeptides. Tandem mass spectrometry is very helpful for this step. Many techniques have been described to identify phosphopetides. Three MS fragmentation methods have been described for phosphopeptide determination including Collision-induced dissociation (CID), Electron capture dissociation (ECD), and Electron transfer dissociation (ETD). Each technique is suitable for detection of various phosphorylation types.



Figure 3. The flow chart of phosphoproteome analysis: The methods of phosphoprotein detection and identification showed in distinct lines. Four techniques were summarized in this chart (indicated by different lines. ProQ DPS; ProQ Dimond phosphoprotein detection, iTRAQ; isobaric peptide tags for relative and absolute quantification, SILAC; stable isotope labeling by amino acids in cell culture, HCD; Higher energy C-trap dissociation, ETD; Electron transfer dissociation, CID; Collision-induced dissociation.

MATERIALS AND METHODS

Shrimp preparation

Specific pathogen free of black tiger shrimp (*P. monodon*) were kindly provided by Somjai Wongtripob, Shrimp Genetic Improvement Center, the National Center for Genetic Engineering and Biotechnology (SGIC, BIOTEC), located in Suratthani, Thailand. About 60 shrimps of approximately 50-100 g of body weight were acclimatized in 500 – 800 L aerated tank containing artificial sea water with 30 ppt salinity.

Hemocyte collection

Shrimp hemolymph was collected from cephalothorax (Hemoceol) of shrimp. Hemolymph was withdrawn by using 21G needle equipped with 5 ml syringe,containing modified Alsever's (AS) anticoagulant solution (19.3 mM sodium citrate, 239.8 mM NaCl, 182.5 mM glucose, 6.2 mM EDTA; pH 7.2). Hemolymph mixed with an equal volume of AS were immediately kept on ice before hemocyte separation, total and differential hemocyte count.

Percoll gradient centrifugation

To isolate for shrimp hemocyte populations, percoll gradient centrifugation was performed. For continuous percoll gradient preparation, percoll solution (70% Percoll, 0.33M NaCl, 700 mOsm/kg) was prepared and then subjected to ultracentrifugation at speed of 50,000 x g for 35 min at 4 °C to generate continuous Percoll gradient. For step of shrimp hemocyte separation, hemolymph sample was collected from shrimp and immediately loaded onto continuous percoll gradient solution and then centrifuged at low speed centrifugation (1,700 xg for 30 min at 4 °C, Beckman GS-15R). All of separated hemocytes bands were then characterized by selected methods to identify the cell types.

Flow cytometry

Shrimp hemolymph was analyzeded by flow cytometry to classify for the populations of hemocyte. After hemolymph collection, 300 µl of hemolymph were loaded into flow cytometric

tube (BD Falcon) and then subjected to flow cytometric analysis using BD FACSCalibur # E6361 flow cytometry. The optimized parameter settings for *P. monodon* hemocyte separation were FSC E00, SSC 400, FL1 443 and FL3 501. A total of 50,000 events were collected for each sample. Three to five individual hemolymph samples were investigated in this step. In addition, each separated hemocyte populations from percoll gradient were also investigated by flow cytometry. All separated bands were collected and 300 µl of cell solution were immediately subjected to flow cytometric analysis using the same parameter setting for hemolymph investigation.

Microscopic examination

Morphological examination of shrimp hemocyte was performed by light microscope. Both hemolymph sample and percoll separated hemocyte samples were evaluated in this step.

YHV preparation and purification

Initial YHV stock (kindly provided by Dr. Apichai Bourchookarn, Prince of Songkla University) was diluted (1:100) in normal saline solution (0.45 M NaCl) and intramuscularly injected to shrimp. After 24 hours or until shrimp reaching moribund stage, the hemolymph was collected and hemocyte was removed by centrifugation (830 xg, 10 min, 4 °C). Hemocyte-free plasma was centrifuged further at high speed at 20,000 xg, 15 min, 4 °C to to remove cell debris. Plasma was then subjected to ultracentrifugation (Beckman Optima XL-100) at 100,000 xg for 1 h at 4 °C. The supernatant was discarded and the pellet was resuspended in normal saline. Aliquot YHV stock solution was stored at -80 °C until used. All step of YHV purification were handled in ice-cold temperature.

YHV injection

For experimental infection, shrimps were separated into two groups: saline injection and YHV injection group. For YHV infection, YHV stock was diluted in normal saline (1:100) and then intramuscularly injected into shrimp (100 µl/20 g shrimp weight). For saline injection

group, only normal saline was injected with the same volume. At decided time points of 6 hpi, 12 hpi, and 24 hpi, hemolymph was collected and further subjected to YHV detection.

RT-PCR

To determine YHV replication level in hemocyte, total RNA was extracted from the hemocyte obtained from either normal or YHV-infected shrimp at 6 hpi, 12 hpi and 24 hpi respectively. For RNA preparation, 150 μl of hemolymph was collected and then mixed with 300 μl TRI[®] reagent (Molecular research Center, Inc.). The total RNA was extracted according to manufacturer instruction. Briefly, hemolymph contained TRI reagent was homogenized with tiny spatula and incubated at RT for 5 min. after that, 200 μl of chloroform was added and then mixed thoroughly followed by incubated for 15 min. To collect aqueous phase, the solution was centrifuged at 12,000 rpm for 15 min at 4 °C. RNA was precipitated with 500 μl of isopropanol for 15 min at room temperature. The aqueous phase was removed by centrifugation. The RNA pellet was kept and then washed twice with 70% ethanol by centrifugation. The pellet was dissolved in RNase – free sterile water (DEPC water) and kept at -20 °C until cDNA systhesis. To determine total RNA concentration, extracted RNA was analyzed by using spectrophotometer (Nano Drop, BIO-RAD). RNA concentration and purity were indicated by two absorption wavelengths of 260 nm and 280 nm respectively. The ratio of two absorption wavelengths (A260/A280) should be 1.9 – 2.0 for high purity RNA sample.

To generate cDNA template, 500 – 1000 ng of total RNA was subjected to cDNA systhesis reaction. Firstly, total RNA was mixed with oligo-dT and heated at 70 °C for 5 min then 20 µl of cDNA reaction mixture contained 2.5 mM MgCl₂, 0.5 mM dNTPs, and ImPromtIITM reverse transcriptase (Promega) were mixed with RNA sample. The cDNA reaction was incubated at 42 °C for 1 h and then finally inactivated the enzyme at 75 °C for 15 min. Further, multiplex PCR was carried out to determine YHV target gene. 25 µl of the PCR reaction was contained cDNA template, 1X *Taq* buffer, 2.5 mM MgCl₂, 0.5 mM dNTPs, 0.5 µM YHV and EF-1a primers mix (table 3), and 1 U/µl *Taq* polymerase (Promega) was subjected to PCR reaction. The PCR cycle were; pre denaturation at 94 °C for 5 min, denaturation at 94 °C for 30 sec, annealing at 55 °C for 30 sec, extension at 72 °C for 45 sec, and final extension at 72 °C for 7 min. A total 25 cycles of PCR reaction were performed. PCR product was

investigated by agarose gel electrophoresis. Briefly, 1.5% agarose gel (Cambex Bioscience, Rockland Inc.) was prepared by using TBE buffer (90 mM Tris-base, 90 mM boric acid, 2 mM EDTA; pH 8.0). 10 µl of PCR product was mixed with loading buffer (15% (w/v) Ficoll 400, 0.01% (w/v) Bromophenol blue) and loaded onto prepared agarose gel by using 1X TBE buffer as an electrophoretic buffer. The electrophoresis was performed at constant voltage of 90 V for 1 h, after complete running, gel was stained with ethidium bromide solution (0.5 µg/ml ethidium bromide) and then visualized by UV spectrometer (Gel Doc model 1000, Bio-Rad).

Semiquantitative RT-PCR.

Total RNA was obtained from five individual shrimps which were infected with YHV. RT-PCR was performed according to the method previously described. Five transcripts of hemocyte protein were evaluated upon YHV infection at 0 hpi, 6 hpi, 12 hpi and 24 hpi respectively by using specific primers (table 3). Shrimp elongation factor – 1 alpha (Ef-1a) was used as internal control gene. The PCR products were visualized on 1.0% agarose gel containing 1X TAE and ethidium bromide staining. The intensities of PCR products were analyzed by densitometer (Amersham Biosciences) and relative intensity of the targeted genes were calculated.

Immunocytochemistry.

To determine the targeted hemocyte cell type for YHV, a detection of YHV particle using specific antibody was carried out. For sample preparation hemolymph samples obtained from 3 individual shrimps of YHV infection group at 6 hpi, 12 hpi, and 24 hpi were subjected to percoll gradient centrifugation. The separated hemocytes bands were collected, 50 μl of all collected cell types were subsequently maintained on 24 – well cell culture plate containing L-15 medium (1X L-15, 1% glucose, 5 g/L NaCl, 15% Fetal bovine serum, 1x Antibiotic-Antimycotic (Gibco)) and incubated for 1 h at 28 °C to allow cell attachment. Further, hemocyte cultures were fixed in fixative solution (10% formaldehyde, 0.45 M NaCl) for 20 min and then washed twice with 1X PBS buffer (137 mM NaCl, 2.7 mM KCl, 8 mM Na₂HPO₄, 1.46 mM KH₂PO₄, pH 7.4). The fixed cell was permeabilized with 0.5% Triton X-100 in PBS buffer for 5 min and then blocked with 10% fetal bovine serum (FBS) for 1 h. Subsequently, cell was

incubated with 1:500 mouse monoclonal anti-gp 116 primary antibody containing 1% FBS for overnight at 4 °C. Further, cell was washed three times, 5 min each, with PBS buffer and then covered with 1: 500 goat anti-mouse Alexa Fluor-546 conjugated secondary antibody (Invitrogen) in PBS buffer for 1 h at RT in the dark. Finally, excess antibody was washed three times with PBS and then incubated with 1: 500 TO-PRO 3 iodide (Invitrogen) for 1 h in the dark to label the nucleus. Stained cell on the slide was coated with anti-fade permount (Invitrogen) before visualized by using Confocal fluorescence scanning microscope (Olympus FluoView™ FV1000). At least 3 non-overlap regions were scan and image captured for each sample.

Co-immunoprecipitation (Co-IP) assay

Shrimp hemocytes were resuspended in ice-cold RIPA buffer [50 mM Tris-HCl pH 8.0, 150 mM NaCl, 2 mM EDTA, 0.1% SDS, 1% NP-40, 1 mM PMSF] on ice for 30 min. Cell lysate was clarified by a centrifugation at 10,000 rpm for 5 min. Totally 500 µg of resolved proteins was incubated with 5 µg of rabbit polyclonal anti-ERK1/2 antibody (Cell Signaling Technology) at 4 °C for 16 h. The mixture was further incubated with 50 µl protein G beads (GE Healthcare) at 4 oC for 4 h. Thereafter, the beads were collected by centrifugation at 2,000 rpm for 2 min and washed twice with ice-cold RIPA buffer. Immunoprecipitated proteins were eluted, separated by SDS-PAGE under reducing condition, and subjected to Western blot analyses. Immunoprecipitation with rabbit IgG (Santa Cruz Biotechnology; Santa Cruz, CA, USA) served as an isotype control for Co-IP

Total hemocyte protein extraction.

Shrimp hemolymph was collected as previous described. Hemocyte pellet was separated by centrifugation (830 x g, 10 min, 4 °C). Further, the pellet was washed three times with ice-cold AS solution by centrifugation. Subsequently, 100 µl of lysis buffer (8 M urea, 2 M thiourea, 4% CHAPS, 50 mM DTT, 1X Protease inhibitor (GE Healthcare)) was added and then cell was homogenized by homogenizer (Sonicator®, Misonix Incorporated). For phosphoprotein detection, the lysis solution will phosphatase inhibitor cocktail (Sigma). Cell debris was removed by centrifugation at 14,000 rpm for 30 min at 4 °C and then the

aqueous phase was collected to a new tube. For protein precipitation, the chloroform-methanol-water protein precipitation method by the ratio of sample: methanol: chloroform: water equal to 1: 4: 1: 3 was performed in this step. In brief, 150-200 μl of protein solution obtained from previous step was mixed with 600 μl of methanol by vortex and then 200 μl of chloroform was added and mixed thoroughly. Finally, 450 μl of sterile water was added, mixed well and then protein pellet was precipitated by centrifugation at 12,000 rpm for 5 min at 4 °C. The protein pellet was collected and washed with 1 ml of methanol using centrifugation. The protein pellet was left for air dry followed by rehydrated with 50 – 100 μl of lysis buffer and then solubilized by using water bath sonicator (TRU-SWEEPTM Crest ultrasonicator) for 15 min followed by centrifugation to remove non-solubilized materials. Protein solution was collected to new tube and kept at -20 °C until determining of protein concentration and electrophoresis. Hemocytes obtained from five-pooled individual shrimp samples were evaluated and triplicate sample was performed for each experimental groups.

Hemocyte protein extraction for each isolated cells types.

To evaluate hemocyte protein expression pattern among different hemocyte populations, hemocyte protein extracted from percoll separated cells was performed. After percoll gradient centrifugation, hemocyte bands were harvested and then hemocyte pellet was collected by centrifugation at 1,700 xg for 5 min at 4 °C. The cell pellet was washed three times with ice-cold AS solution by centrifuged at 830 xg for 10 min each to remove the remaining percoll beads. Subsequently, cell pellet was lysed with lysis solution and then subjected to protein extraction method as previously described.

Determination of protein concentration

To determine hemocyte protein concentration, Bradford's assay was performed. The reaction of colorimetric assay was performed by Bradford's assay. The calibration curve was prepared by using bovine serum albumin (BSA) as protein standard. Each of the reaction was mixed well by vortex and then 180 μ l of reaction were loaded into a flat bottom 96-well plate. Determination of protein concentration was performed using micro-plate reader at wavelength

of 595 nm in Bradford assay mode. The concentration of protein sample was calculated based on standard curve. Three replicate reactions of protein sample were evaluated in this step.

SDS-PAGE

SDS-PAGE was performed to evaluate hemocyte protein expression pattern for both total protein obtained from mixed hemocytes population and isolated hemocyte cell types from percoll centrifugation. A 10 – 20 µg of prepared protein samples were mixed with 5X sample buffer (62.5 mM Tris-HCl, pH 6.8, 10% (w/v) SDS, 20% (v/v) glycerol, 100 mM Dithiothreitol (DTT), 0.1% (w/v) Bromophenol Blue) by the ratio of 1: 4 to get 1X sample buffer concentration. The solution of denaturing SDS-PAGE gel was prepared as shown in table 6-7. The electrophoresis was performed using Hoefer mini-VE gel electrophoresis system (GE Healthcare) under tris-glycine buffer system (25 mM Tris-HCl, pH8.3, 193 mM glycine, 0.1% SDS). Electrophoresis condition was carried out by constant voltage at 110 – 120 V for 1 – 1.5 h or until the tracking dye reaches the bottom of the gel. After a complete running, gel was fixed with fixative solution (50% methanol, 10% acetic acid) for phosphoprotein detection followed by CBB-G staining.

Two-dimensional gel electrophoresis

To obtain a high resolution of total protein separation, 2-DE was performed to evaluate differential levels of of both phosphorylated protein and non-phosphorylated proteins in YHV targeted cells. 2-DE protein separation consists of the two following steps;

Isoelectric focusing (IEF)

To separate proteins based on their isoelectric point (*p*I), extracted hemocytes protein was subjected to IEF step. Total 300 μg of prepared hemocyte protein obtained from five-pooled semigranular cell or granular cell was rehydrated with rehydration buffer containing IPG buffer (8 M urea, 2 M Thiourea, 4% (v/v) CHAPS, 50 mM DTT, 1X protease inhibitor, 1X phosphatase inhibitor (Sigma), 0.002% bromophenol blue, 0.5% IPG buffer (GE Healthcare)). The solution was adjusted to 250 μl by rehydration buffer and then was centrifuged at 12,000 rpm for 5 min. the IEF step was performed on IPG strip pH 3-10, non-linear, 13 cm long (GE

Healthcare). The IPG strips were rehydrated at 20 °C for 6 h at 50 μA per strip followed by isoelectric focusing by using step and hold mode (SH) and increased voltage up to 8000 V.

Second dimensional SDS-PAGE

After completion of IEF step, the strip was subjected to second dimensional protein separation by SDS-PAGE. The strip was deamidated in equilibration buffer containing DTT (30% (w/v) glycerol, 20% (w/v) sucrose, 2% (w/v) SDS, 50 mM Tris-HCI, pH 8.8 and 0.002% (w/v) Bromophenol blue, 100 mM DTT) for 15 min at RT with rocking. Subsequently, strip was alkylated in the same buffer replacing DTT with IAA (250 mM IAA) for 15 min. the strip was further loaded onto a prepared 12.5% SDS-PAGE gel (table 7) running on Hoefer 600 Ruby electrophoresis system (Amersham Biosciences). The Pepermintstick phosphoprotein standard marker (Invitrogen) was used by dipping 10 µl of marker on filter paper and placed at the acidic side of the strip. The electrophoresis was performed using tris-glycine electrophoresis buffer and electrical voltage was started at 100 V for 1 h followed by constant voltage at 150 V in cold temperature until tracking dye reach to the gel bottom. Subsequently, SDS gel was fixed in fixative solution (50% methanol, 10% acetic acid) for 15 min and then replaced with new fixative solution for overnight at 4 °C. The fixed gel can be stored in fixative solution at cold temperature until protein staining.

Phosphoprotein detection by ProQ Diamond phosphoprotein staining

To determine phosphorylated protein in both 1D and 2D gel, fluorescence dye staining was developed in this study. Firstly, the fixed gel was stained for phosphoprotein using ProQ[®] Diamond phosphoprotein staining dye (Molecular Probes, Invitrogen). Briefly, the fixed gel was rinsed with milliQ water three times, 15 min each, to remove remaining SDS. Subsequently, the gel was subjected to a modified fluorescence staining method according to previous report. In summary, the gel was soaked in three-fold diluted ProQ[®] Diamond fluorescence dye for 2 h in the dark with agitation (50 rpm) at RT. Further, stained gel was destained three times with destaining solution (50 mM Sodium acetate; pH 4.0, 20% Acetronitrile) for 30 min each by replacing the new destaining solution in each step. Finally, stained gel was scanned and image captured by using Typhoon Trio fluorescence scanner (Amersham Biosciences).

Total protein detection by Sypro Ruby

To determine protein spots or protein bands on the same gel after phosphoprotein detection by ProQ Diamond, the gel was directly stained with three-fold diluted Sypro Ruby dye (Molecular Probes, Invitrogen) for overnight in the dark with agitation at 4 °C (table 8). Further, stained gel was washed with destaining solution (10% methanol, 7% acetic acid) for 30 min and then washed with deionized water for 5 min. The stained gel was then scanned to capture for the image.

Total protein detection by CBB-G250.

To visualize protein spot and protein bands, all of the gels obtained from fluorescence dye staining were subjected to CBB-G staining. The gels were incubated with CBB-G working solution (10% (w/v) ammonium sulfate, 2% (v/v) phosphoric acid, 0.001% (w/v) CBB-G250) for overnight with agitation at RT. The stained gel was washed with deionized water for 2 days or until the gel background was clear. The gels were then scanned and captured for images by using densitometer (ImageScanner, PowerLook 1120 USG, Amersham Biosciences). The parameters of gel scanning were set in transmissive mode and 300 dots per inch (dpi) resolution.

Image acquisition and analysis

Three replicates of 2D gels obtained from SGC and GC in both control and YHV infected groups were saved as .GEL file format from a fluorescence scanner. To analyze both differential phosphoprotein and non-phosphorylated protein expression by Image Master 2D platinum software version 5.0 (Amersham Biosciences), .GEL files were then saved as Melanie file (.Mel). For image analysis, three replicate gels of control and YHV infected samples at 1 hpi were analyzed for SGC and GC. Significant change for both phosphorylated and non-phosphorylated proteins were statistically determined by Student's t test (p < 0.05). The ratio of differential phosphorylated proteins and non-phosphorylated proteins were calculated based on percentage of protein spot volume between samples.

For SDS-PAGE analysis, three replicate samples obtained from HC, SGC and GC were evaluated. Predominated protein expression among each cell type of hemocyte was

visually determined based on intensity of standard protein marker. The predominated protein bands were further excised for in-gel digestion and identification by MS/MS analysis.

Protein identification by mass spectrometry

In-gel digestion

For in-gel digestion, gel pieces were washed with 50% acetonitrile (ACN) in 25 mM ammonium bicarbonate (AB); pH 8.5 for 15 min to 1 h to remove the remaining CBB-G dye. Further, gel pieces were dehydrated with 100% ACN for 5 min and then protein was reduced by 10 mM dithithreitol (DTT) in 25 mM AB for 1 h at RT. Subsequently, gel pieces were alkylated by 100 mM iodoacetamide (IAA) in 25 mM AB for 1 h at RT in the dark. After dehydrated with 100% ACN, gel pieces were rehydrated and incubated with 10 - 20 ng/µl of sequencing grade – modified trypsin (Promega) in 25 mM AB; pH 8.5 at 37 °C for overnight. Finally, digested peptides were extracted by 50% (v/v), acetonitrile containing 5% (v/v) formic acid for two times with vortexing. Peptides solution were combined and evaporated by vacuum then kept at -80 °C until mass spectrometric analysis.

NanoLC-ESI-MS/MS

Tryptic digested peptides were dissolved in 0.1% (v/v) formic acid (FA) containing 25 mM AB; pH 8.5 before loading to MS/MS sampling vials. Identification of peptide mass and amino acid sequences were processed by using liquid chromatography-nano-electrospray ionization tandem mass spectrometry (nanoLC-ESI-MS/MS).

Database search

For MS/MS peptides ion search by mascot search engine (www.matrixscience.com), the parameters for MS/MS ions searching were set using NCBInr databases including invertebrates-EST databases. The carbamidomethyl (C), oxidation (M) and phospho (S, T, Y) were set for fixed modification, and variable modification repectively. Tryptic enzyme digestion was selected and allowed up to three miss cleavage sites. The peptide tolerance was \pm 1.2 Da and \pm 0.6 Da for MS/MS tolerance. The peptide charges were 1+, 2+, and 3+. ESI-QUAD-TOF was set for instrument type and mascot generic file (.mgf) was an input for searching. The significant hit of identified peptide with p < 0.05 and highest MOWSE score was reported for protein spot identification.

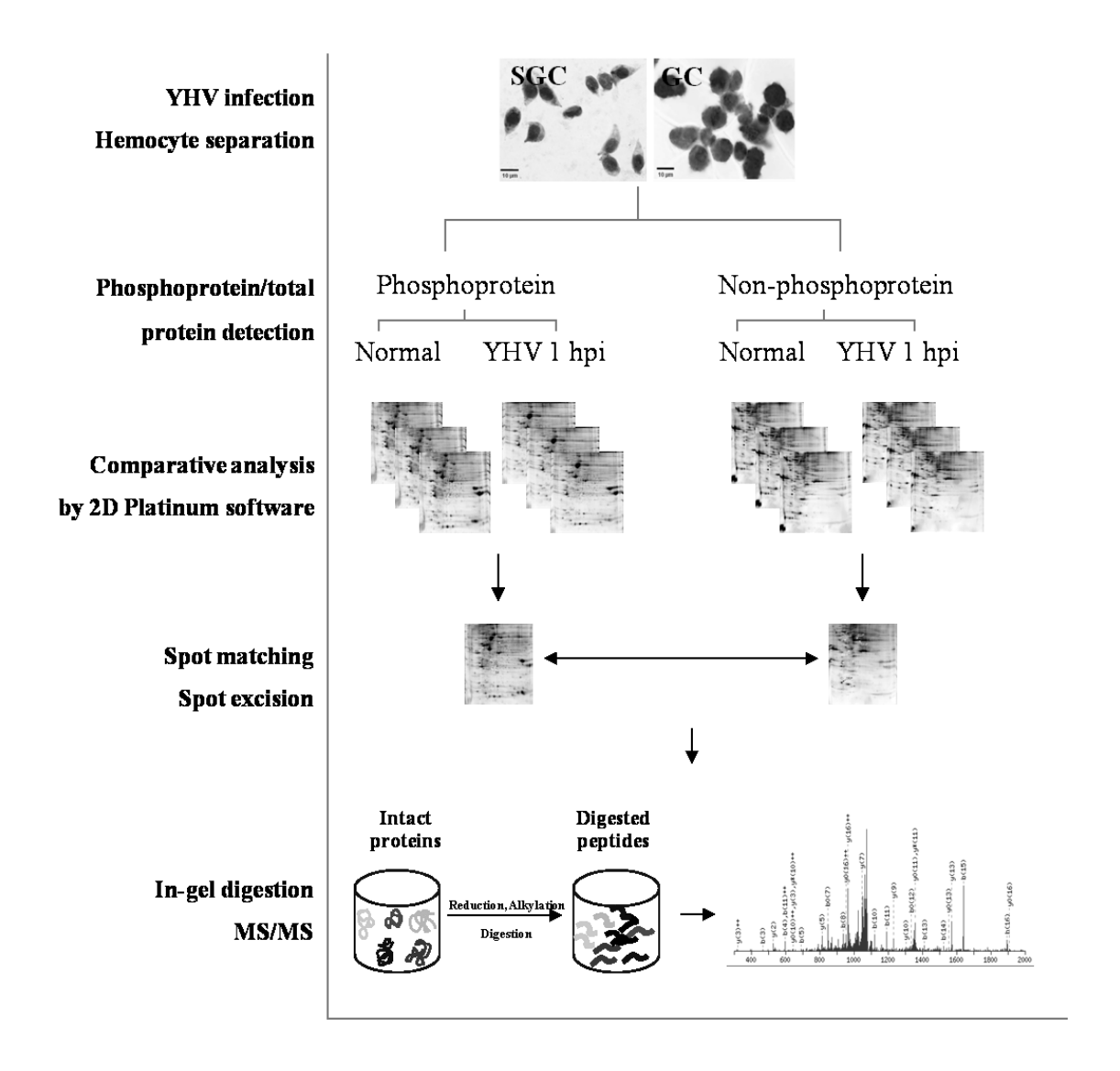


Figure 4. Differential phosphoproteomics analysis workflow of YHV-infected hemocytes. The diagram showed analysis workflow of differential phosphoprotein and total protein in YHV-infected hemocytes.

Production of recombinant protein and polyclonal antibody against MRLC MRLC cDNA amplification and purification

Hemocyte RNA was extracted by Tri reagent similar to the previously described method. To obtain partial sequence of shrimp hemocyte myosin regulatory light chain (MRLC), RT-PCR was performed. The cDNA was synthesized by incubating 1 µg of extracted RNA

with DNase 1 (Promega) containing 1X DNase buffer (40 mM Tris-HCI; pH 7.9, 10 mM NaCl, 6 mM MgCl₂ and 10 mM CaCl₂) for 15 min at 37 °C. The reaction was then incubated with 2.5 mM EDTA at 55 °C for 15 min to stop the DNase reaction. The reaction of cDNA synthesis contained oligo-dT (Promega), 1 mM dNTPs (Promega), 1X First strand buffer (Invitrogen), 5 mM DTT, 1X RNase out (Invitrogen), and Superscript III reverse transcriptase (Invitrogen). The reaction was incubated with the following conditions; RT 5 min, 50 °C, 60 min, and 70 °C 15 min. The cDNA template was kept at -20 °C for stock.

PCR was then performed to amplify the MRLC target gene. The PCR reaction contains; 1X Ex *Taq* buffer (Takara Bio, Inc.), 2.5 mM dNTPs, 1 mM MRLC primers (Table 3), and Ex *Taq* polymerase. The condition of PCR reaction was followed by an initial denaturation at 95 °C for 3 min, denaturation at 95 °C for 30 sec, extension at 72 °C for 30 sec, and final extension at 72 °C for 5 min. The PCR product was either subjected to PCR extraction process or kept at -20 °C until extraction step. For PCR product extraction, approximately 300 µg of PCR product was determined on 0.8% agarose gel. The single band of amplified gene was excised and cut into small pieces and then PCR extraction from gel was performed by using Gel PCR extraction kit (GeneAid) according to instruction from manufacturer. Briefly, 300 µg of PCR product in agarose gel was mixed with 500 µl of DF buffer and then incubated at 55 °C for 15 min to melt agarose gel. After cooling at RT, 800 µl of solution was transferred to prepared DF column and then the flow-through was removed by centrifugation. Subsequently, W1 buffer was added and removed by centrifugation again. The column was washed by wash buffer and then PCR product was eluted using elution buffer by centrifugation. The eluted fraction was kept at -20 °C for ligation process

MRLC ligation

Approximately $30-50~\mu g$ of purified PCR product obtained from previous step was subjected to ligation reaction. Amplified MRLC was ligated to pGEM $^{\circ}$ - T easy vector (Promega) to evaluate for nucleotide sequences. Briefly, PCR product was incubated with 1 μg of pGEM $^{\circ}$ - T easy vector (Promega) containing ligation Ver. 2 buffer (Takara, Bio, Inc.) and then incubated at 16 $^{\circ}$ C for overnight. Subsequently, recombinant plasmid was transformed to *Escherichia coli* strain DH5 Ω competent cell (RBC Biosciences, Taiwan) and then incubated

at 42 °C for 90 sec. Transformant was cultured in LB broth at 37 °C for 30 min before spreading on LB agar plate containing (100 μg/ml) ampicillin antibiotic and then further incubated at 37 °C for 16 h. The transformed cell was checked by colony growth and restriction enzyme digestion to identify MRLC positive clone. Approximately 10 – 20 colonies were checked by colony PCR as previously described. The positive clone was transferred to a new LB agar plate and kept as master plate. To analyze for the positive clone, recombinant plasmid was extracted by mini prep plasmid DNA extraction kit (GeneAid) by following the manufacturer protocol. The purified recombinant plasmid was kept at -20 °C for ligation to pET 28b (+) vector (Invitrogen) and cut by restriction enzyme. To perform restriction analysis for recombinant plasmid, the digestion reaction was prepared in 10 μl of DNA plasmid, 1 μl of *Eco* RI restriction enzyme (table 2) and then incubated at 37 °C for 4 h. The reaction was inactivated at 65 °C for 20 min followed by a resolving on 0.8% agarose electrophoresis. Further, the positive clone containing MRLC gene was then subjected to DNA sequencing process to verify for the MRLC sequences before ligation to pET 28b (+) protein expression system.

Plasmid ligation and protein expression

For MRLC recombinant protein expression, the pET28b (+) protein expression system was developed. For ligation reaction, the recombinant plasmid obtained from previous section and pET 28b (+) vector (Novagen) were digested with two selected restriction enzymes, *Hind* III and *Xho* I (table 2) using buffer 2 and 1X BSA (Promega). The reaction was incubated at 37 °C for 4 h following an inactivation at 65 °C for 20 min. Both digested reaction were combined for ligation step containing Ligation Ver. 2 buffer. The ligation reaction was incubated at 16 °C for overnight. The recombinant plasmid (pET 28b (+) MRLC) was transformed into *E. coli* strain BL21 (DE) competent cell (RBC Bioscience, Taiwan). The positive clone was identified by colony PCR and then positive colony was kept as master plate by growing on LB agar plate containing 100 µg/ml of kanamycin at 37 °C for 16 hours.

For MRLC protein expression, the positive clone was cultured in LB broth containing kanamycin and then incubated at 37 $^{\circ}$ C for 16 h. to determine MRLC expression level in small scale, 60 μ l of bacterial cultured was transferred to new LB broth and then incubated at 37 $^{\circ}$ C

for 1 – 1.5 h (OD_{600} = 0.5). After that, 200 µl of bacterial cultured was collected for no-induction sample and MRLC expression induction by 1 mM IPTG (Promega). After 3 h post induction, 200 µl of bacterial cultured was collected for IPTG induction sample. To determine protein expression level, both non induction and IPTG induction sample were centrifuged at 3000 rpm for 10 min to collect cell pellet. The pellet was resuspended in PBS buffer and then sonicated for 1 min. The bacterial cell lysate was centrifuged at 12000 rpm for 5 min to collect both supernatant and non-soluble part. To determine protein expression, both supernatant and pellet were mixed with 5X sample buffer and then incubated at 95 $^{\circ}$ C for 10 min before resolving on 12.5% SDS-PAGE and CBB-G staining.

In addition, MRLC expression in *E. coli* system was confirmed by Western blot analysis. Briefly, *E. coli* obtained from the previous step was separated on 12.5% SDS-PAGE and then transferred to PVDF membrane (GE Healthcare) using wet blot protein transfer system (Amersham Biosciences). Further, PVDF membrane was blocked with blocking solution (5% skimmed milk, 1X TBS; pH 7.5, 0.5% Tween-20) at 4 °C for overnight. Subsequently, membrane was covered with mouse anti-6X His primary antibody (Abcam) containing 5% skimmed milk, 0.5% TBST; pH 7.5 and incubated at RT for 1 h. The membrane was then incubated with secondary antibody (goat anti-mouse HRP-conjugated secondary antibody) containing 5% skimmed milk, 0.5% TBST; pH 7.5 at RT for 2 h. Finally, after membrane washing, the immuno complex signal was enhanced by Western Lightning (Perkin Elmer) and exposed to X-ray film.

Protein purification

For large scale MRLC expression, the positive clone was cultured in 20 ml of LB broth containing kanamycin at 37 $^{\circ}$ C for 16 h. Subsequently, 10 ml of bacterial cultured was transferred to 500 ml of LB broth with antibiotic and then incubated at 37 $^{\circ}$ C for 2 h to obtain OD₆₀₀ equal to 0.5 – 0.8. After that protein expression was induced by 1 mM IPTG for 3 h of incubation. Further, the bacterial pellet was collected by centrifugation at 8,000 rpm for 10 min. The cell pellet was resuspended in buffer A (10% glycerol, 1X PBS; pH 7.5) and then sonicated for 30 min on ice. The lysate was centrifuged at 9,000 rpm for 15 min at 4 $^{\circ}$ C to obtain inclusion part. Subsequently, the inclusion was resuspended with buffer B (1.5% *N*-

lauryl sarcosine, 1X PBS; pH 7.5) and mixed well by vortexing for 1 h to dissolve unsoluble protein. Further, dissolved His-tag MRLC protein was purified by Ni — NTA agarose bead (Qiagen). Ni — NTA agarose bead was washed with buffer C (50 mM Tris-Cl; pH 8.0, 500 mM NaCl, 20 mM imidazole) and incubated with dissolved *E. coli* lysate for overnight at 4 °C with rotation. After that, agarose bead was collected by centrifugation at 9,000 rpm for 10 min and then washed with buffer C by centrifugation. Finally, MRLC was eluted by sequential elution buffer. For protein elution step, 1.5 — 2 ml of agarose bead containing MRLC protein was applied to column (Econo-column, Bio-Rad) and then differential concentration of elution buffer (elution buffer 1 — 6) was applied. Only eluate obtained from elution buffer 3 (50 mM Tris-Cl; pH 8.0, 500 mM NaCl, 60 mM imidazole) and buffer 4 (50 mM Tris-Cl; pH 8.0, 500 mM NaCl, 100 mM imidazole) were collected and pooled together. The concentration of purify MRLC was determined by Bradford's assay according to previously described method.

Antibody production

Approximately 1.8 mg of purified MRLC was subjected to polyclonal antibody production. 0.5 mg of purified protein antigen was immunized to rabbit and then the antibody level was boosted twice by equal volume of purified protein once for every 2weeks. The serum obtained from immunized rabbit was collected and antibody titer against shrimp MRLC was determined by enzyme-linked immunosorbent assay (ELISA).

Western blot analysis

Determination of MRLC phosphorylation and protein expression level in YHV infected hemocyte were evaluated to confirm with 2 – DE analysis. To determine hemocyte MRLC phosphorylation level, anti-phospho-MRLC in shrimp hemocyte was obtained by using phospho-specific antibody against human MRLC-p20. Based on mass spectrometric result in this investigation, the sequence alignment of *Sylla paramamosain* (gi|262401074) MRLC phosphopeptide (QRATpSNVFA) recognition by myosin light chain kinase (MLCK) enzyme was identical to human MRLC. Therefore, antibody against human phospho-MRLC can cross react with shrimp hemocyte MRLC and commercially available for this experiment.

For Western blot analysis, 10 µg of total protein obtained from both total hemocyte and percoll separated granular cell (GC) were separated on 12.5% SDS-PAGE. The resolving proteins were transferred onto PVDF membrane (GE Healthcare) by using semidry blotting system (Amersham Biosciences). The PVDF membrane was blocked in blocking solution (5% BSA, 0.1% TBST; pH 7.5) for overnight at 4 °C. Subsequently, membrane was incubated with rabbit anti-phosphoMRLC primary antibody (Cell Signaling) for overnight at 4 °C with rocking. After washing, the membrane was further incubated with goat anti-rabbit HRP-conjugated secondary antibody (Santacruz) for 2 h at RT. The excess antibody was washed three times with 1X PBS and then immunoreactive band was determined by ECL-plus chemiluminescent (Pierce). To determine MRLC expression level on the same membrane, after MRLC phosphorylation detection, the membrane was soaked in mild stripping solution (1.5% (w/v) glycine, 0.1% (w/v) SDS, 1% (v/v) Tween-20; pH 2.2) for 10 min following 1X PBS washing to remove immune complexes. Further, the membrane was blocked with 5% skimmed milk containing 0.5% TBST for overnight followed by incubation with polyclonal rabbit anti-MRLC primary antibody for 2 h at RT with rocking. The membrane was washed with PBS and then incubated with goat anti-rabbit HRP-conjugated secondary antibody for 2 h at RT. Finally, the immunoreactive band was determined by ECL-plus chemiluminescent substrate (Pierce). In this experiment, two replicates hemocyte protein sample obtained from five-pooled individual shrimps investigated both normal YHV infection were in and hpi.

To determine the level of antimicrobial peptide, crustin Pm1, shrimp hemocyte was collected from four individual samples upon YHV infection at 0 hpi, 6 hpi, 12 hpi, and 24 hpi. Total hemocyte protein and plasma protein were precipitated using methanol-chloroform-water and determined for protein concentration by Bradford's assay similar to method previously described. 15 mg of total protein from both hemocyte and plasma were separated on 12.5% SDS – PAGE followed by Western blot analysis. Tubulin expression level was used as an internal control. The intensities of crustin Pm1 and tubulin from Western blot result were analyzed by densitometer.

Hemocyte phagocytic activity assay

To determine whether the molecular function of MRLC phosphorylation is associated with immune response, determination of shrimp hemocyte phagocytic activity during an inhibition of MRLC phosphorylation was investigated.

Inhibition of MRLC phosphorylation

To evaluate the functional role of MRLC phosphorylation, *in vitro* inhibition of MRLC phosphorylation in hemocyte was established. Briefly, the optimal concentration of myosin regulartory ligh chain kinase(MLCK) inhibitor was determined for hemocyte culture based on mammalian cell studied. For shrimp hemocyte, 10 μM and 50 μM of ML-9 (Sigma Aldrich), a specific inhibitor of myosin light chain kinase, were supplemented in hemocyte culture medium. To monitor MRLC phosphorylation level, total protein was collected at different periods post inhibition including 30 min, 1 h, 2 h, 6 h, 12 h, and 24 h. Phospho-MRLC and MRLC expression level were then investigated by Western blot analysis.

Hemocyte phagocytosis assay

MRLC phosphorylation inhibition, hemocyte phagocytosis investigated. At optimal concentration of inhibitor and investigated time point, hemocyte culture was incubated with shrimp serum sensitized sheep red blood cell (SRBC). To prepare SRBC, sheep red blood cell was washed twice with PBS by centrifugation. Sheep red blood cell was further incubated with shrimp serum at RT for 1 h. The sensitized sheep red blood cell was fixed with fixative solution (10% formaldehyde) for 20 min and then washed three times with PBS. Fixed SRBC was diluted to obtain 10^{5} cell/ml and then kept at 4° C until used. To determine hemocyte phagocytosis, after incubation with SRBC at 28 °C for 1 h, hemocyte culture was fixed with fixative solution (10% formaldehyde, 0.45 M NaCl) for 20 min and then stained by Rose Bengal and Hematoxylin. Stained cell was investigated and the numbers of phagocytosed cells were counted by light microscope (Olympus). The activity of hemocyte phagocytosis was reported in term of phagocytic index using the following the formula;

A total of 100 cells were investigated per shrimp sample, and 10 shrimps were evaluated for each group. The significant change of hemocyte phagocytic activity between normal and MRLC phosphorylation inhibition was statistically determined by Student's t test (p < 0.05).

In vitro study of MRLC phosphoryltion inhibition and YHV replication

Five individual shrimps were used for normal and YHV infection group. Diluted YHV stock (1:100, 0.45 M NaCl) was intramuscularly injected to infected group, while normal group was injected with normal saline. After 2 hpi, hemolymph was collected and then hemocyte was cultured on 24-well plate containing L-15 medium. To evaluate the role of MRLC phosphorylation and YHV infection level in hemocyte, hemocyte obtained from YHV infected shrimps were separated into two batches. One batch was cultured in L-15 medium supplemented with two types of MLCK inhibitors (ML-7, and ML-9) in various concentrations (10 μ M and 50 μ M) while another one group was maintained in L-15 medium containing 2% dimethylsulfoxide (DMSO). At 24 h post treatment, YHV infected hemocyte was examined by immunofluorescence detection. The method of YHV detection was similar to previously described.

The number of YHV positive granular cell was count from confocal image. Total 500 of hemocytes (100 cell/shrimp) of each experimental group were demonstrated. The significantly infectivity based on fluorescence positive cell comparing between each group were statistically analyzed by $Student's\ t$ test (p < 0.05)

In vivo study of MRLC phosphoryltion inhibition and YHV replication Inhibition of MRLC phosphorylation in shrimp

Study of MRLC phosphorylation and YHV replication in shrimp was performed using 20 g body weight of adult shrimp. 10 shrimps/group were separated into four experimental groups including normal shrimp (saline injection), no inhibition (saline injection followed by YHV infection), and two groups of MRLC inhibition shrimp (1 mg/kg ML-7 or 10 mg/kg ML-7 injection followed by YHV infection). Diluted YHV stock was intramuscularly injected post 2 h

of ML-7 injection. The culmulative mortality was observed at 12 hpi, 18 hpi and 24 hpi. At the same time, the hemolymph was randomly collected from five shrimp per group to determine YHV replication level in each condition. In this experiment, the toxicity of ML-7 inhibitor to shrimp was monitored in normal shrimp by injected at the same concentration similar to experimental condition and the mortality rate was investigated.

Calculation of YHV replication

The hemolymph obtained from each groups were maintained in L-15 medium for 1 hour before subjected to analysis by immunofluorescence detection. Total 500 cells from five individual shrimps (100 cell/shrimp) were count from confocal image. The number of YHV positive GC cell at various time points were calculated (cells/100 cell of hemocyte). In addition, YHV replication level in granular cell was also demonstrated by determination of relative fluorescence intensity in YHV positive cell. Determination of fluorescence intensity was demonstrated by Image J analysis software (version 1.45S). The relative fluorescence intensity was demonstrated by the corrected total cell fluorescence value (CTCF) following the formula;

CTCF = Integrated Density - (Area of selected cell x Mean fluorescence of background readings)

Total 20 of GC cell in each experimental group (n = 5) from confocal image were used to calculated for the fluorescence intensity. *Student's t* test (p < 0.05) was used to determine the significance of difference of YHV replication level in each experimental condition based on fluorescence intensity.

In vivo study of caspase-3 inhibition and YHV infection

To evaluate to role of apoptosis induction in YHV infected shrimp and YHV replication, inhibition of the key apoptosis regulator protein caspase-3 was established. 10 individual shrimps were separated into normal (without inhibitor), YHV infection (without inhibitor), and two inhibitor injected groups. In this experiment, irreversible caspase-3 inhibitor [Ac-DEVD-CMK] (Merck) was used. For caspase-3 inhibited groups, 1 mg/kg and 10 mg/kg of inhibitor

were evaluated. After 2 h post inhibitor injection, diluted YHV was subsequently injected and shrimp mortality rate was observed at 12 hpi, 24 hpi, 30 hpi, and 36 hpi. YHV replication level in hemocyte was then investigated. Randomly collected hemolymph samples from five shrimps in each condition were subjected to YHV detection by immunofluorescence. The relative fluorescence intensity corresponding to YHV replication in hemocyte was calculated using ImageJ similar to previously described. Differences in fluorescence intensity comparing between each experiment condition was statistically analyzed by $Student's\ t$ test (p < 0.05).

RESULTS AND DISCUSSION

1. Characterization of Penaeus monodon hemocytes

Characterization of black tiger shrimp hemolymph by light microscope revealed at least three types of hemocytes. After staining by Rose Bengal and hematoxylin, they were classified as hyaline cell (HC with small cell size, high content of nucleus and no granules), semi-granular cell (SGC medium cell size, oval or elongated shape, high volume of cytoplasm with lots of small and large granules), and granular cell (GC- large cell size, oval and elongated shape, high volume of cytoplasm with large granule).

Analysis of hemocytes by flow cytometry (FC) also showed a mixture of three cell types based on their cell size and granularity. These cell types can be classified into three populations of small cell and non-granule containing (SSC score $< 10^{1}$), small size of granular containing cell (SSC score 10^{2} - 10^{3}), and large size of granular containing cell (SSC $> 10^{3}$).

Moreover Percoll gradient centrifugation at optimal condition showed three separation bands of cells. To confirm the results from FC, each isolated bands were individually evaluated. The result had confirmed that the three isolated bands of cell were detected in distinct cytogram region. Light microscope data indicated that the homogenous cell population was clearly observed in each percoll separated bands. This result revealed that percoll gradient centrifugation successfully separated the hemocytes of black tiger shrimp without disturbing their morphology and cell viability.

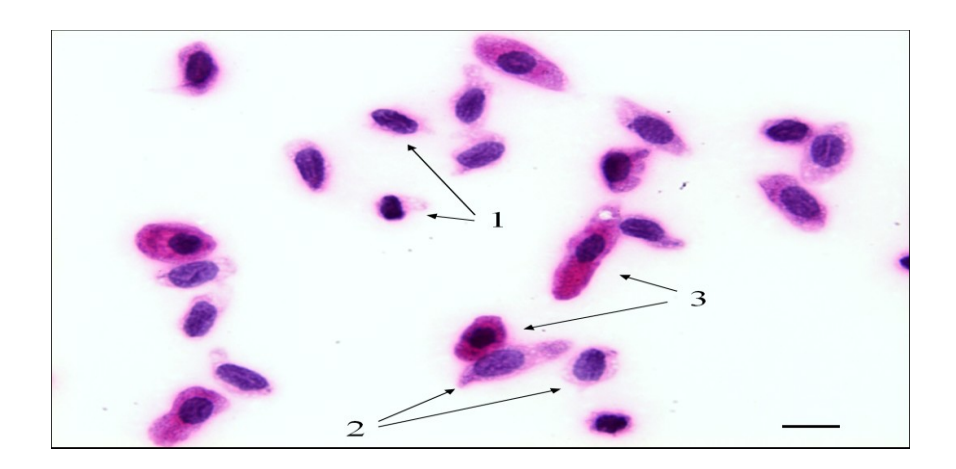


Figure 5. *P. monodon* hemocytes stained with Rose Bengal (pink for granule detection) and hematoxylin (blue for nucleus detection) under light-microscope (100X).

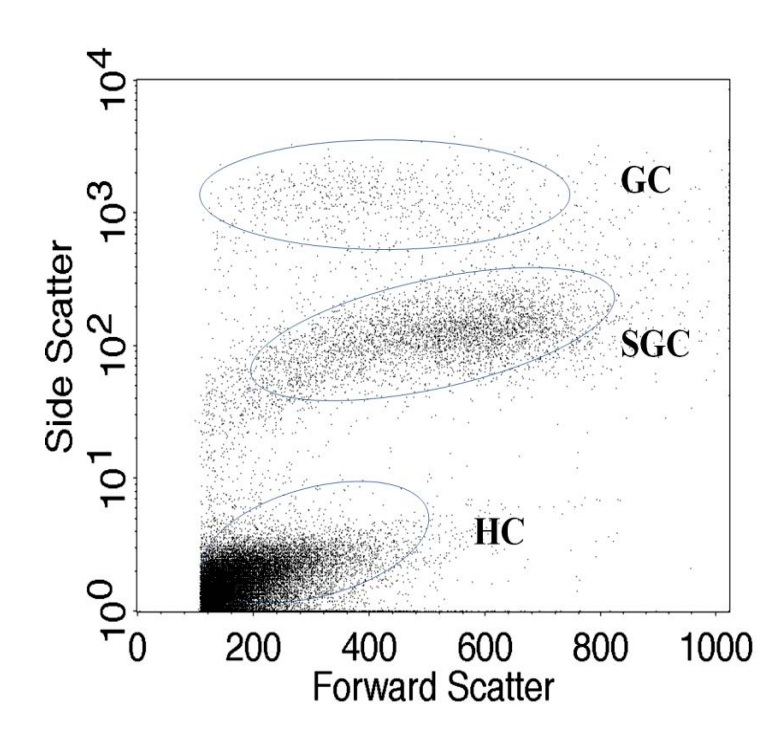


Figure 6. Analysis of *P. monodon* hemocytes by flow cytometry revealed three types of cell population in cytogram.

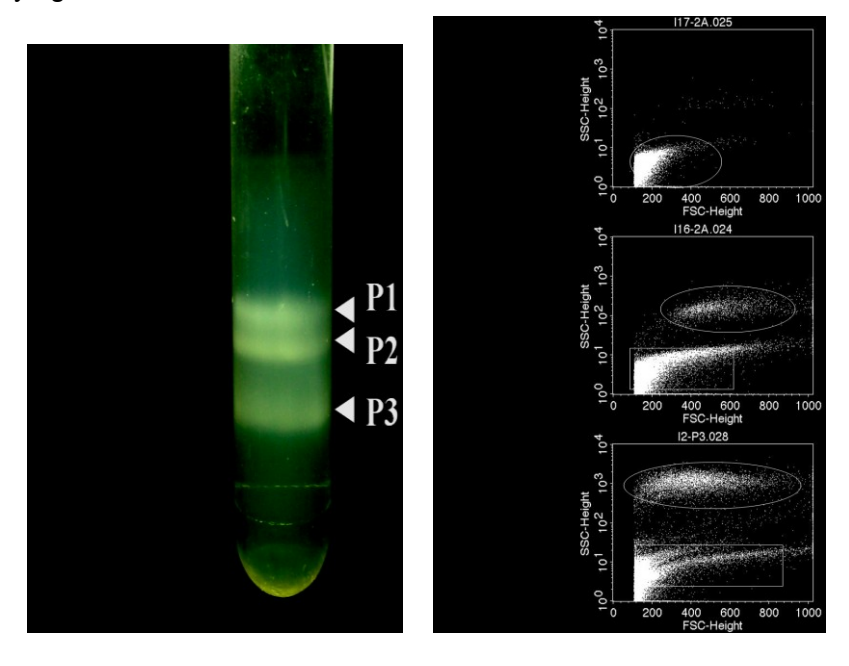


Figure 7. Separation of shrimp hemocyte by percoll gradient centrifugation revealed three separated bands of hemocytes (indicated by arrow heads). The optimal condition for hemocyte separation is 70% percoll solution containing 0.33 M NaCl (osmolarity = 700 mOsm/Kg).

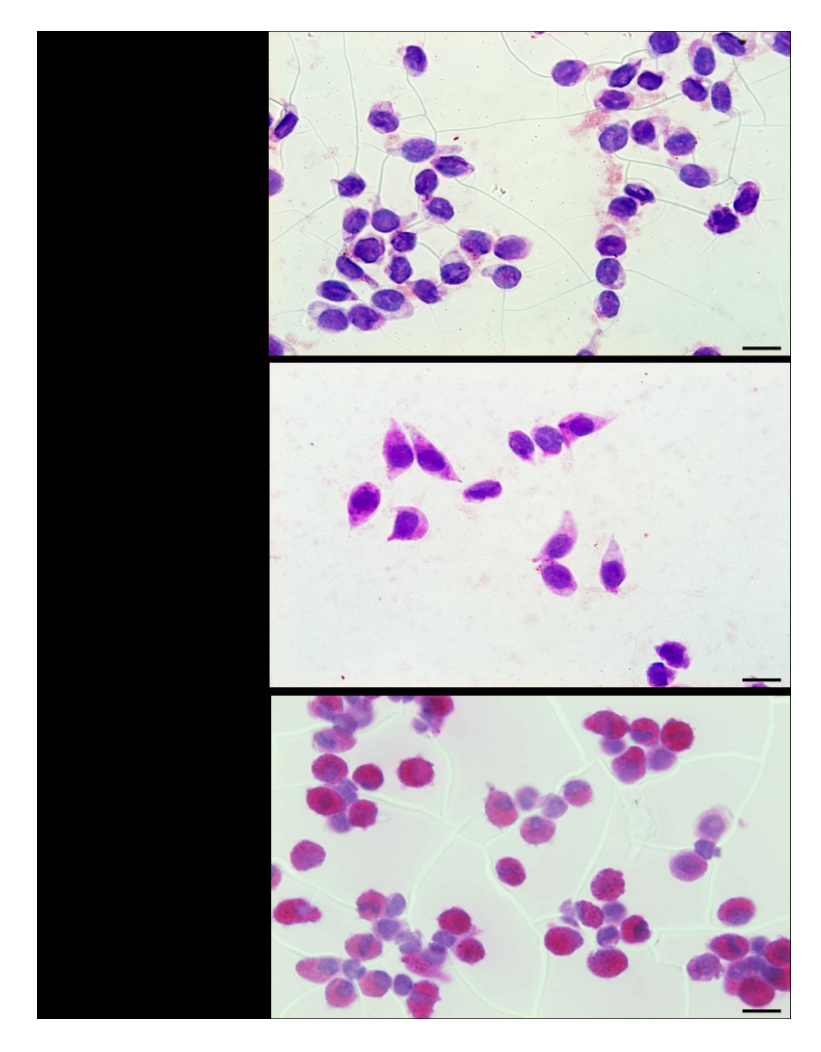


Figure 8. Morphology of *P. monodon* **hemocyte.** The cell characteristics was investigated by light microscope after percoll separation.

2. Analysis of total *P.vannamei* hemocytes under TSV infection.

Alterations in C- and N-terminal fragments of hemocyanin in TSV infected hemocytes

Expression proteomics using 2-DE (totally 4 gels derived from 12 individual shrimps per group were analyzed) revealed up-regulation of the C-terminal hemocyanin fragments (labeled as C1-C4; TSV-infected/control ratios were ranged from 1.50 ± 0.15 to 2.25 ± 0.26 folds), whereas the N-terminal fragments were down-regulated (labeled as N1-N3; TSVinfected/ control ratios were ranged from 0.37 ± 0.19 to 0.53 ± 0.11 folds). Amino acid sequence of the N-terminus (1^{st} -230th residues) and C-terminus (438^{th} - 648th residues) of hemocyanin were identified by nanoLC-ESI-MS/MS (Accession no. CAA57880; MS/MS ions scores were ranged from 74 to 334), and were used for production of rabbit polyclonal

antibodies against these two respective fragments. Note that we used the pl range of 4-7 in the present study because our initial screening using the broader pl range of 3-10 demonstrated that almost all of hemocyte proteins had pl range of 4-7

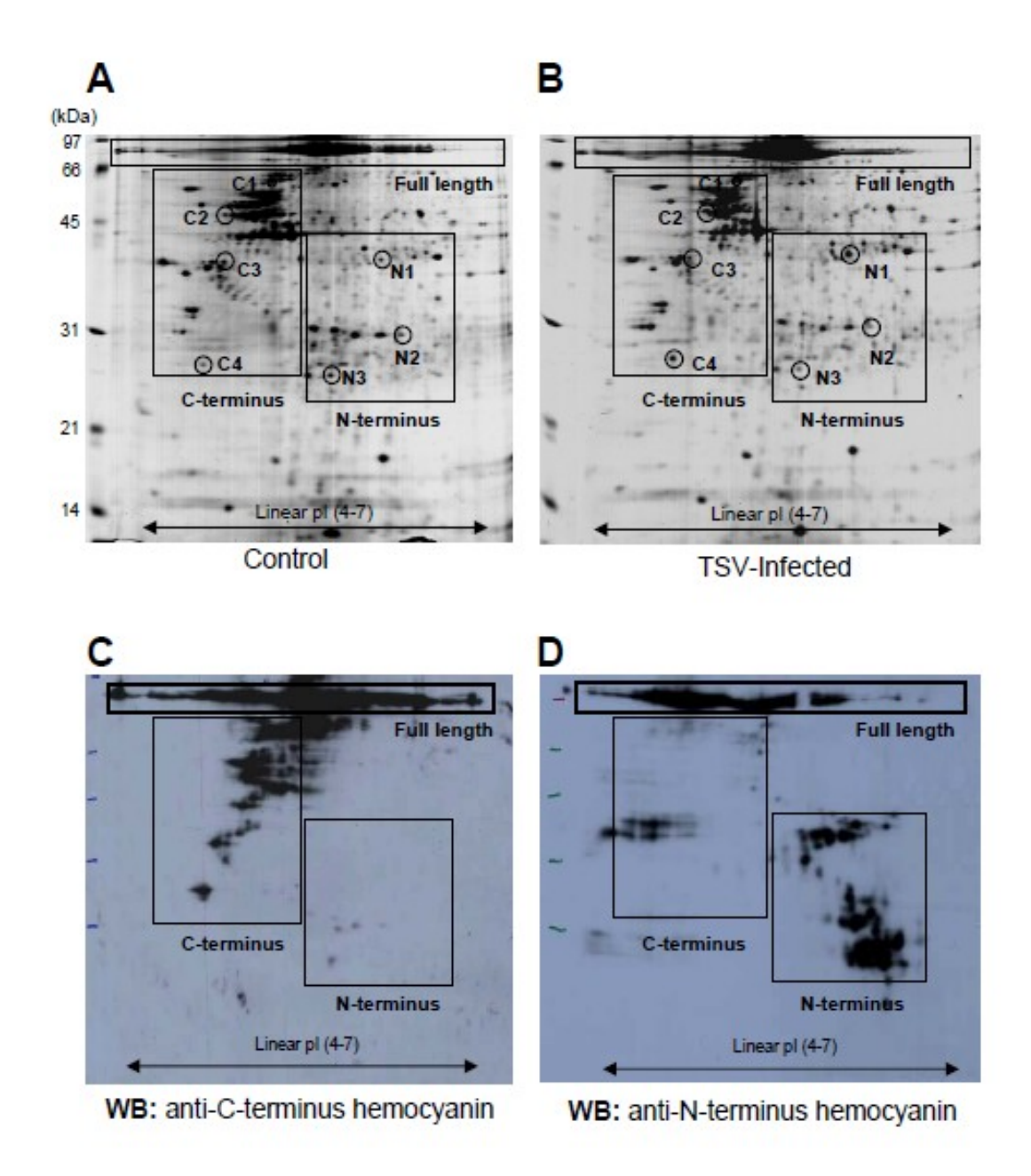


Figure 9. Alterations in C- and N-terminal fragments of hemocyanin in TSV infected hemocytes of *P. vannamei*. (A) and (B) show proteome maps of altered C- and N-terminal fragments of hemocyanin (n = 4 gels derived from 12 individual shrimps for each group; totally 8 gels were analyzed). (C) and (D) show 2-D Western blot analysis of C- and N-terminal hemocyanin, respectively.

C-terminal hemocyanin fragments underwent serine phosphorylation

The C-terminal hemocyanin fragments were localized in the more acidic region, whereas the N-terminal fragments were localized in the less acidic region in 2-D gels. Calculation of their theoretical pl by the "ProtParam" tool using their sequences revealed that the C-terminus had a more acidic pl (approximately 5.16; with 37 negatively charged amino acid residues), whereas the N-terminus had a less acidic pl (approximately 6.04; with 27 negatively charged amino acid residues), consistent to their actual positions in 2-D gels. Moreover, the expression proteomics data were confirmed by 2-D Western blot analysis using specific antibodies 11 against the C- and N-termini of hemocyanin, strengthened our results by 2-DE and pl calculation. These selective locales of the C- and N-termini of hemocyanin drew our attention for further functional analyses of the C- and N-terminal hemocyanin fragments. One of the possibilities of this difference in pl of the C- and N-termini could be the process of posttranslational modification (PTM). The most likely PTM that caused pl shift was phosphorylation, which might cause a pl shift towards the acidic end (up to >1 pl unit shift). We thus screened for potential phosphorylation sites in the C-terminal hemocyanin compared to the N-terminus. Using the "NetPhos 2.0 Server" for prediction of possible phosphorylation sites revealed greater number of phospho-serine (7 residues) in the Cterminus, whereas only 2 phospho-serine residues were predicted in the N-terminus. There were comparable numbers of potential phospho-threonine and phospho-tyrosine residues predicted in the C- and Ntermini of hemocyanin. We then validated our prediction by 1-D Western blot analysis for phospho-serine, Cterminal, and N-terminal hemocyanin. Our data shows that serine phosphorylation was observed only in the C-terminus, not in the N-terminus of hemocyanin. We then hypothesized that serine phosphorylation in the C-terminal hemocyanin fragments might be the key for differential regulation of the C-terminus compared to the N-terminus of hemocyanin.

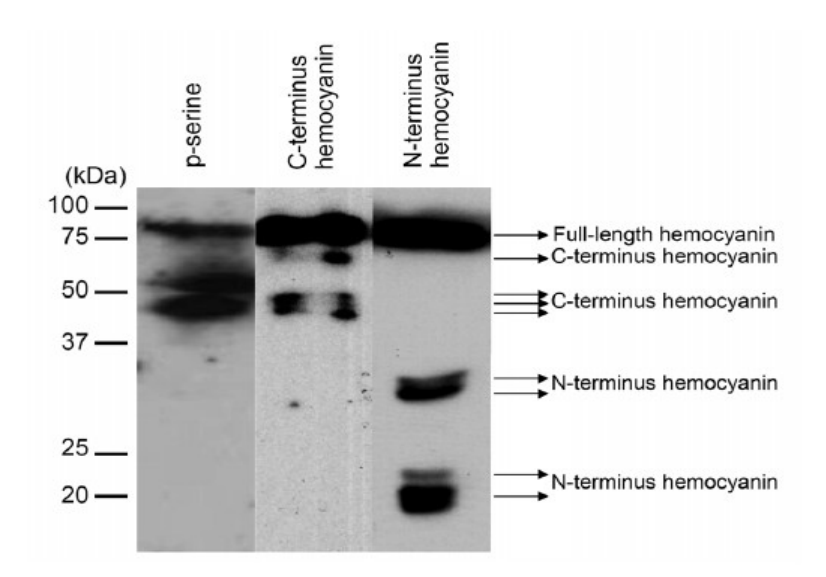


Figure 10. Western blot analyses of phospho-serine (p-serine), C-terminus, and N-terminus of hemocyanin. Immunoreactive bands corresponding to full-length, C-terminus, and N-terminus of hemocyanin are indicated with arrows and legends.

C-terminal hemocyanin interacted with ERK1/2

To further investigate the differential roles of C- and N-termini of hemocyanin in shrimp hemocytes, "Scansite" (version 2.0) software was employed for motif scan in the C-terminus, compared to the N-terminus of hemocyanin. The scan was performed against all 65 individual motifs and 12 motif groups available in the Scansite, using the "high stringency" criteria indicated in the software. Only ERK D-domain, which is required for activation 12 of ERK1/2 effector kinase, was identified as a kinase-binding site in the C-terminal hemocyanin at 527th valine residue, whereas none of individual motifs and motif groups was identified in the Nterminus (data not shown). This data strongly suggested that ERK interacted with the Cterminal hemocyanin, leading to serine phosphorylation in this terminus. The motif scan results were confirmed by co-immunoprecipitation (Co-IP) to address potential interaction between the C-terminal hemocyanin and ERK1/2. Co-IP using anti-ERK1/2 and the resulting complexed proteins were examined with 1-D Western blot analysis using anti-C-terminal hemocyanin. The results showed that the C-terminus of hemocyanin bound to ERK1/2, whereas the isotype control yielded none of the C-terminal fragments. However, the full-length, but not C-terminus, hemocyanin could be pulled down from the IgG isotype control sample, suggesting the nonspecific binding of the full-length hemocyanin to protein G bead surfaces. This result was not

surprising as hemocyanin is normally sticky and almost always pulled down by Co-IP (similar to albumin in mammalians). Western blot analysis for ERK1/2 confirmed the positive ERK1/2 band at the expected size, whereas the isotype control sample showed a faint band of ERK1/2. This result again was not unexpected, as the full-length of hemocyanin that was somehow pulled down by the isotype IgG also contained the 527th valine; thus, should be able to bind to ERK1/2. However, the ERK1/2 band in the isotype control sample was not as prominent as the one present in the ERK1/2 Co-IP sample. Because the C-terminal hemocyanin fragments were up-regulated in hemocytes of *P. vannamei* during TSV infection, we then further hypothesized that ERK1/2 as the interacting protein of the C-terminal hemocyanin should be also up-regulated in the TSV-infected hemocytes. 1-D Western blot analysis was performed to address this hypothesis. It illustrates that ERK1/2 level was also up-regulated in the TSV-infected hemocytes.

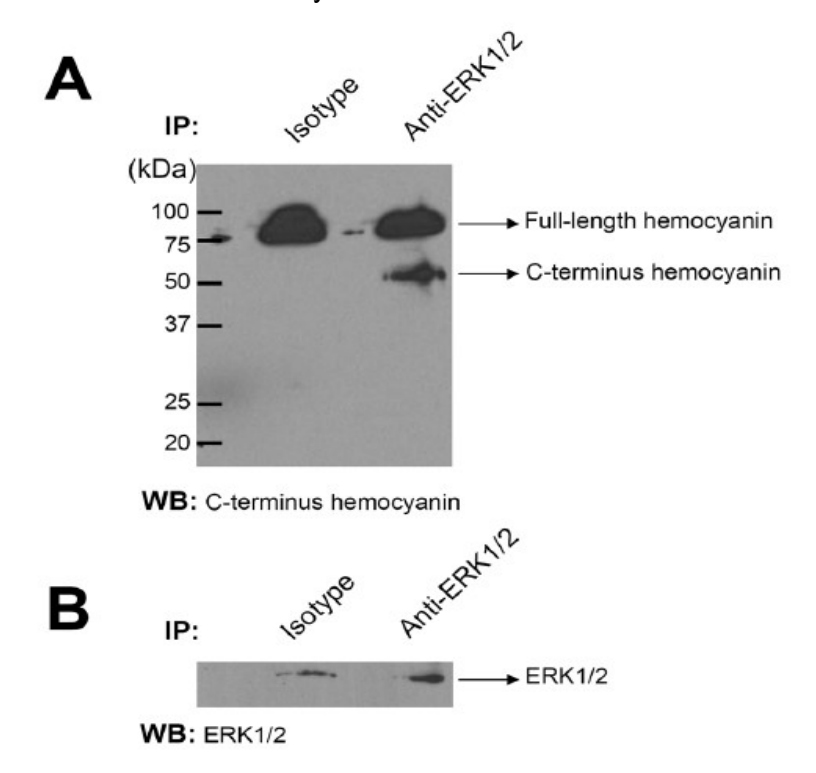


Figure 11. C-terminal hemocyanin bound to ERK1/2 as demonstrated by Co-IP using anti-ERK1/2. (A): The resulting complexed proteins were examined with 1-D Western blot analysis using anti-C-terminal hemocyanin. (B): The resulting complexed proteins were examined with 1-D Western blot analysis using anti-ERK1/2. Rabbit IgG served as the isotype control in a parallel experiment.

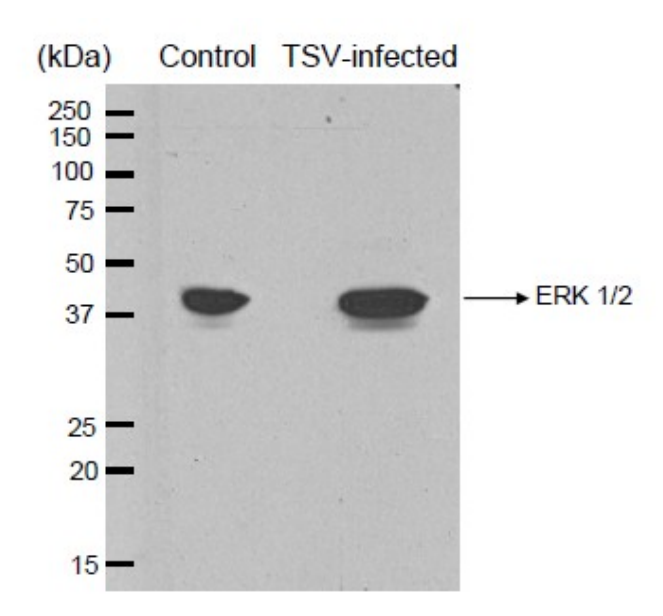


Figure 12. Western blot analysis of ERK1/2 in TSV-infected hemocytes compared to the mock (uninfected) control. Immunoreactive band of ERK1/2 is indicated with arrow and legend.

3. Analysis of protein expression for each hemocyte cell types

Analysis of hemocyte protein expression indicated distinct pattern among the three isolated cell types. Granular containing cells (SGC and GC) showed somewhat similar expression profile while the non-granular containing cell (HC) was quite different. Some protein bands were observed predominately in one type of hemocytes suggesting their specific roles in that hemocyte. SDS - PAGE analysis demonstrated at least eight protein bands with differential expression when compare between non-granular and granular containing cell. High resolution protein separation by 2-DE comparing between non granular cell and granular containing cells clearly showed that most of highly expressed proteins were synthesized in granular containing hemocytes. Their abundance may be associated with the functional roles in immune defense of granular hemocytes. Identification of these highly expressed proteins of hemocyte by mass spectrometry showed that were associated with many crucial functions in shrimp immune system. In addition, some proteins in hemocytes also supported the hemocyte functions that have been previously characterized. In this experiment, transglutaminase (TGase) is highly presented in hyaline cell suggesting that this cell is differentiated or closely related to hemocyte progenitor cell. On the other hand, Protease inhibitors (alpha-2 macroglobulin and Kazal-type proteinase inhibitor) and antimicrobial peptides (Crustins) are expressed in granular containing cell, indicating that most of effective molecules regulating shrimp immune responses are present in late differentiated cells of SGC and GC.

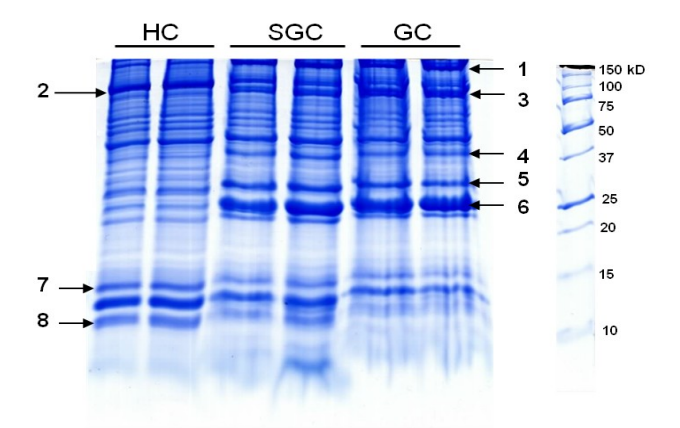


Figure 13. SDS-PAGE analysis revealed expression patterns of hyaline (HC), semigranular (SGC), and granular cell (GC). The arrows and numbers indicated the predominated bands of proteins expression when compare among each cell types.

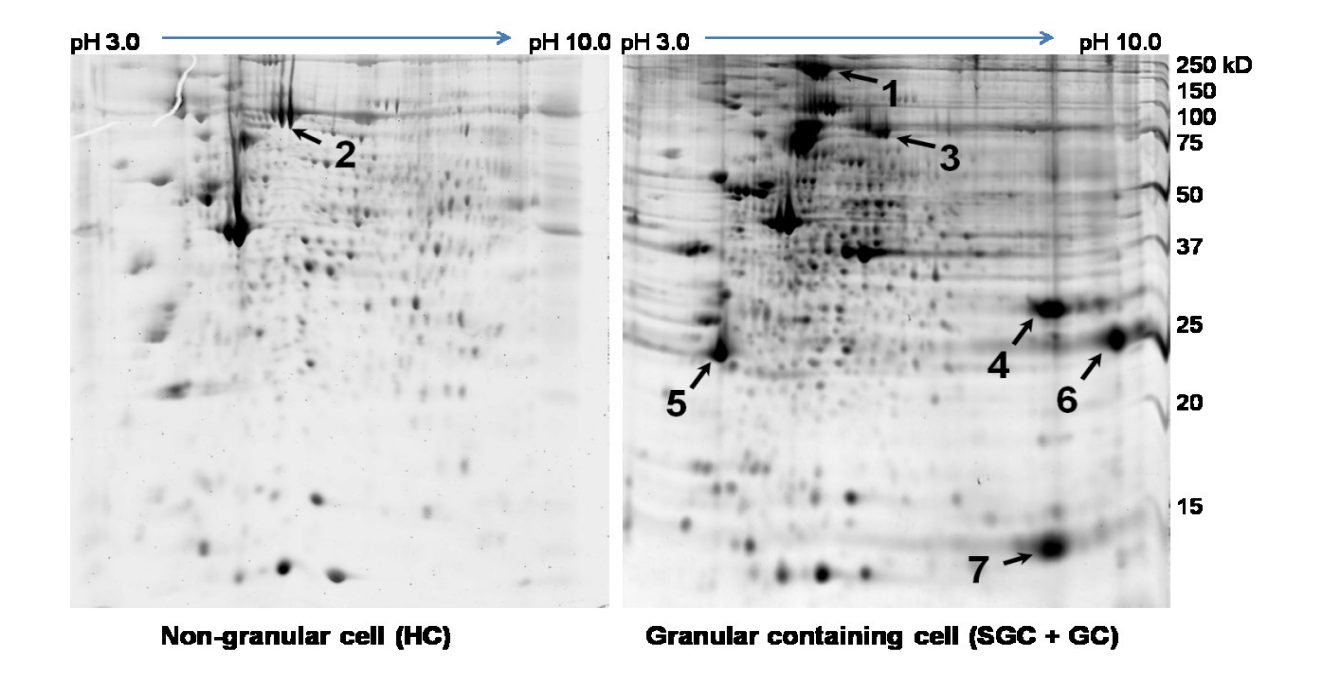


Figure 14. High resolution protein separation by 2-DE demonstrated the pattern of hemocyte protein expression comparing between non-granular containing cell (HC, left panel) and granular containing cells (SGC and GC, right panel). The numbers indicated predominately expressed protein spots.

Spot No.	Cell type	Protein [Organism]	Acc. No.	Observed MW(kD)/p/	lon score <i>i</i> Seq. coverage.	Possible function
1	SGC/GC	Alpha-2 macroglobulin	gi 126661688	168.5/5.7	180/3%	Protease inhibitor, ProPo system
		[Litopenaeus vannamei]				
2	HC	Transglutaminase [Penaeus monodon]	gi 33694274	85.5/3.31	1117/33%	Clotting system, hemocyte homeostasis
3	SGC/GC	Hemocyanin [Litopenaeus vannamei]	gi 854403	74.9/5.27	219/7%	Phenoloxidase, antimicrobial activity
4	SGC/GC	Kazal-type proteinase inhibitor [Penaeus monodon]	gi 33087164	30.5/8.48	1012/54%	Proteinase inhibitor, bacteriostatic activity
5	SGC/GC	Alpha-2 macroglobulin fragment [Penaeus monodon]	gi 60549971	32.7/5.04	531/32%	Syntenin binding, proteinase inhibitor
6	SGC/GC	Crustin <i>Pm</i> 4 antimicrobial peptide	gi 229459067	24.9/9.0	312/28%	Antimicrobial activity
7	SGC/GC	[Penaeus monodon] Crustin Pm1 antimicrobial peptide	gi 229459065	16.2/8.4	138/23%	Antimicrobial activity
		[Penaeus monodon]				

Table1: Protein identification from each cell types of *P. monodon* hemocytes.

4. YHV infection in P. monodon hemocytes

Infection of yellow head virus in black tiger shrimp hemocyte was revealed when the replication level of YHV gene was detected at 12 hours post injection using RT-PCR. This result suggested that the viral gene replication before assembly occurs within 12 hours after virus penetration. Therefore, detection of YHV infection in shrimp by PCR analysis should determined at more than 12 hours after virus invasion. However, at this YHV concentration (1:100 of diluted YHV stock, approximately 10⁶ copies/µI), high sensitivity of detection method including nested PCR may show the positive result since 6 hours post infection. Agarose gel electrophoresis demonstrated that YHV gene (helicase, 854 bp) was amplified since 12 hpi, and high level of gene expression was found at 24 hours post infection.

To investigate the interaction between YHV and hemocyte, detection of YHV in infected hemocytes was performed by immunocytochemistry. The result revealed that YHV interacted only with specific cell types. The YHV positive signal (indicated by red color) was found mainly in granular containing cells including semigranular (SGC) and granular cell (GC). Meanwhile, YHV positive cell observed in non granular cell (HC) was rarely or not found. Interestingly, the signal of YHV was found in GC cell since an early period of infection. It is possible that YHV may be more preferably to interact with GC cell than other cell types. This specific interaction between YHV and hemocyte could help us speculate on the mechanism for host and virus interaction which is associated with specific receptors or binding proteins presented in specific hemocytes.

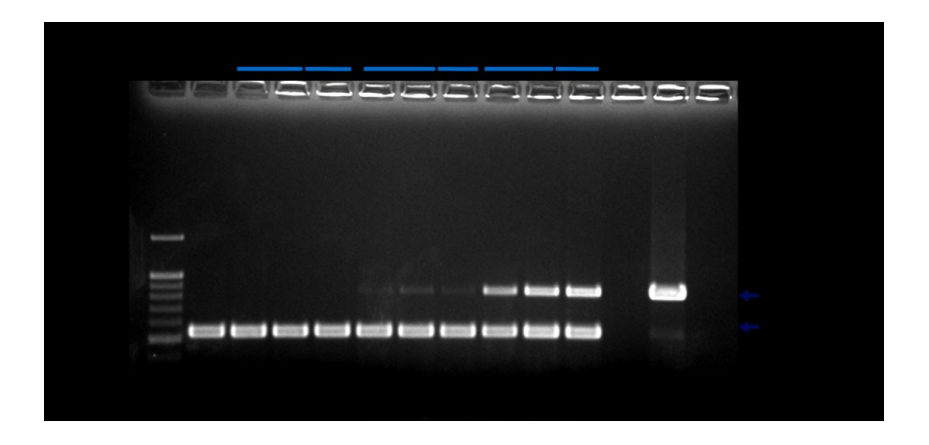


Figure 15. Amplification of YHV helicase gene in hemocytes at various time points showed YHV gene amplification by RT-PCR at least 12 hpi. C = control non-infected shrimp.

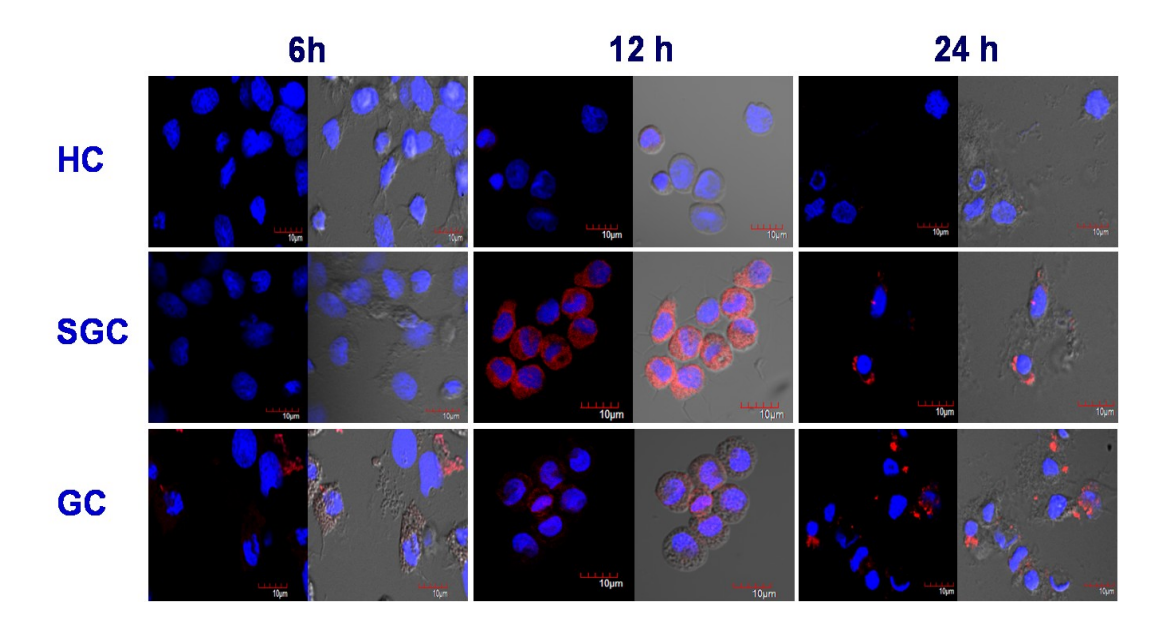


Figure 16. Immunofluorescence detection of YHV in infected hemocytes during 6 – 24 hpi. Detection of YHV particle was revealed by anti-gp116 antibody. Image analysis indicated that YHV particle was detected in cytoplasmic region of SGC and GC (red signal).

5. Crustin*Pm*1 modulation upon YHV infection

Crustin Pm1 is one of the identified proteins which showed predominately expressed in granular containing cells. Western blot analysis also confirmed that Crustin Pm1 is specifically expressed in two types of granulated cell. Determination of Crustin Pm1 expression using indirect immunofluorescence was revealed that Crustin Pm1 is mainly presented in granular cells and suggested to be membrane associated protein based on the position of signal detection. This result indicated that Crustin Pm1 may be useful for hemocyte protein marker.

The mRNA transcript of crustinPm1 antimicrobial peptide showed interestingly modulated upon YHV infection. The level of hemocyte mRNA of crustinPm 1 was up-regulated since early infection (6-12 hpi). In addition, monitoring of secreted level of crustin Pm1 also revealed that more secreted crustin Pm1 was observed in 6 hpi (p = 0.11) while decreasing of expression level was observed in hemocyte (p = 0.25). However, the level of both expression and secretion of hemocyte crustin Pm1 were significantly depleted at 12 hpi and especially in moribund stage.

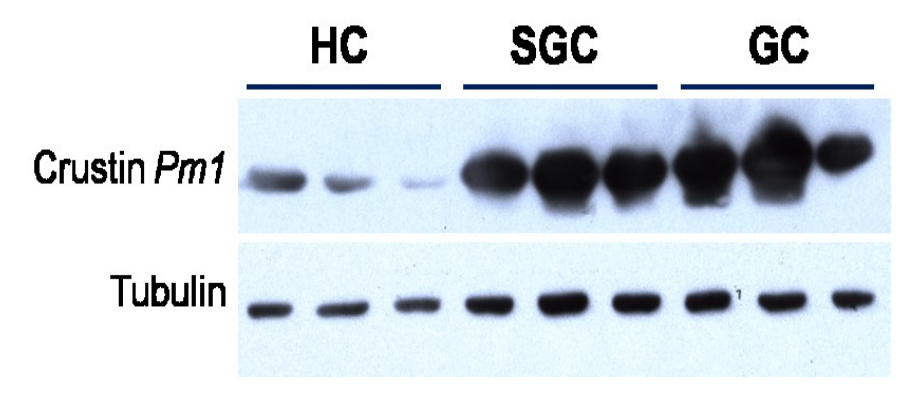


Figure 17. Crustin*Pm*1 expression in hemocyte detected by Western blot analysis revealed different expression level among hemocyte cell types. Crustin*Pm*1 was highly expressed in granulated cells (SGC and GC).

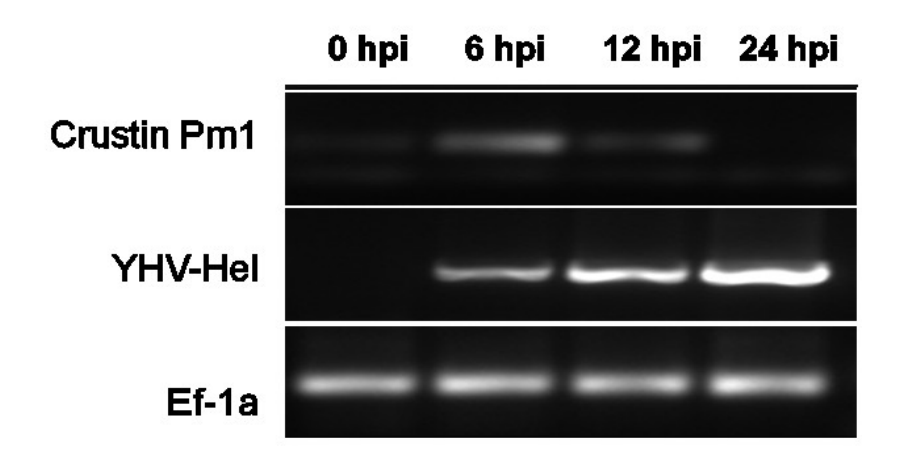


Figure 18. Crustin *Pm*1 mRNA expression was monitored at various times after YHV infection. RT-PCR indicated up-regulation of mRNA expression at 6 and 12 hpi

6. Phosphoproteome and proteome analysis of YHV-infected hemocytes

Evaluation of differential protein phosphorylation in shrimp hemocyte post YHV infection indicated that alteration of hemocyte protein phosphorylation was initiated since early periods of infection. Detection of phosphoprotein by specific fluorescence dye indicated increase of hemocyte protein phosphorylation level during 30 min to 2 hours after YHV inoculation. This phenomenon implied that hemocyte responses to virus infection may be through the function phosphoprotein. These proteins could be activated immediately and regulated shortly when hemocyte interacts with the virus.

To explore the targeted phosphoproteins, protein separation using two dimensional gel electrophoresis coupled with multiplex protein staining was established. In this work, YHV

infected SGC and GC were first evaluated. 2-DE result showed that hemocyte proteins were significantly altered in both phosphorylation level and expression level post in an early period of 1 hour post YHV infection. Some of differential phosphorylated proteins were identified in YHV infected hemocytes. Most of identified phosphorylated proteins in GC are related to immune response. This is suggesting that GC cell play a prominent role or act as the first line of defense cell when shrimp exposes to virus. From 300-400 proteins spots detected in SGC and GC, haft of these can be stained by ProQ Dimond.

The result of differential phosphoprotein identification described the biological function of YHV-targeted hemocytes in metabolic process (glycolysis). One of immune associated protein i.e. prophenoloxidase activating enzyme 2, showed an increase in phosphorylation level. This might be suggesting that ProPO system is involved in antiviral defense mechanism. In addition, some of the identified proteins indicated the activity of hemocyte in association with phosphorylation of cytoskeletal protein, actin and myosin. Differential non phosphorylated proteins also supported that proteins involving in metabolism, motility, and immune response are altered during an early period of YHV infection.

However, many of the phosphorylated proteins could not be identified in this experiment. We have found that most of differential phosphorylated proteins are present in very low abundance. Our detection of phosphorylated protein using 2-DE and multiplex protein staining technique may not be the best choice for detection of low abundant phosphoproteins.

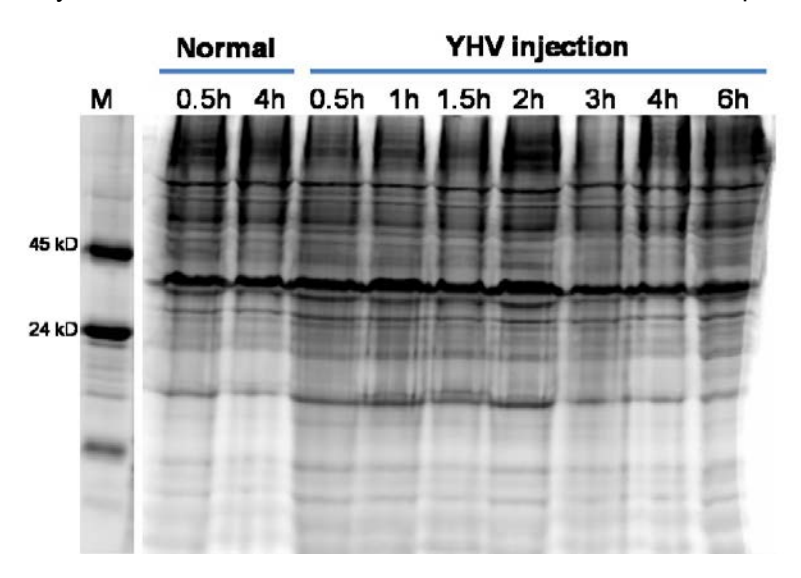


Figure 19. Time course analysis of differential phosphorylated protein in shrimp hemocyte post virus infection. Phosphorylation was observed in an early period of infection (0.5-2 h).

	SGC		GC	
Number of protein spot [↑]	Normal	YHV	Normal	YHV
Sypro Ruby staining (total protein)	405	418	273	252
Pro Q Diamond staining (phosphoprotein)	241	250	188	195
Differential phosphorylated proteins ^a *	2		11	
Differential proteins*	4		9	

Table 2. Differential phosphoproteome and proteome of YHV infected hemocytes

^{*} The number of significant protein spot was statistically analyzed by *Student't* test (T \geq 2.57, $p \leq$ 0.05).

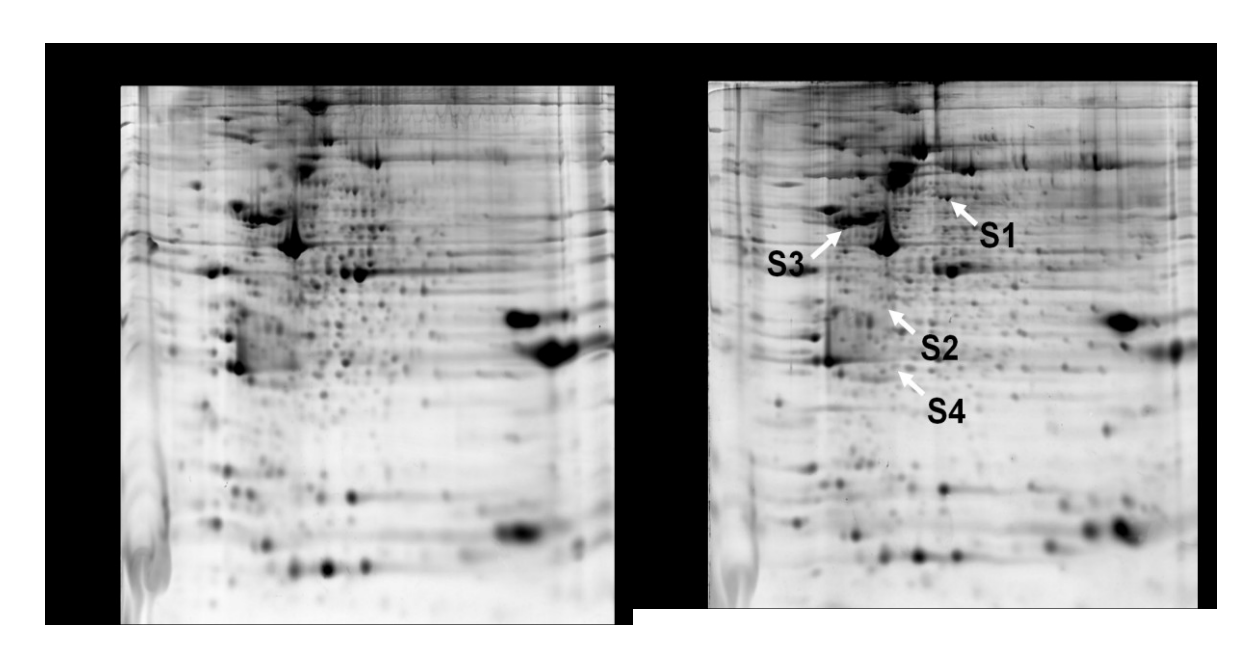


Figure 20. Proteomic analysis between normal (left) and YHV infected (right) SGC at 1 hour post infection. Protein was detected by Sypro Ruby. Four spots of proteins (S1 – S4) were differentially expressed in YHV infected SGC.

[†]The protein sample was obtained from three replicates gels (5 pooled-shrimps/gels).

^aThe proteins showed different phosphorylated level but maintained expression level.

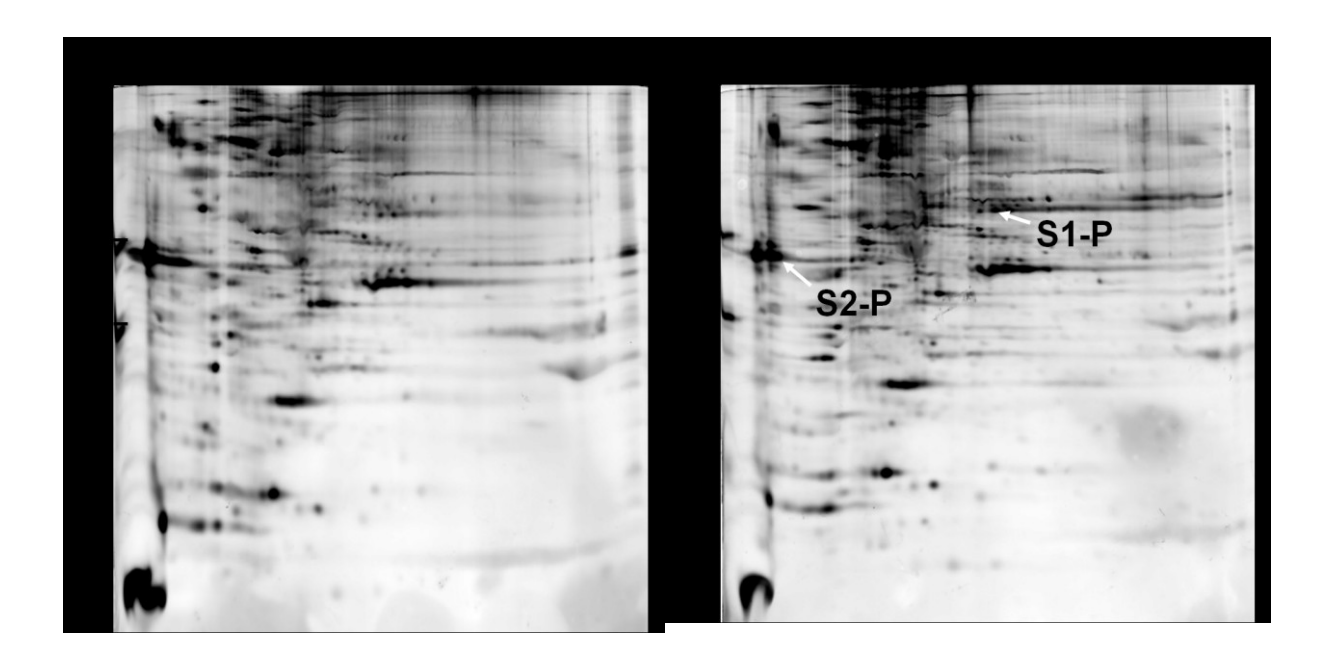


Figure 21. Phosphoproteomic analysis between normal (left) and YHV infected (right) SGC at 1 hour post infection. Two protein spots (S1-P and S2-P) were significantly phosphorylated as detected by ProQ DPS staining.

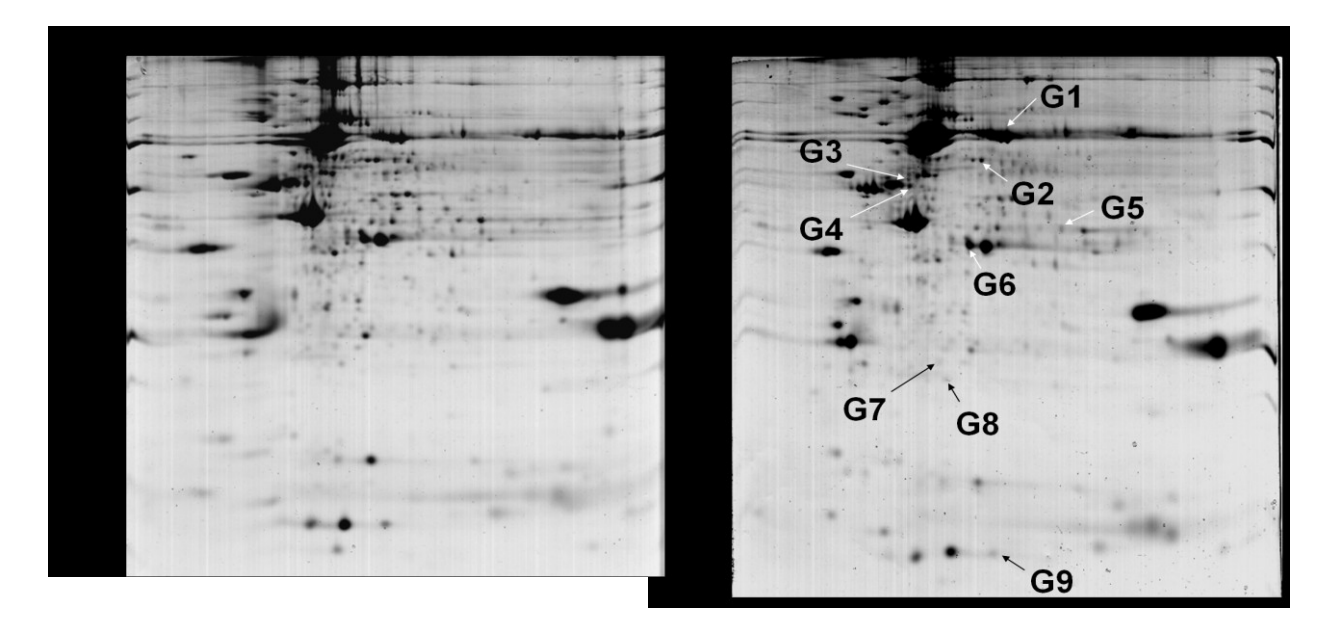


Figure 22. Proteomic analysis between normal (left) and YHV infected (right) GC at 1 hour post infection. Protein was detected by Sypro Ruby. Nine spots of proteins (G1 – G9) were differentially expressed in YHV infected SGC.

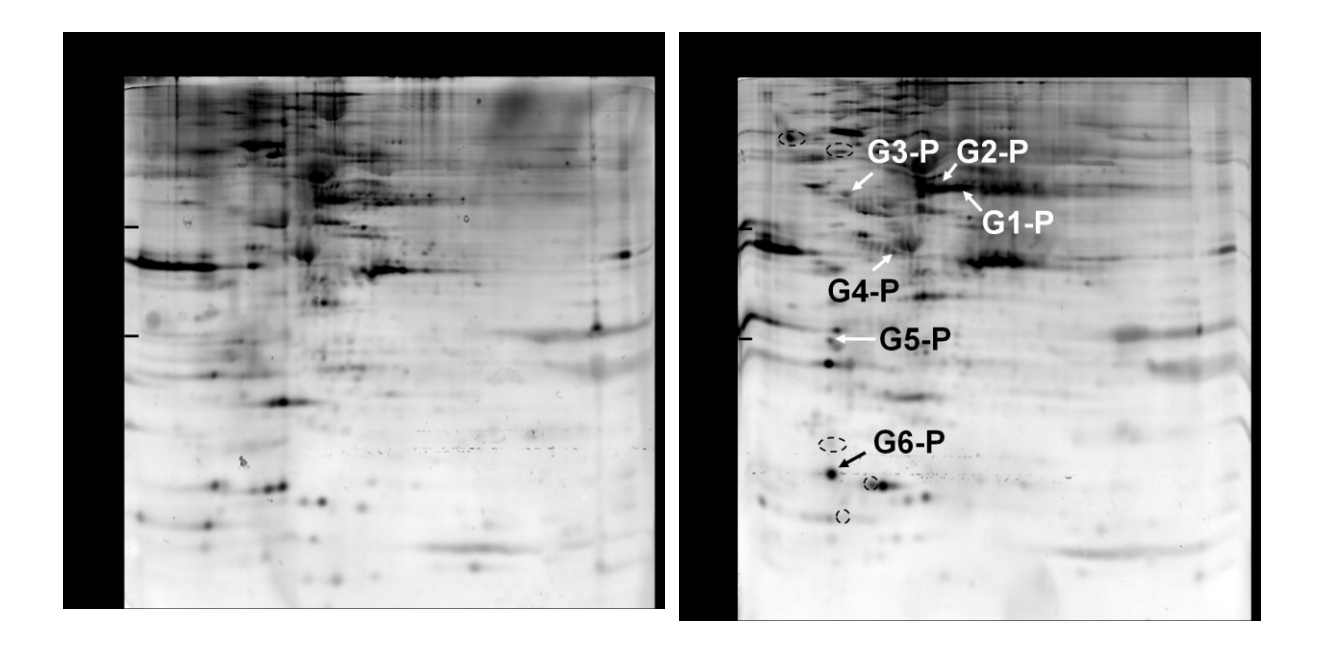


Figure 23. Phosphoproteomic analysis between normal (left) and YHV infected (right) GC at 1 hour post infection. Six protein spots (G1-P and G6-P) were significantly phosphorylated as detected by ProQ DPS staining.

			MW (kD)	Ratio	
Spot No.	Protein [organism]	Acc. No.	/b/	(YHV/ control)	Biological Function
Semigran	Semigranular cell (SGC)				
S1	EST0034 similar to transketolase [Dario rerio]	CF805601	37.9/6.15	0.64	Energy reserve metabolic process
S 2	LV_LO_RA003O21r Litopenaeus vannamei lymphoid	FE148139	27.5/6.02	1.45	
ć	organ cDNA library [<i>Litopenaeus vannamei</i>]			-	
S 83	F1-AI P synthase beta subunit [Litopenaeus vannamei] IV GI RA27F16r I itonenaeus vannamei cills cDNA	gi 1/U//9040 FF084657	55.9/5.03 27.6/7.15	3.27	ATP hydrolysis
	lihran II ifonananis vannamail			į	
Granular cell (GC)	ell (GC)				
5	Hemocyanin [Penaeus monodon]	gi 16612121	51.1/5.10	1.73	Oxygen transport, antimicrobial activity
G 2	PmTwN02G02.scf similar to hemocyanin [Litopenaeus	GO074804	19.0/4.90	0.22	
	vannamei]				
63	Tubulin alpha chain [Penaeus monodon]	gi 47498000	50.9/4.99	0.46	Microtubule-based movement, protein
					polymerization
G4	Tubulin beta-l chain [Homarus americanus]	gi 3915087	52.3/4.88	0.34	Microtubule-based movement
G5	LV_HC_RA032102r Litopenaeus vannamei hemocyte	FE099864	30.5/7.63	0.59	ı
	cDNA library [Litopenaeus vannamei]				
99	allergen Pen m 2 [Penaeus monodon]	gi 27463265	40.3/6.05	0.5	ATP/protein binding
C 2	Peroxiredoxin-6 [Lepeophtheirus salmonis]	gi 225712978	24.6/5.44	0.58	Lipid degradation
89 89	PmTwN55G06.scf similar to Crustacean calcium-	GO079665	17.3/6.93	0.65	Calcium ion binding
	binding protein 23 (CCBP-23 protein) [Orconectes				
	limosus]				
69	ED_501 P. monodon SSH hemocyte library Penaeus	EG026283	26.0/9.0	0.47	Oxygen transport, antimicrobial activity
	monodon cDNA clone P2029				

Table 3 Lists of non-phosphorylated proteins identification from YHV-infected of P. monodon hemocytes at 1 hour post infection.

Spot		:	MW KD)	Ratio	:
- No.	Protein [organism]	Acc. No.	ld/	(YHV/ control)	Biological function
Semigra	Semigranular cell (SGC)				
S1-P	Phosphopyruvate hydratase [Penaeus monodon]	gi 3885968	47.8/6.18	2.19	Glycolysis
S2-P	Beta-actin [<i>Litopenaeus vannamei</i>]	gi 10304437	42.2/5.3	0.55	Cell motility
Granula	Granular cell (GC)				
G1-P	LV_HP_RA13G17r Litopenaeus vannamei hepatopancreas cDNA library [Litopenaeus vannameil	FE129934	18.1/9.34	4.09	•
G2-P	AG-N-N01-0326-W similar to prophenoloxidase-activating enzyme 2 [Penaeus monodon]	GW996495	25.9/5.53	1.55	Prophenoloxidase activity
G3-P	Protein disulfide isomerase [<i>Litopenaeus</i> vannamei]	gi 225382096	55.8/4.64	.0.67*	Cell redox homeostasis
G4-P	LV_ES_RA14F10r Litopenaeus vannamei eyestalk cDNA library [Litopenaeus vannamei]	FE051092	24.9/9.21	3.73	•
G5-P	14-3-3-like protein [Penaeus monodon]	gi 66774602	28.2/4.61	2.05	Protein binding/Apoptosis
G6-P	Putative myosin regulatory light chain 2 smooth muscle [Scylla paramamosain]	gi 262401075	19.8/4.55	2.05	Cell motility, phagocytosis

Table 4. Lists of phosphorylated proteins identification from YHV-infected of P. monodon hemocytes at 1 hour post infection.

7. Myosin regulatory light chain phosphorylation in YHV infected GC

Differential phosphorylation of Myosin regulatory light chain in YHV infected GC was clearly detected by fluorescence dye staining. The 2-DE gels indicated that MRLC was highly phosphorylated while maintained its expression level at 1 hpi. MRLC is one of the proteins that plays crucial role in regulation of cytoskeletal proteins such as myosin and actin. Upon YHV infection, phosphorylated MRLC (MRLC-p) was significantly increased suggesting its role associated with immune response. Sequence alignment of MRLC among human and invertebrates indicated highly conserved amino acid sequences especially in phosphorylation recognition site at Serine residue. To study the role of MRLC phosphorylation associated with hemocyte immune response against YHV, molecular cloning of recombinant *Pm*MRLC was carried out. *Pm*MRLC gene was cloned based on the MRLC sequence obtained from mass spectrometric result (gil262401075). 378 base pairs (124 deduced amino acid sequences) of partial *Pm*MRLC sequence was amplified and verified. The *E. coli* expression system was used for large scale *Pm*MRLC expression. The purified *Pm*MRLC was verified by anti-His6 antibody and used for antigen immunization in rabbit to produce polyclonal antibody.

Confirmation of *Pm*MRLC phosphorylation by Western blotting also supported that *Pm*MRLC-p is increased at 1 h after YHV infection in GC. Meanwhile, the total *Pm*MRLC expression remains constant. Time course analysis of *Pm*MRLC phosphorylation during YHV infection showed continuously up-regulation of *Pm*MRLC-p and reached for up to 6 hpi before going down to regular level at 24 hpi.

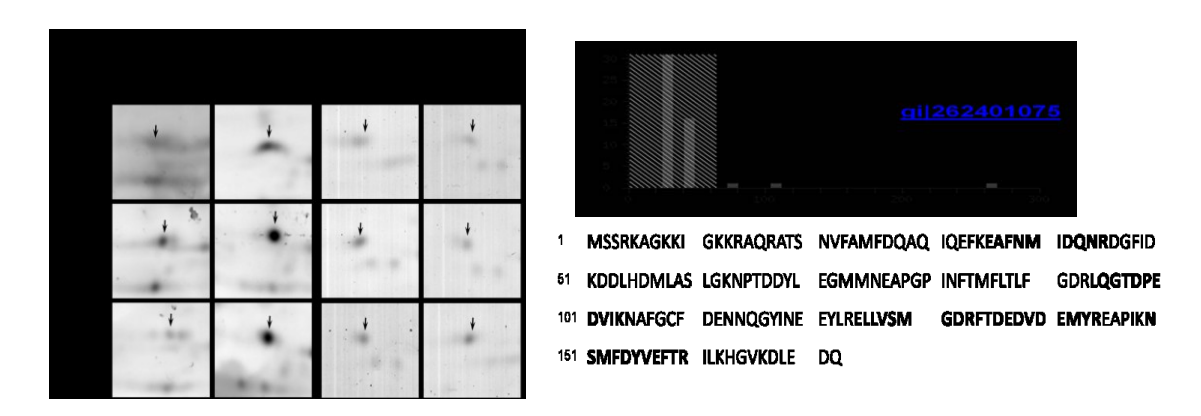


Figure 24. Differential phosphorylation level of myosin regulatory light chain (*Pm*MRLC). Mascot score showed the score of peptides hit (MOWSE = 265) and the number of peptides matched (shown in bold).

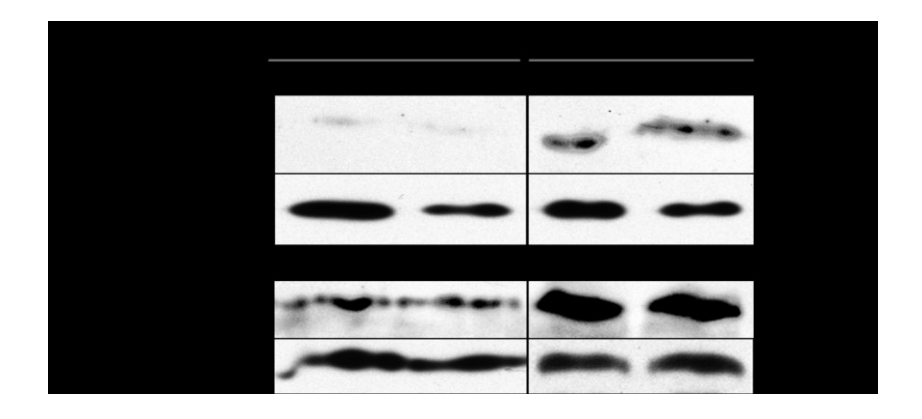


Figure 25. Western blot analysis of MRLC expression and phosphoprylation and in YHV infected granular (GC) hemocyte.

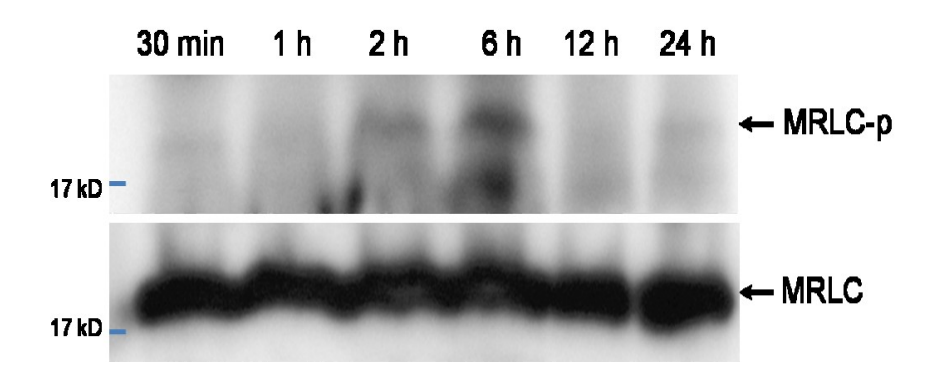


Figure 26. Time course analysis of PmMRLC phosphorylation level in YHV infected GC.

8. <u>PmMRLC phosphorylation associated with actin polymerization</u>

We have detected high level of phosphorylation of *Pm*MRLC in viral infected GC. In other systems, it was found that regulation of actin remodeling involved with phospho-MRLC. In our work, actin showed very low signal at 0 hpi. After 2 hour post infection, rearrangement of actin at the plasma membrane position is clearly observed, and increased in 6 hpi. This result indicated that *Pm*MRLC phosphorylation may associate with actin remodeling in GC and regulate hemocyte immune response during YHV infection.

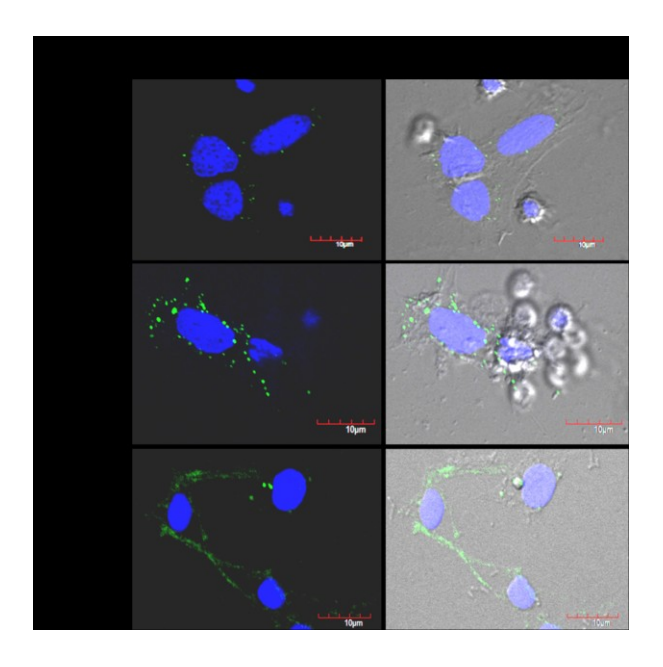


Figure 27. Immunofluorescence detection of actin (green) polymerization.

9. Inhibition of MRLC phosphorylation affected hemocyte phagocytosis activity

Cytoskeletal proteins associated with immune cell phagocytic activity were previously reported in both vertebrate and invertebrate systems. In shrimp, hemocyte phagocytosis regulated by MRLC phosphorylation mechanism may be related to antiviral activity. Analysis of hemocyte phagocytosis using sheep red blood cell (SRBC) ingestion showed that phagocytosis is mainly exist in granular containing hemocytes (i.e. SGC and GC). In hyaline cell, lower activity is observed. SRBC clumping was routinely observed when incubated with granular hemocytes. This phenomenon may suggest that GC can play a crucial role in pathogen entrapping as the first line of defense mechanism.

To further evaluate the relationship between MRLC phosphorylation and hemocyte phagocytosis, two types of myosin light chain kinase (MLCK) specific inhibitors (ML-7 and ML-9) were applied for inhibition assay. Inhibition of MLCK showed a decrease of MRLC phosphorylation in hemocyte at 2 hours after inhibitors supplemented. Both inhibitors showed effective inhibition of MLCK activity at 10 µM *in vitro*. Upon MRLC phosphorylation inhibition, hemocyte phagocytosis was examined. The result indicated that both inhibitors were significantly diminished phagocytic activity of the granular containing cells. These data could demonstrate that MRLC phosphorylation is involved in hemocyte phagocytosis activity.

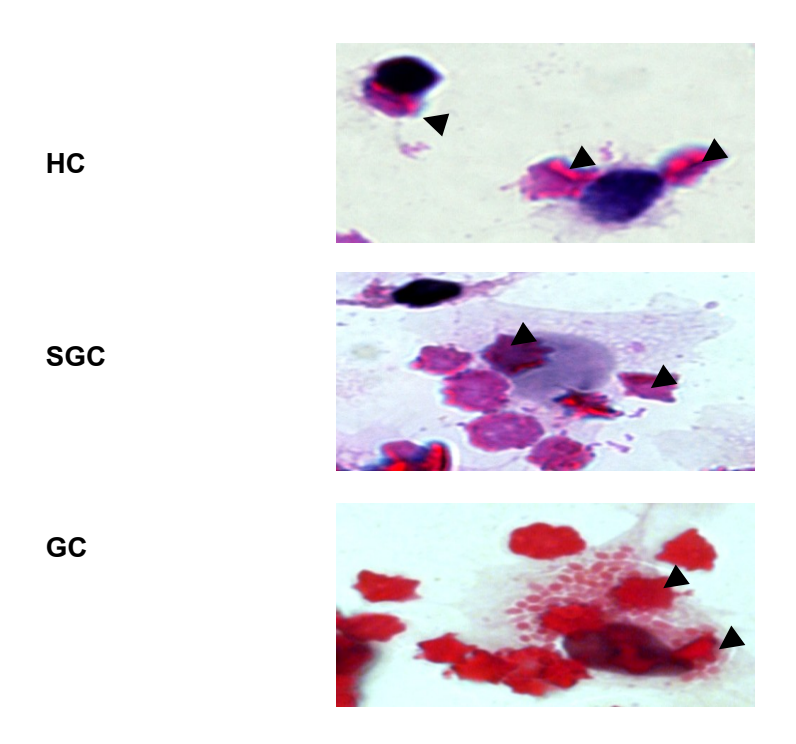


Figure 28. Detection of hemocyte phagocytic activity by sheep red blood cell ingestion.

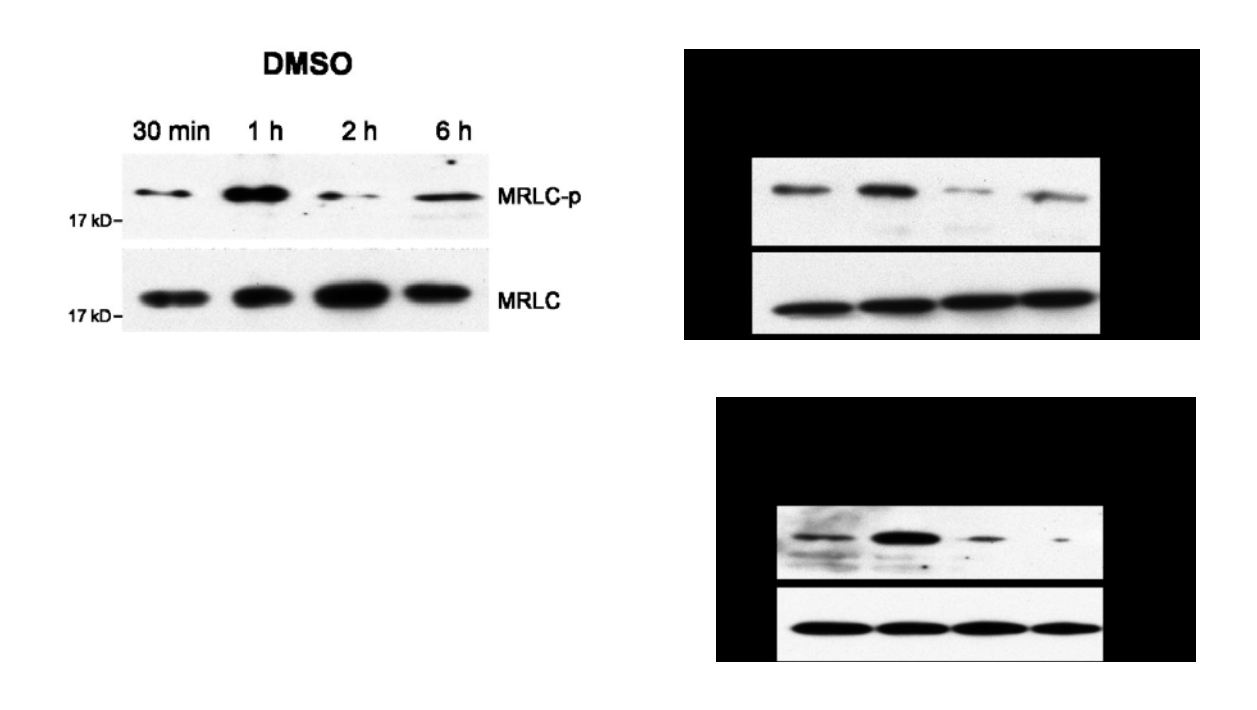


Figure 29. Inhibition study of MRLC phosphorylation in shrimp hemocytes using 10 μ M ML-7 and 10 μ M ML-9 respectively. At 2 hours post inhibition, MRLC-p was decreased in both inhibitors test.

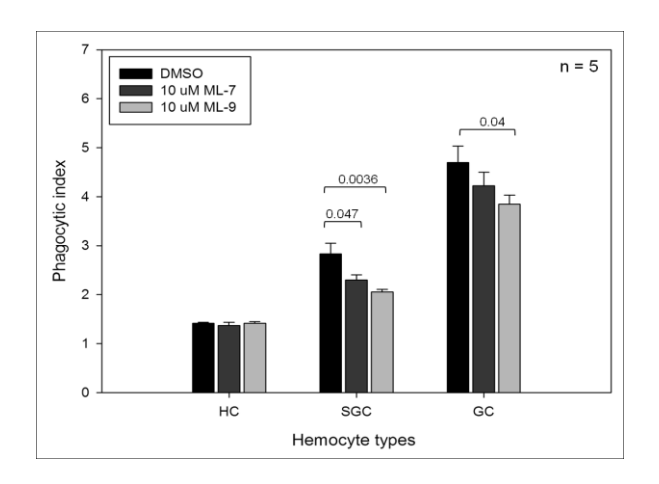


Figure 30. Hemocyte phagocytosis activity upon MRLC-p inhibition. The correlation of MRLC-p and hemocyte defense response was determined by hemocyte phagocytic activity (PI). High activity of phagocytosis was observed in granular containing cells of control shrimp (black bar). Both inhibitors, ML-7 and ML-9 significantly affected hemocyte phagocytosis.

10. Inhibition of MRLC phosphorylation induced YHV infection in vitro and in vivo

To evaluate the role of MRLC phosphorylation in YHV response, *in vitro* study of YHV infection upon inhibition of MRLC was investigated. After shrimp infected with YHV, viral replication level in primary hemocyte culture was monitored. The result showed an increase of replication in MLCK suppressed conditions. Both MLCK inhibitors showed similar effect in primary hemocyte culture. In addition, comparison among the YHV-infected cells indicated that suppression of MLCK activity lead to higher infection in GC cell.

In vivo study for the role of MRLC phosphorylation also supported an in vitro study. In vivo inhibition of MRLC phosphorylation induced YHV multiplication and caused rapid mortality in shrimp. Two concentrations of selected MLCK inhibitor (ML-7) were tested in shrimp. After inhibitor injection, experimental infection of YHV was carried out. During an inhibition of MRLC phosphorylation, shrimp mortality increased especially in high dose of MLCK inhibitor injection. Immunofluorescence detection of YHV in infected shrimp revealed highly increased of infected hemocytes after inhibition. Detection of YHV in infected GC also revealed a significant increase of YHV positive GC cell when shrimp was exposed to 10 mg/kg of ML-7. In addition, Immunofluorescence signal count (CTCF) showed high replication of YHV in infected GC. This investigation, demonstrated that inhibition of MRLC phosphorylation affected hemocyte antiviral response in shrimp.

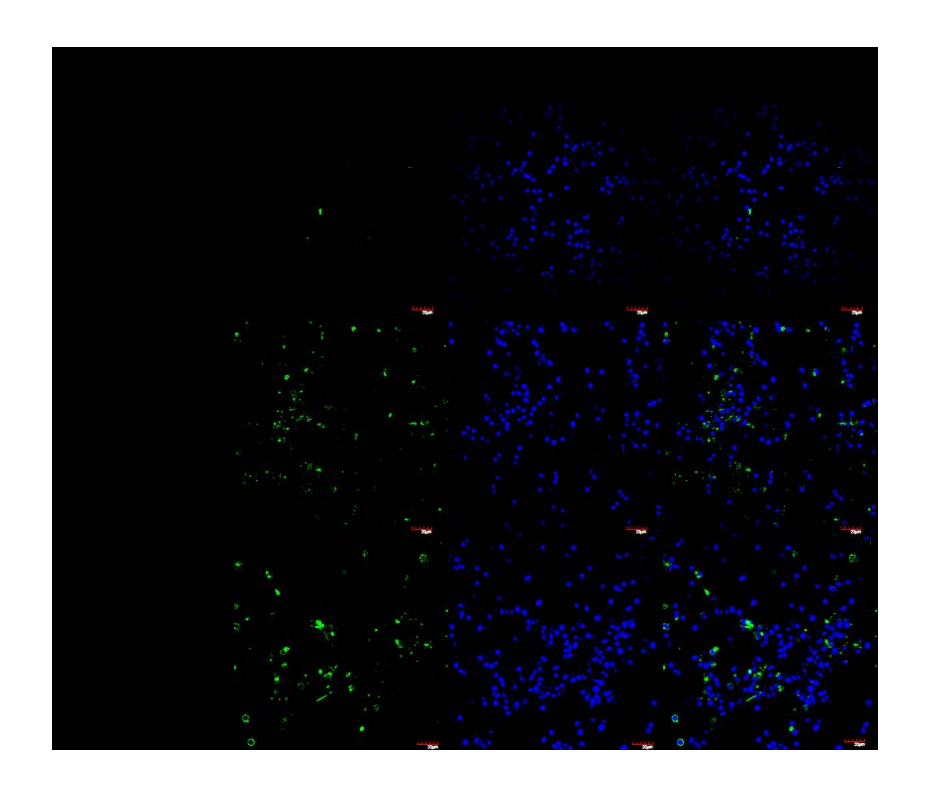


Figure 31. Inhibition of MRLC phosphorylation increased YHV infection in vitro.

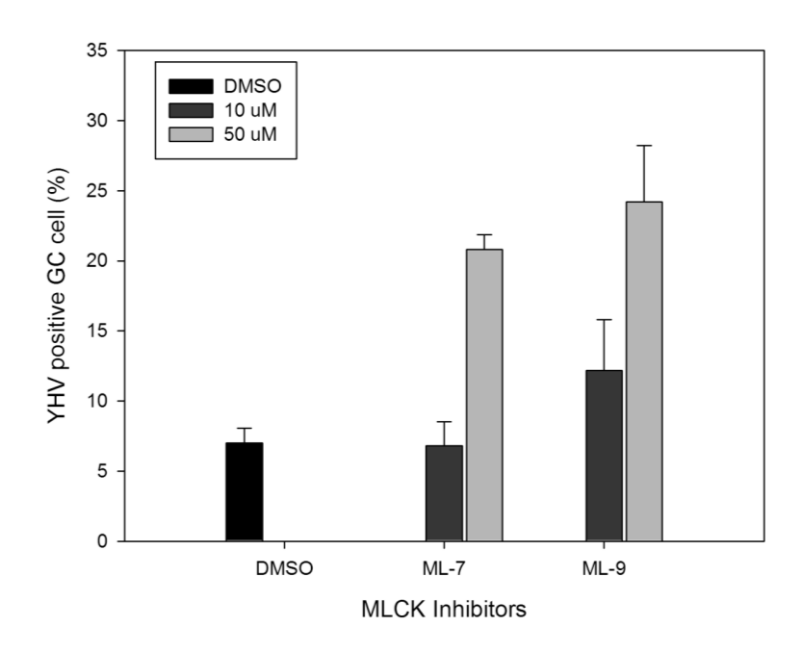


Figure 32. In vitro inhibition of MRLC phosphorylation and YHV infection in GC cell.

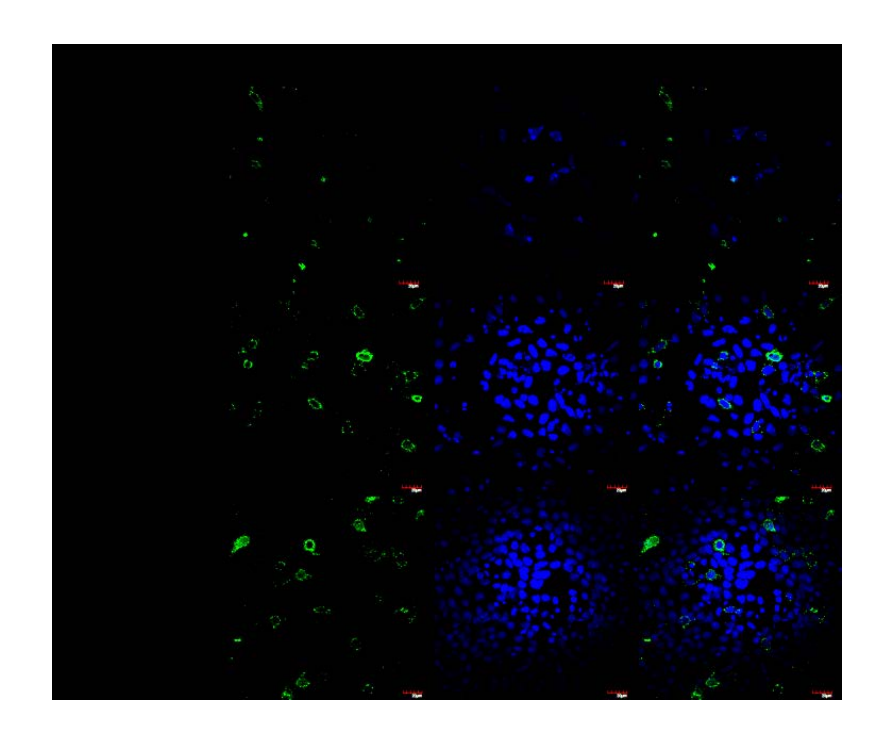


Figure 33. Immunofluorescence detection of YHV infected hemocyte post MRLC. Anti-gp 116 (YHV) was determined by Alexafluor-488 (indicated by green color) and nucleus was stained by DAPI (indicated by blue color). YHV (green signal) in hemocyte was observed at 12 hpi.

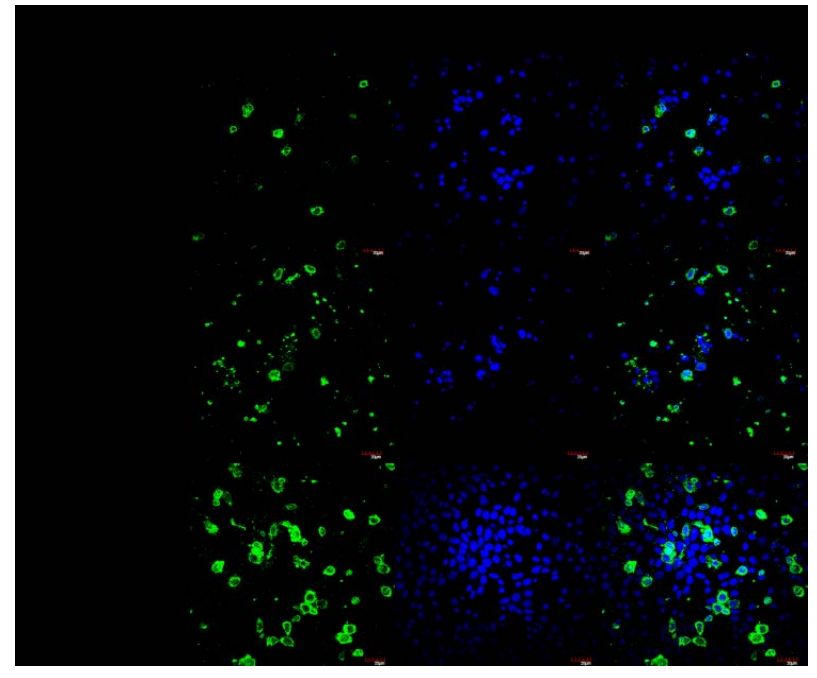


Figure 34. Immunofluorescence detection of YHV infected hemocyte post MRLC phosphorylation inhibition. Anti-gp 116 (YHV) was determined by Alexafluor-488 (indicated by green color) and nucleus was stained by DAPI (indicated by blue color). YHV (green signal) in hemocyte was observed at 24 hpi.

CONCLUDING SUMMARY

- 1. Isolation and characterization of *P. monodon* hemocytes based on their granularity and cell sizes revealed at least three populations of cell types. Percoll gradient centrifugation using 70% continuous gradient solution yielded three separated bands of hemocyte cells. Microscopic and flow cytometric examination confirmed three distinct cell types of hemocytes representing in each isolated bands. These cells are classiflied as hyaline, semigranular, and granular hemocytes.
- 2. Protein expression profiling of each hemocytes revealed cell type specific protein patterns. The granular containing hemocytes (SGC and GC) showed similar protein expression pattern which is different from the non-granular cell. In comparison the granular containing cells showed at least seven predominant expressed proteins as observed by SDS-PAGE and 2-DE. These identified proteins are hemocytes proteins with involving roles in immune responses.
- 3. Analysis of YHV infected hemocytes revealed that SGC and GC are the viral targets. Viral infection in GC was detected since an early period of infection, meanwhile high viral replication level was found in SGC at late phase of infection. In contrast, YHV infection in HC is rarely found. It was suggested that YHV infects only on specific type of hemocyte targets and the interaction may rely on specific receptors.
- 4. Phosphoproteomic analysis of YHV infected hemocytes indicated differential phophorylation of hemocyte proteins in an early state post YHV interaction. 2-DE coupled with multiplex protein detection indicated both phosphorylation and dephosphorylation.
- 5. P. monodon myosin regulatory light chain (PmMRLC) in GC is modulated in its phosphorylation level upon YHV infection. Investigation on the role of PmMRLC indicates an association with hemocyte phagocytosis and regulating of actin

rearrangement. Inhibition of *Pm*MRLC phosphorylation showed a significant decrease of hemocytes phagocytic activity, leading to an increase in YHV replication. The results demonstrated that *Pm*MRLC phosphorylation is essential for an antiviral response of shrimp hemocyte.

- Caspase 3 in GC demonstrated an increased phosphorylation upon YHV infection.
 The role of caspase 3 upon YHV infection is proposed to be associated with PKC kinase activity and shrimp survival.
- 7. During TSV infection on the hemocytes of *P. vannamei*. C-terminal hemocyanin fragments were up-regulated. ERK1/2. Our co-immunoprecipitation results showed that the C-terminus of hemocyanin bound to ERK1/2 and undergoes phosphorylation.
- 8. We have demonstrated that the analysis of proteomics and phosphoproteomics of viral infected hemocytes can reveal the molecular responses of several hemocyte proteins. These proteins have functional roles in defensive pathways that help protect the cells from viral pathogen.

Outputs

Publications from this research project

Taengchaiyaphum S, Havanapan P, Roytrakul S, Lo CF, Sritunyalucksana K, Krittanai C*. (2013) Phosphorylation is required for myosin regulatory light chain (PmMRLC) to control yellow head virus infection in shrimp hemocytes. Fish & Shellfish Immunology. 34(5):1042-9.

Impact Factor (2011) = 3.322

Havanapan, P., Kanlaya, R., Bourchookarn, A., Krittanai, C. and Thongboonkerd, V. (2009) C-terminal hemocyanin from hemocytes of *Penaeus vannamei* interacts with ERK1/2 and undergoes serine phosphorylation. Journal of Proteome Research. 8(5): 2476-83.

Impact Factor (2011): 5.113

Publication resulting from indirect support of this funding

- Somboonna N, Mangkalanan S, Udompetcharaporn A, Krittanai C, Sritunyalucksana K, Flegel T. (2010) Mud crab susceptibility to disease from white spot syndrome virus is species-dependent. BMC Research Notes. 20; 3: 315.
 Impact Factor (2011): -
- 2. Pathaichindachote1 W, Rungrod A, Audtho1 M, Soonsanga S, Krittanai C. and Promdonkoy B.* (2012) Isoleucine at position 150 of Cyt2Aa toxin from *Bacillus thuringiensis* plays an important role during membrane binding and oligomerization. Biochemistry and Molecular Biology Reports. 46(3):175-80.
 Impact Factor (2011): 2.276
- 3. Thammachat S, Pungtanom N, Kidsanguan S, Pathaichindachote W, Promdonkoy B, Krittanai C. (2010) Amino acid substitution on Beta1 and alphaF of Cyt2Aa2 affects molecular interaction of protoxin. Biochemistry and Molecular Biology Reports.

43(6):427-31.

Impact Factor (2011): 2.276

4. Sangcharoen, A., Tepanant, W., Kidsanguan, S., Promdonkoy, B. and Krittanai, C.

(2009) Investigation of the Unfolding Pathway of Bacillus thuringiensis Cyt2Aa2 Toxin

Reveals an Unfolding Intermediate. Journal of Biotechnology. 141(3), 137-41.

Impact Factor (2011): 3.045

Presentations in research conferences

1. Sekson Mangkalanan, Piyachat Sa-nguanrat, Tanatchaporn Utairangsee, Timothy W.

Flegel, Kallaya. Sritunyalucksana, and Chartchai Krittanai. Hemocytic Response in

Persistent WSSV Infection in the Mud Crab, Scylla olivacea. Oral Presentation in

The 12th Congress of the International Society of Developmental and Comparative

Immunology, July 9-13, 2012, Hilton Fukuoka Sea Hawk Hotel, Fukuoka, Japan.

2. Phattara-orn Havanapan, Suparat Taengchaiyaphum, Nuanwan Phungthanom and

Chartchai Krittanai Study of Biotinylated Proteins from Hyaline and Granular

Containing Hemocytes of Penaeus monodon. Poster Presentation in the 6th

International Symposium of the Protein Society of Thailand, August 29-31, 2012,

Chulabhorn Research Institute Convention Center, Bangkok, Thailand.

3. Chartchai Kritanai. *Proteomic Analysis*. Plenary Lecture in International Workshop in

Protein Expression and Purification Strategies (PEP) 2011, October 3-7, 2011, Faculty

of Medicine, Chulalongkorn University, Thailand.

4. Chartchai Krittanai and SuparatTaengchaiyaphum 2-D Blue Native PAGE in Shrimp

Proteomics. The TRF Senior Scholar Conference "Disease Proteomics in Thailand",

August 30, 2011, Chulabhorn Research Institute, Bangkok, Thailand.

s. Seksan Mangkalanan, Nuanwan Pungtanom, Sittiruk Roytrakul, KallayaSritunyalucksana,

Piyachat Sanguanrut and Chartchai Krittanai Response of Mud Crab (Scylla olivacea)

64

Hemocyte to Persistent Infection of Whilte Spot Syndrome Virus. Oral Presentation in the 37th Congress on Science and Technology of Thailand, October 10-12, 2011, Centara Grand at Central World, Bangkok, Thailand.

- Phattara-orn Havanapan, Suparat Taengchaiyaphum, Nuanwan Phungthanom, Sittiruk
 Roytrakul and Chartchai Krittanai *Phosphoproteomic Analysis of Penaeus*monodon Hyaline Hemocytes upon Yellow Head Virus Infection Oral Presentation
 in The 37th Congress on Science and Technology of Thailand, 10-12 October 2011,
 Centara Grand at Central World, Bangkok, Thailand.
- 7. Suparat Taengchaiyaphum, Atchara Paemanee, Nuanwan Pungtanom, Phattara-orn Havanapan, Apinunt Udomkit, Sittiruk Roytrakul, Kallaya Sritunyalucksana and Chartchai Krittanai Phosphoproteomic *Analysis of Penaeus monodon Hemocytes:***The role of Granular Cell in Early State of Yellow Head Virus Infection.** Poster Presentation in the 6th International Symposium of the Protein Society of Thailand.

 *August 31-September 2, 2011, Chulabhorn Research Institute Convention Center, Bangkok, Thailand.
- Suparat Taengchaiyaphum and Chartchai Krittanai. Characterization of
 Phosphorylated Proteins in Viral-Infected Tissues of Peneaus monodon. Oral
 Presentation in RGJ-Ph.D Congress X, April, 3-5 2009. Jomtian Palm Beach, Pattaya,
 Chonburi, Thailand.

3. Training of graduate students

Mr. Suparat Taechaiyaphum (Ph.D. Graduate)

Mr. Sekson Mangkalanan (Ph.D. Graduate)

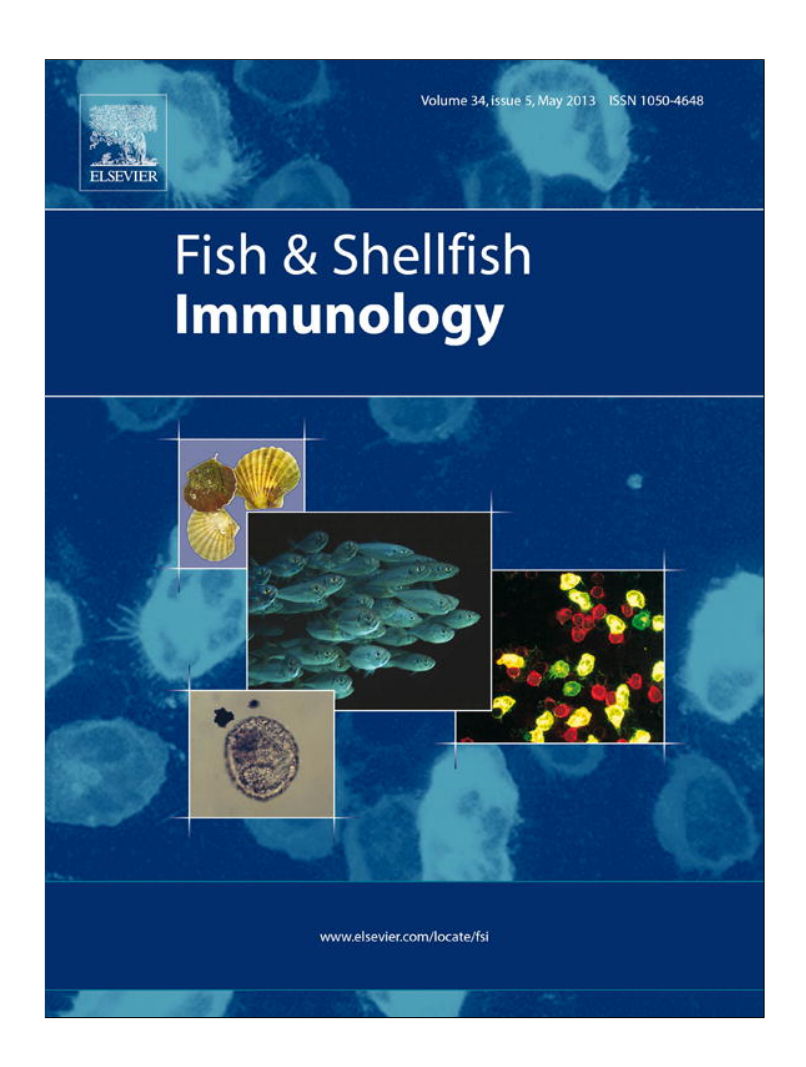
Mrs. Phatta-Orn Havanapan (Ph.D. Graduate)

Mr. Apichai Bourchookarn (Ph.D. Graduate)

ภาคผนวก

Publications & Reprints

Provided for non-commercial research and education use. Not for reproduction, distribution or commercial use.



This article appeared in a journal published by Elsevier. The attached copy is furnished to the author for internal non-commercial research and education use, including for instruction at the authors institution and sharing with colleagues.

Other uses, including reproduction and distribution, or selling or licensing copies, or posting to personal, institutional or third party websites are prohibited.

In most cases authors are permitted to post their version of the article (e.g. in Word or Tex form) to their personal website or institutional repository. Authors requiring further information regarding Elsevier's archiving and manuscript policies are encouraged to visit:

http://www.elsevier.com/authorsrights

Author's personal copy

Fish & Shellfish Immunology 34 (2013) 1042-1049



Contents lists available at SciVerse ScienceDirect

Fish & Shellfish Immunology

journal homepage: www.elsevier.com/locate/fsi



Phosphorylation is required for myosin regulatory light chain (*Pm*MRLC) to control yellow head virus infection in shrimp hemocytes

Suparat Taengchaiyaphum ^a, Phattara-orn Havanapan ^a, Sittiruk Roytrakul ^b, Chu-Fang Lo ^d, Kallaya Sritunyalucksana ^{c,e}, Chartchai Krittanai ^{a,*}

- ^a Institute of Molecular Biosciences, Mahidol University, Salaya Campus, Salaya, Nakhonpathom 73170, Thailand
- ^b Genome Institute, National Center for Genetic Engineering and Biotechnology (BIOTEC), Pathumthani 12120, Thailand
- ^c Center of Excellence for Shrimp Molecular Biology and Biotechnology, Mahidol University, Bangkok 10400, Thailand
- ^d Institute of Zoology, National Taiwan University, Taipei 106, Taiwan, ROC
- e Shrimp-Virus Interaction Laboratory (ASVI), National Center for Genetic Engineering and Biotechnology (BIOTEC), Thailand Science Park, Pathumthani 12120, Thailand

ARTICLE INFO

Article history: Received 10 September 2012 Received in revised form 17 December 2012 Accepted 23 December 2012 Available online 19 January 2013

Keywords:
P. monodon
Granular hemocyte
Yellow head virus
phosphoproteome
Myosin regulatory light chain (MRLC)

ABSTRACT

The cellular signal-transduction process is largely controlled by protein phosphorylation. Shrimp infected with yellow head virus show dramatic changes in their hemocyte phosphoproteomic patterns, and aberrant activation of phosphorylation-based signaling networks has been implicated in a number of diseases. In this study, we focused on phosphorylation of *Penaeus monodon* myosin regulatory light chain (PmMRLC) that is induced at an early hour post YHV infection and is concomitant with cellular actin remodeling. In shrimp cell cultures, this phosphorylation was inhibited by the myosin light chain kinase (MLCK) inhibitors ML-7 and ML-9, suggesting that PmMLC phosphorylation is MLCK pathwaydependent. Blocking PmMRLC phosphorylation resulted in increased replication of YHV and reduction of phagocytic activities of shrimp hemocytes called semigranular cells (SGC) and granular cells (GC). Injection of MLCK inhibitors prior to YHV challenge resulted in dose-dependent elevation in quantity of YHV-positive GC and cytoplasmic YHV protein, coincident with high shrimp mortality. Altogether, we demonstrated that PmMRLC phosphorylation increases after YHV infection in shrimp and that inhibition of the phosphorylation leads to increased YHV replication, reduced hemocyte phagocytic activity (probably through actin remodeling) and subsequent shrimp death. Thus, further studies on the MLCK activation pathway may lead to new strategies in development and implementation of therapy for YHV infections in shrimp.

© 2013 Elsevier Ltd. All rights reserved.

1. Introduction

Yellow head disease is one of the causes of severe shrimp mortality. The causative agent is yellow head virus (YHV), an enveloped virus with a positive-sense, single stranded RNA genome belonging to the genus *Okavirus* (order: Nidovirales and family: *Roniviridae*) [1,2]. The lymphoid organ is a major YHV target. However, other host tissues also susceptible to YHV replication include gills, muscles and hemocytes [3]. In the giant or black tiger

Abbreviations: CHAPS, 3-[(3-cholamidopropyl) dimethylamino]-1-propanesulfonate; DTT, dithiothreitol; NaOAc, sodium acetate; SDS-PAGE, sodium dodecyl sulfate polyacrylamide gel electrophoresis; 2-DE, two dimensional gel electrophoresis; LC-MS/MS, liquid chromatography mass spectrometry; RT-PCR, reverse transcriptase polymerase chain reaction; YHV, yellow head virus; MRLC, myosin regulatory light chain.

shrimp (*Penaeus monodon*), granule-containing hemocytes (i.e., semigranular and granular cells) have been reported to be targets of several viruses including YHV and white spot syndrome virus (WSSV) [4]. Analysis of hemocyte proteins and their posttranslational modifications such as phosphorylation is considered important for identification of disease markers and targets for therapeutic drug design.

In this study, we show that several immune related proteins and cytoskeletal proteins in shrimp hemocytes are significantly changed in both phosphorylation level and expression level upon YHV infection. One of these is myosin regulatory light chain (MRLC) in shrimp granular hemocytes. Its phosphorylation level is significantly increased during the early hours of YHV infection although its total protein level is constantly maintained. MRLC phosphorylation (MRLC-p) regulates many biological functions of the cell including cell motility, membrane structure regulation and cell signaling [5,6]. Suppression of MRLC phosphorylation inhibited influenza A virus replication in host cells, suggesting that MRLC is associated with the

^{*} Corresponding author. Tel.: +66 2 441 9003x1410; fax: +66 2 441 1013. E-mail address: chartchai.kri@mahidol.ac.th (C. Krittanai).

viral propagation cycle in infected cells [7]. In kuruma shrimp, myosin and their light chain has been reported as a WSSV-interacting protein involved in the antiviral defense mechanism of shrimp immune cells. High expression of the myosin light chain subunit was investigated in WSSV resistant shrimp and was strongly related to shrimp antiviral, phagocytosis activity [8]. From our work, *in vitro* and *in vivo* suppression of the *Pm*MRLC phosphorylation by MLCK inhibitors suggested that the MLCK dependent pathway regulated anti-YHV activity in shrimp hemocytes.

2. Materials and methods

2.1. Shrimp preparation

Shrimp of 30–50 g body weight were obtained from the Shrimp Genetic Improvement Center (SGIC, Suratthani, Thailand). Shrimp were maintained in aerated 800 L-tanks containing artificial sea water at 30 ppt for two days. Intermolt shrimp were used for experiments.

2.2. YHV infection and hemocyte isolation

The purified virus preparation was diluted in saline solution (0.45 M NaCl) before intramuscular injection into shrimp (100 µl/20 g shrimp, 5 shrimp/group). The control shrimp were injected with saline solution only. Shrimp hemolymph was collected from the hemocoel (cephalothorax part) using a 21-gauge needle equipped with a 5 ml syringe containing an equal volume of cold modified Alsever's (AS) anticoagulant solution (19.3 mM tri-sodium citrate, 239.8 mM NaCl, 182.5 mM glucose, 6.2 mM EDTA; pH 7.2) [9] and immediately kept on ice. For separation of hemocyte subpopulations, percoll gradient centrifugation was established as previously described by Soderhall and Smith [10]. Briefly, continuous percoll (GE Healthcare) gradient solution (70% percoll, 0.33 M NaCl, pH 7.0, Osmolarity 700 mOsm/kg) was generated by ultracentrifugation (Beckman Optima XL-100) at $50,000 \times g$, 35-42 min and then the hemolymph was loaded onto the preformed percoll gradient and centrifuged at $1700 \times g$, 4 °C for 30 min. The granular hemocytes located in the lowest band in the tube were collected.

2.3. 2-DE and multiplex protein staining

Hemocyte proteins were extracted using the chloroformmethanol-water precipitation method and the protein concentration was measured using Bradford reagent [11]. To perform isoelectric focusing (IEF), a total 300 µg of hemocyte protein was separated on a non-linear IPG strip pH 3–10, 13 cm (GE Healthcare) using the IPGphor II system (GE Healthcare). The IEF step was performed at 20 °C with a continuous increase of voltage (up to 8000 V) to reach 25000 Vh. For the second dimension, the strip was equilibrated with 100 mM DTT containing equilibration buffer (6 M urea, 2% SDS, 30% glycerol, 50 mM Tris-HCl; pH 8.8 and 0.002% bromophenol blue) and subsequently by 250 mM iodoacetamide in the same buffer. Protein on the equilibrated strip was further separated on 12.5% polyacrylamide using an SE600 Ruby electrophoresis system (GE Healthcare) at 120 V until the tracking dye reached to bottom of the gel. For multiplex protein staining, the gel was fixed in fixative solution (50% methanol, 10% acetic acid) overnight prior to sequential protein staining by ProQ Diamond® and Sypro Ruby® fluorescence dye (Molecular Probes, Invitrogen) respectively. Briefly, the fixed gel was stained with ProQ Diamond dye for 1.5 h in the dark and then destained with destaining solution before visualization and image capture using a Typhoon Trio fluorescence scanner (Amersham Biosciences). Subsequently, the gel was re-stained with Sypro Ruby dye overnight in the dark with agitation. The gel was destained with destaining solution (10% methanol, 7% acetic acid) and the image was re-captured. The parameter settings for image capture for both ProQ Diamond and Sypro Ruby were those recommended by the manufacturer. Finally, the gel was stained with Coomassie brilliant blue G solution overnight before destaining with MilliQ until the background was clear.

2.4. Image analysis, in-gel digestion and LC-MS/MS

Differential phosphoproteins and non-phosphorylated proteins were analyzed using Image Master 2D Platinum software version 5.0 (Amersham Biosciences). Three replicate gels were compared between normal and YHV-infected shrimp. Differential phosphoprotein and non-phosphorylated protein profiles were statistically analyzed using Student's t test ($p \le 0.05$). Significantly different phosphoprotein and non-phosphorylated protein spots were excised and subjected to in-gel digestion followed by mass spectrometry. For in-gel tryptic digestion, protein spots were dehydrated with 100% acetronitrile (ACN) and then reduced with 10 mM DTT in 25 mM ammonium bicarbonate (AB). Gel pieces were further alkylated with 100 mM iodoacetamide in 10 mM AB in the dark. After that, protein was digested overnight with sequencinggrade modified trypsin solution (10 ng/µl trypsin containing 50% ACN in 25 mM AB). Digested peptides were extracted by 0.1% formic acid in 50% ACN and the volume was reduced by vacuum. The digested peptides were dissolved in 0.1% formic acid and then subjected to nano-LC coupled with ESI-MS/MS to determine peptide masses and to identify amino acids. A database search for protein identification was performed using the Mascot search engine (http://www.matrixscience.com). Only protein hits with significant ion scores are reported.

2.5. Production of anti-PmMRLC antibody and Western blot analysis

Shrimp PmMRLC was cloned from hemocyte mRNA using primers designed based on the mass spectrometry result (gi|262401075) and expressed in the Escherichia coli system. Total RNA was extracted from hemocytes using Trizol® reagent (Molecular Probe, Invitrogen) and a partial sequence of MRLC was amplified by RT-PCR using a forward primer with a restriction enzyme (Hind III) site (5'-GGG AAG CTT GAA GCC TTC AAT ATG ATT-3') and a reverse primer (XhoI) (5'-GGG CTC GAG GGT AAA CTC CAC ATA GTC-3'). The amplified fragment of PmMRLC (372 bp) was cloned into pET28b (+) vector (Novagen) with a 6× His-tag and expressed in the E. coli system with strain BL21 (RBC Bioscience). Expressed *Pm*MRLC was purified by using Ni-NTA agarose (Qiagen) and eluted under denaturing conditions (50 mM Tris-Cl, 500 mM NaCl, 250 mM imidazole, pH 8.0). The concentration of purified PmMRLC was determined by Bradford's method and analyzed by SDS-PAGE. The amount of 1.8 mg of purified PmMRLC was used to immunize a rabbit. The titer of antiserum was determined by enzyme-linked immunosorbent assay (ELISA).

Phosphorylation of *Pm*MRLC was determined using the western blot method. Total protein extracted from granular cells ($20~\mu g$) was separated by SDS-PAGE, before transfer to a PVDF membrane (GE Healthcare) using a semidry blotting system (Amersham Biosciences). Protein on the PVDF membrane was soaked overnight at 4 °C in blocking solution (5% bovine serum albumin, $1 \times$ TBS, 0.1% tween-20) followed by incubation overnight with 1:1000 antiphospho-MRLC antibody (Cell Signaling). Subsequently the membrane was incubated with HRP-conjugated goat anti-rabbit secondary antibody (Santacruz). Immunoreactive bands were detected using ECL plus the western blot detection system (GE Healthcare). Protein on the PVDF membrane was further used to check total *Pm*MRLC expression level. After phospho-MRLC detection, the membrane was washed with mild stripping solution (1.5% (w/v)

glycine, 0.1% (w/v) SDS, 1% (v/v) Tween-20; pH 2.2) to remove reactive immune complexes. The membrane was blocked again overnight in blocking solution followed by incubation overnight at 4 $^{\circ}$ C with 1:10,000 rabbit anti-shrimp PmMRLC antibody. The immunoreactive band was detected as previously described. The PmMRLC phosphorylation was monitored in five individual shrimp at various times post YHV infection. The intensity was determined by densitometer and relative phosphorylation ratio was calculated.

2.6. Immunoflourescence detection of actin polymerization

To determine the role of actin during YHV infection in GC cells, hemocytes were collected from non-infected or YHV-infected shrimp at 0 h, 2 h and 6 h post infection and maintained in L-15 medium for 1 h. The hemocyte culture was fixed with 10% formaldehyde (10% formaldehyde in 0.45 M NaCl) for 20 min. The fixed cells were permeabilized with 0.1% Triton X-100 (0.1% Triton X-100 in $1\times$ PBS; pH 7.0) and subsequently incubated with blocking solution (10% fetal bovine serum in $1\times$ PBS). Further, hemocytes were incubated with mouse monoclonal anti-actin antibody (Sigma) overnight at 4 °C, followed by extensive washing and incubated with anti-mouse Alexafluor-488 conjugated secondary antibody (Invitrogen). To detect the fluorescence signal, the cells were stained with DAPI containing anti-fade permount (Invitrogen) before scanning by microscopy (Olympus Fluoview 1000).

2.7. Hemocyte phagocytic activity assay

Shrimp hemocytes were separated by percoll gradient centrifugation and maintained on 24-well cell culture plates containing L-15 medium. Three subpopulations of hemocytes were separately collected in the medium supplemented with 10 μM ML-7 or 10 μM ML-9 (Sigma) for 2 h. Shrimp serum-sensitized sheep red blood cells (SRBC) were added and incubated at 28 °C for 1 h. The incubated cell culture was fixed and stained with Rose Bengal and hematoxylin as previously described by Sritunyalucksana et al. [12]. The number of phagocytic cells was determined by light microscopy. A total 100 hemocytes with phagocytic activity against SRBC were examined to determine phagocytic index (i.e., the number of SRBC ingested per number of SRBC ingesting hemocyte). Differences in hemocyte phagocytic activity between normal and inhibitor-treated hemocytes were considered statistically significant when Student's t test gave p < 0.05.

2.8. Inhibition of PmMRLC phosphorylation in primary hemocyte cultures challenged with YHV

PmMRLC phosphorylation in YHV-infected hemocytes was first determined in primary hemocyte cell cultures. Diluted YHV stock was injected to healthy shrimp and then hemolymph was collected 2 h post injection. Subsequently, the hemocytes were cultured in 24-well plates containing L-15 medium supplemented with 10 μ M or 50 μ M of MLCK inhibitors (ML-7 or ML-9, Sigma). For the non-inhibitor-supplemented control group, L-15 medium was added with inhibitor solvent, 2% dimethylsulfoxide (DMSO). Hemocyte cultures were maintained at 28 °C for 24 h. The culture medium was then removed and the hemocytes were fixed with 10% formaldehyde (10% formaldehyde in 0.45 M NaCl) for 20 min. YHV-infected hemocytes were detected by the immunofluorescence technique. Briefly, mouse monoclonal anti-gp116 primary antibody (kindly provided by Dr. Paisarn Sithigorngul, Srinakarinwirot University, Prasanmit) was incubated overnight at 4 °C with fixed hemocytes. The immune complex was

subsequently detected by exposure for 1 h at RT to goat antimouse Alexafluor-546 conjugated secondary antibody (Molecular Probe, Invitrogen). For nucleus detection, the slide was counterstained for 1 h at RT with TO-PRO-3 iodide (Molecular Probe, Invitrogen). To detect fluorescence signals, slides were examined using a Confocal laser scanning microscope (Olympus FluoViewTM FV1000). Three non-overlapping regions were examined for each slide and there was 1 slide each for 5 individual shrimp from each group with a total of 20 cells counted from each slide for the calculation of mean numbers of GC per hundred cells for each group. Differences were considered to be statistically significant when $p \leq 0.05$ by Student's t test).

2.9. In vivo inhibition of PmMRLC phosphorylation and effect on YHV replication

Shrimp were injected intramuscularly with two concentrations of the MRLC phosphorylation inhibitor ML-7 (1 and 10 mg/kg) in a total volume of 50 μ l saline solution (0.45 M NaCl) into shrimp with a fresh weight of 20 g. The control group consisted of shrimp injected with saline solution only. Each group consisted of 3 replicates of 10 shrimp each. At 2 h post inhibitor injection, 100 µl YHV virus stock at 1:100 dilution was injected into each shrimp. Thereafter, shrimp mortality was recorded at 12, 18 and 36 hpi. The toxicity of the inhibitor was also monitored in shrimp. The cumulative percent mortality was compared by Student's t test and differences were considered to be statistically significant at $p \le 0.05$). To investigate YHV infection and level of replication in hemocytes, hemolymph collected arbitrarily from five individual shrimp in each group at 12 and 24 hpi were subjected to YHV detection by immunofluorescence assay using a primary antibody against the YHV envelope protein gp-116 [13] and YHV infection levels were determined by analysis of relative fluorescence intensities. Calculation of corrected total cell fluorescence (CTCF) was achieved by Image J analysis software [14].

3. Results

3.1. Shrimp MRLC is phosphorylated after YHV infection

When the phosphoproteomic pattern of infected hemocytes was examined to evaluate the shrimp response to YHV infection, it was found that protein phosphorylation changed as early as 30 min-2 h after virus injection (data not shown). Our previous study revealed that the target hemocyte subpopulation for YHV infection was granule-containing cells. In this study, phosphoproteomic analysis of YHV-infected granular (GC) at 1 h post YHV injection was achieved by high resolution protein separation (2-DE). The results of multiplex protein detection (phosphoprotein and total protein expression) are shown in Fig. 1A. A number of protein spots with significant changes in both phosphorylation level and expression level were found. Data on identification of some of these spots by mass spectrometry is shown in Table 1. Differences in phosphorylated proteins and non-phosphorylated proteins during YHV infection could be classified into three major groups including immune related and stress induced proteins, proteins associated with metabolic processes and cytoskeletal proteins. However, almost all of the phosphoproteins in YHVtargeted hemocytes were unknown (indicated by dash-circles). One exception was myosin regulatory light chain (MRLC) where the 2-DE gel showed an increase in the phosphorylated form, even though the level of protein expression remained constant [Fig. 1B].

P. monodon MRLC cDNA was cloned and referred as *Pm*MRLC. An MRLC alignment carried out to compare deduced amino acid

S. Taengchaiyaphum et al. / Fish & Shellfish Immunology 34 (2013) 1042-1049

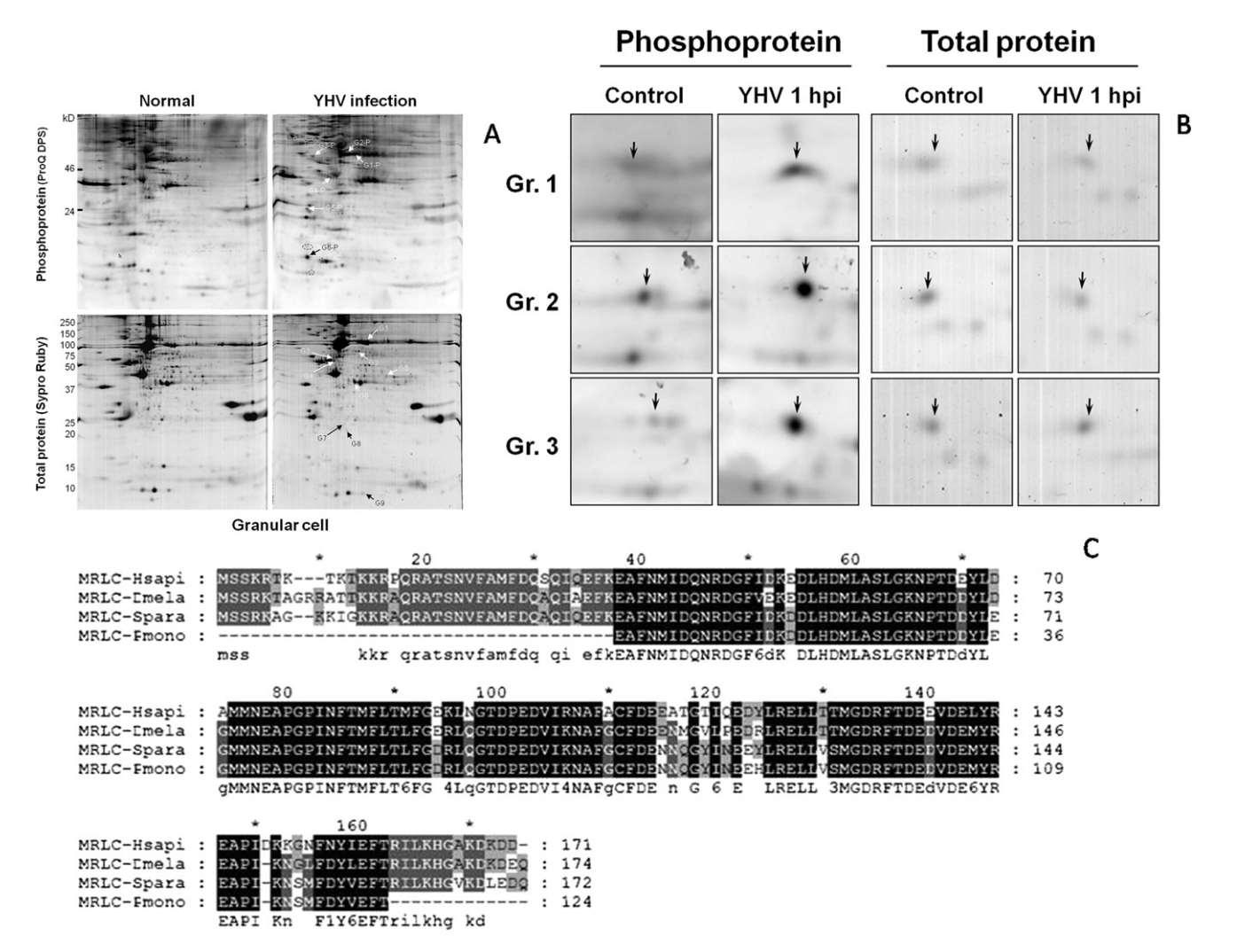


Fig. 1. (A) 2-D electrophoresis profiling of GC phosphorylated proteins (ProQ DPS stained, upper panel) and total proteins (Sypro Ruby stained, lower panel) at 1 h post YHV injection. Differences in phosphorylated and non-phosphorylated proteins are indicated by arrows. (B) Zoom-in on phosphorylated MRLC protein spots and total protein spots from GC of YHV-infected and normal shrimp. (C) Amino acid sequence alignment of MRLC from humans, the fruit fly, crabs and black tiger shrimp showing highly conserved amino acids by grey and black outlines.

sequences among shrimp (*P. monodon*), a crab (*Scylla paramamosain*), the fruit fly (*Drosophila melanogaster*) and humans (*Homo sapiens*) indicated that MRLC is highly conserved evolutionarily in both amino acid sequence and phosphorylation site (QRATpSNVFA) among eukaryotes [Fig. 1C].

3.2. YHV activates MRLC phosphorylation and cellular actin remodeling

Confirmation of *Pm*MRLC phosphorylation using antiphosphoserine (Ser-19) antibody successfully detected the corresponding shrimp protein by Western blot analysis. Time-course analysis of MRLC phosphorylation in GC confirmed that induction of MRLC phosphorylation occurred from 1 h up to 6 h post YHV infection and then returned to the normal level from 12 h post infection onwards. During this interval, constant expression of MRLC protein was observed [Fig. 2, left panel]. These results suggested that YHV infection induced MRLC phosphorylation early after YHV injection. Using immunofluorescence to determine MRLC phosphorylation associated with actin function in GC of YHV-infected shrimp, it was found that activation of MRLC phosphorylation in YHV-infected GC was strongly associated with actin

polymerization [Fig. 2, right panel]. Rearrangement of filamentous actin was observed within 6 h post YHV injection and this corresponded with the MRLC phosphorylation level. The results indicated that YHV infection led to actin reformation through induction of MRLC phosphorylation.

3.3. PmMRLC phosphorylation is associated with hemocyte phagocytic activity

To determine the role of phosphorylated PmMRLC in hemocyte defense activity and especially in phagocytosis, two specific MLCK inhibitors (ML-9 and ML-7) were used. For both, the optimal concentration of 10 μ M resulted in significant reduction in PmMRLC phosphorylation within 2 h after hemocyte exposure [Fig. 3]. With respect to the role of PmMRLC phosphorylation in hemocyte phagocytic activity, phagocytosis activity against SRBC of shrimp hemocytes [Fig. 4, left panel] revealed that normally high phagocytic indices of GC and SGC were dramatically reduced by inhibition of PmMRLC phosphorylation [Fig. 4, right panel]. The results indicated that PmMRLC phosphorylation is linked to phagocytic activity of shrimp hemocytes.

Table 1List of differentially phosphorylated proteins in YHV-infected granular hemocytes at 1 h post challenge.

Spot no.	Protein [organism]	Acc. no.	Observed MW (kDa)/pI	YHV/control	Biological function
Phosphop	rotein				
G1-P	LV_HP_RA13G17r Litopenaeus vannamei hepatopancreas cDNA library [Litopenaeus vannamei]	FE129934	18.1/9.34	4.09	-
G2-P	similar to prophenoloxidase-activating enzyme 2 [Penaeus monodon]	GW996495	25.9/5.53	1.55	Prophenoloxidase activity
G3-P	protein disulfide isomerase [Litopenaeus vannamei]	gi 225382096	55.8/4.64	0.67 ^a	Cell redox homeostasis
G4-P	LV_ES_RA14F10r Litopenaeus vannamei eyestalk cDNA library [Litopenaeus vannamei]	FE051092	24.9/9.21	3.73	_
G5-P	14-3-3-like protein [Penaeus monodon]	gi 66774602	28.2/4.61	2.05	Protein binding/Apoptosis
G6-P	Putative myosin regulatory light chain 2 smooth muscle [Scylla paramamosain]	gi 262401075	19.8/4.55	2.05	Cell motility, phagocytosis
Non-phos	phoprotein				
G1	Hemocyanin [Penaeus monodon]	gi 16612121	51.1/5.10	1.73	Oxygen transport, antimicrobial activity
G2	PmTwN02G02.scf similar to hemocyanin [Litopenaeus vannamei]	G0074804	19.0/4.90	0.22	_
G3	Tubulin alpha chain [Penaeus monodon]	gi 47498000	50.9/4.99	0.46	Microtubule-based movement
G4	Tubulin beta-I chain [Homarus americanus]	gi 3915087	52.3/4.88	0.34	Microtubule-based movement
G5	LV_HC_RA032102r Litopenaeus vannamei hemocyte cDNA library [Litopenaeus vannamei]	FE099864	30.5/7.63	0.59	_
G6	allergen Pen m 2 [Penaeus monodon]	gi 27463265	40.3/6.05	0.5	ATP/protein binding
G7	Peroxiredoxin-6 [Lepeophtheirus salmonis]	gi 225712978	24.6/5.44	0.58	Lipid degradation
G8	similar to Crustacean calcium-binding protein 23 (CCBP-23 protein) [Orconectes limosus]	G0079665	17.3/6.93	0.65	Calcium ion binding
G9	ED_501 <i>P. monodon</i> SSH hemocyte library <i>Penaeus monodon</i> cDNA clone P2029	EG026283	26.0/9.0	0.47	_

^a The intensity value was observed only in YHV-infected hemocyte. Identified protein table was not included unknown or unidentified proteins.

3.4. Blocking PmMRLC phosphorylation enhances YHV replication in cell cultures

Addition of *Pm*MRLC phosphorylation inhibitors to shrimp cell cultures prior to YHV challenge resulted in significantly higher replication of YHV than in cultures without the inhibitors [Fig. 5, left panel]. In addition, the inhibitory effect of both inhibitors was shown to be dose-dependent [Fig. 5, right panel].

3.5. Blocking of PmMRLC phosphorylation in vivo increases YHV replication and numbers of YHV-positive GC

Shrimp injected with *Pm*MRLC phosphorylation inhibitors prior to virus injection showed higher YHV levels than control shrimp by YHV-positive immunofluorescence intensity of GC [Fig. 6A]. Specifically, corrected total cell fluorescence (CTCF) showed higher levels of YHV in GC when *Pm*MRLC phosphorylation was blocked at

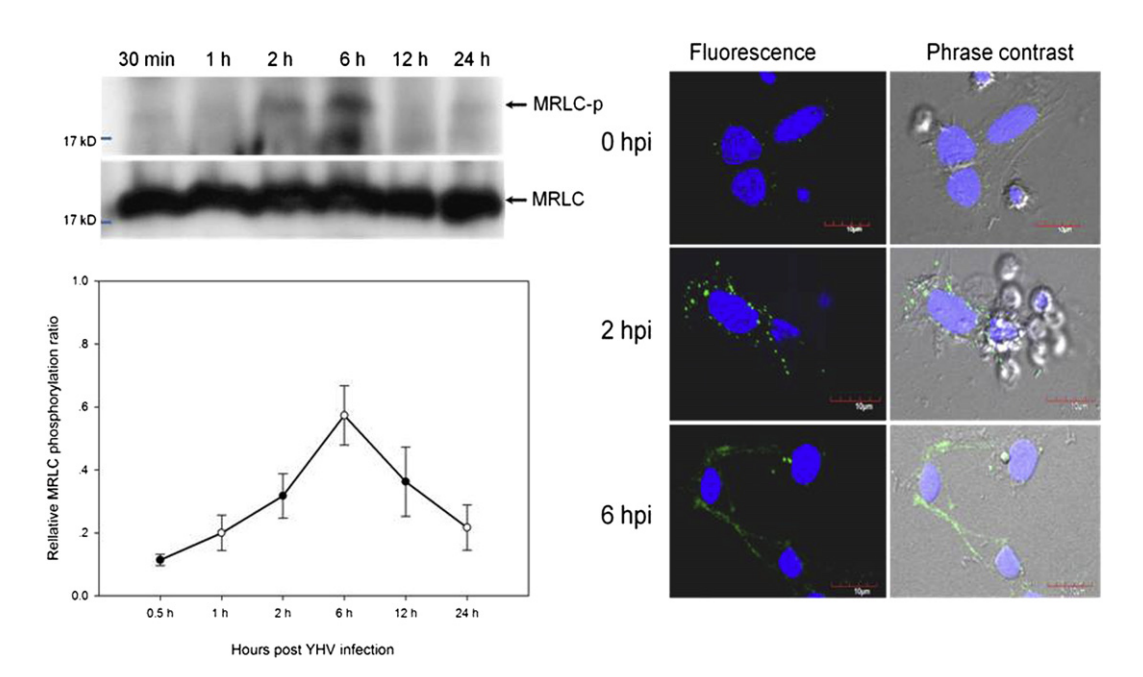


Fig. 2. Time-course analysis for phosphorylated MRLC after GC exposure to YHV. The left panel shows by western blot detection and by measurement of total MRLC expression that the relative level of PmMRLC phosphorylation in GC increased during the early phase of YHV infection (n=5). In the right panel, analysis of hemocyte actin rearrangement by immunofluorescence (green) reveals reformation of globular actin and more polymerization corresponding to an increase in MRLC phosphorylation level. [For interpretation of color referred in this figure legend, the reader is referred to web version of the article.]

S. Taengchaiyaphum et al. / Fish & Shellfish Immunology 34 (2013) 1042–1049

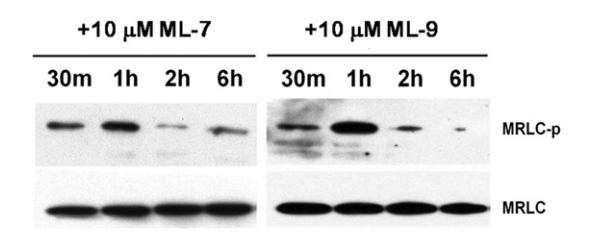


Fig. 3. Effect of MLCK inhibitors on PmMRLC phosphorylation in GC. PmMRLC phosphorylation decreased from 2 h to 6 h post exposure in MLCK inhibitor-treated GC compared with non-treated GC.

10 mg/kg (44 μ M) of ML-7 when compared to shrimp injected with saline (p < 0.001) at both 12 hpi and 24 hpi (p < 0.01). These results indicated that phosphorylation was an essential process in limiting YHV levels in target hemocytes.

3.6. Blocking of MRLC phosphorylation in YHV-infected shrimp results in high mortality

Higher levels of YHV replication and higher numbers of infected GC corresponded with higher cumulative mortality in the ML-7

injected group when compared to the saline-injected control group at both 18 hpi (p < 0.05) and 24 hpi (p < 0.05) [Fig. 7].

4. Discussion

In both vertebrates and invertebrates, phosphorylation is one of the most important posttranslational modifications (PTM) associated with many biological processes including signal-transduction, metabolic pathways, cell cycle regulation and immune response pathways [15–17]. For example, the shrimp STAT protein and hemocyanin responses to viral infection are regulated by phosphorylation processes [18,19].

Here we have shown by phosphoproteomic profiling of GC that YHV induces protein phosphorylation early after infection and that one of the most significantly affected proteins in GC is the cytoskeletal protein *PmMRLC* (within 1 hpi). In other organisms, MRLCs have been reported to be involved in regulation of myosin and actin function [6]. Myosin light chain kinase (MLCK) and myosin light chain phosphatase are two major enzymes regulating MRLC phosphorylation [5,6]. Characterization of MRLC function during influenza A virus (IAV) infection indicated that induction of MRLC phosphorylation enhanced IAV proliferation in cell cultures [7]. A previous study on polymorphonuclear leukocyte (PMNL)

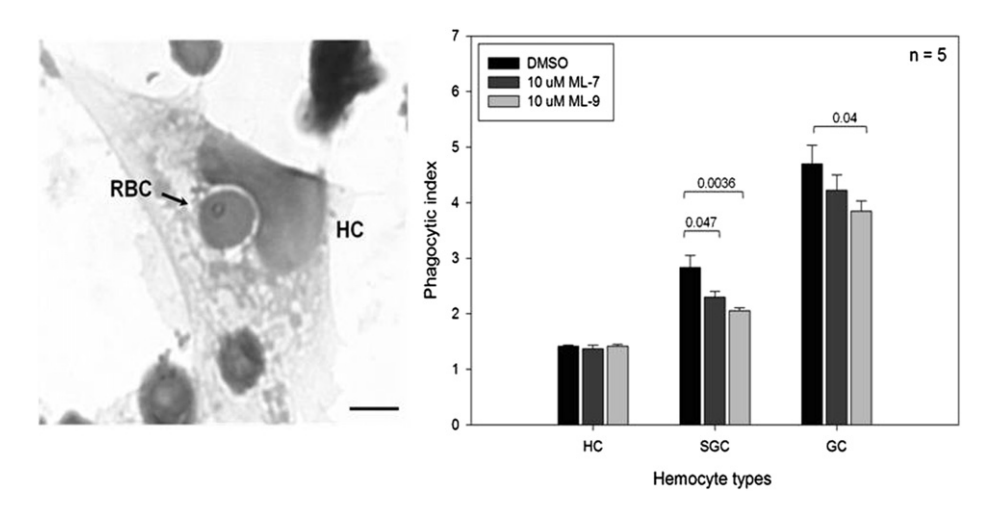


Fig. 4. Effect of MLCK inhibitors on hemocyte phagocytic activity. Hemocyte phagocytic activity for sheep red blood cells (left panel) was significantly reduced (right panel) for both heomcyte types (*p* values given in brackets above the bars).

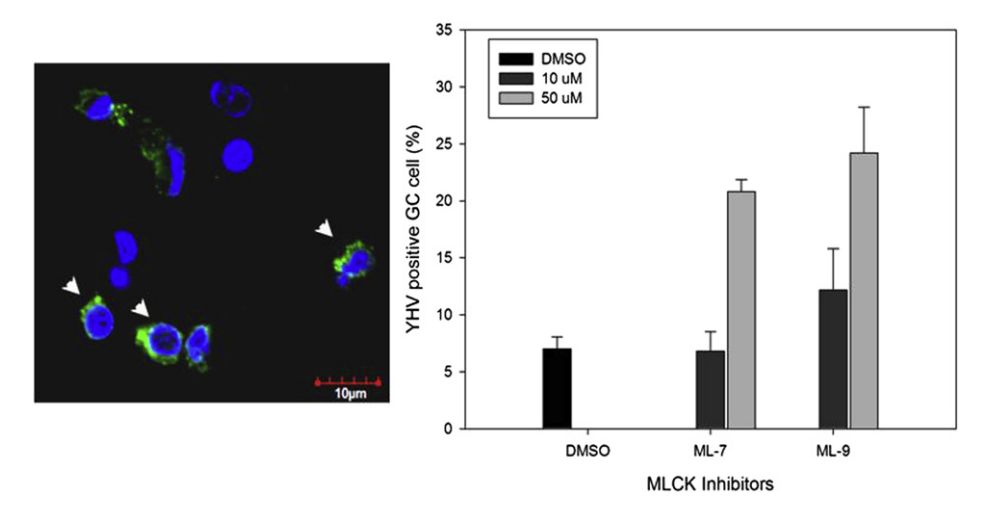


Fig. 5. Effect of two MLCK inhibitors on YHV replication in hemocyte cultures. At 24 h post exposure to both inhibitors, YHV-positive GC (left panel, green immunofluorescence) increased in percentage (right panel). [For interpretation of color referred in this figure legend, the reader is referred to web version of the article.]

S. Taengchaiyaphum et al. / Fish & Shellfish Immunology 34 (2013) 1042-1049

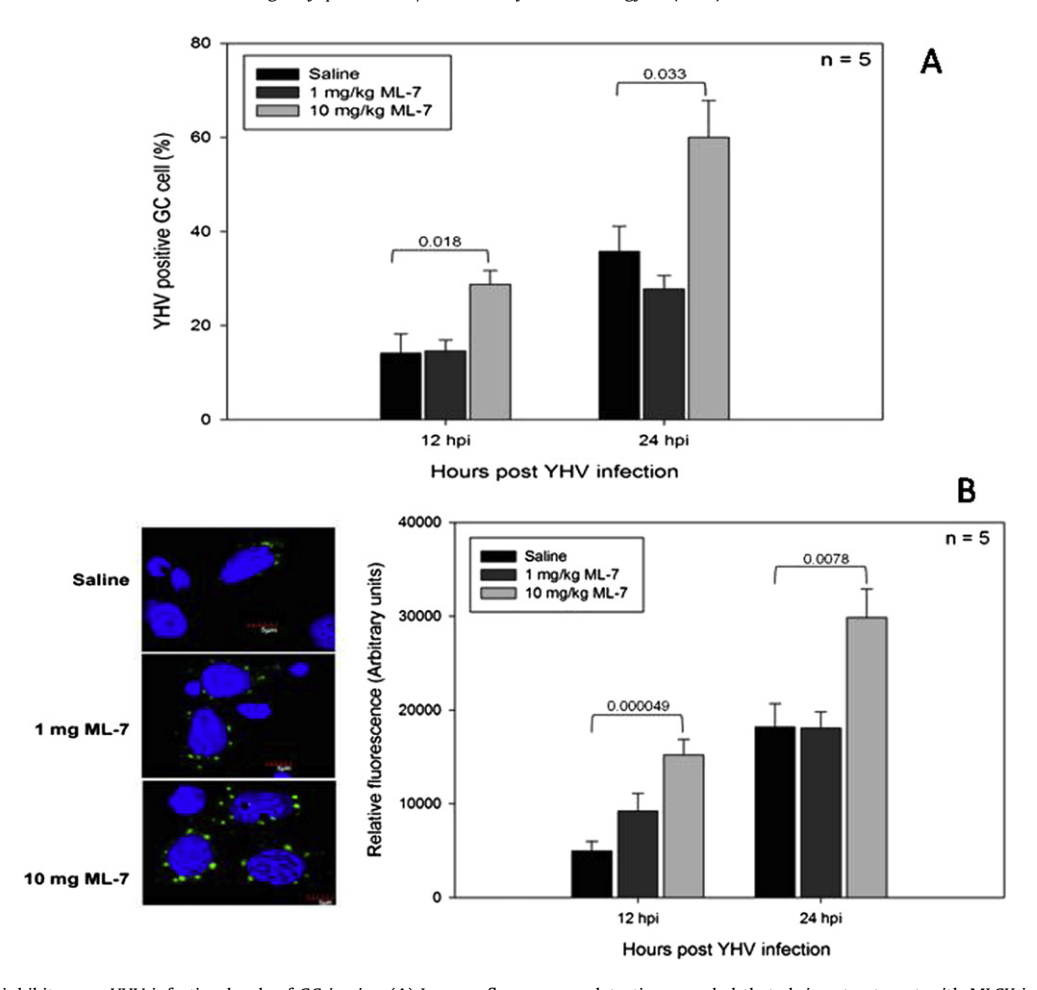


Fig. 6. Effect of MLCK inhibitors on YHV infection levels of GC *in vivo*. (A) Immunofluorescence detection revealed that shrimp treatment with MLCK inhibitors increased the percentage of YHV immunopositive GC (infected cells) when compared to untreated shrimp. (B) Determination of YHV replication level in GC by relative fluorescence intensity indicated higher levels of YHV replication in shrimp treated with MLCK inhibitors when compared to untreated shrimp.

phagocytosis also showed that MRLC phosphorylation played a crucial role for phagocytic activity [20]. Myosin X is associated with phagosome formation that is related to the process of ingestion completion [21]. Altogether, this information suggested that

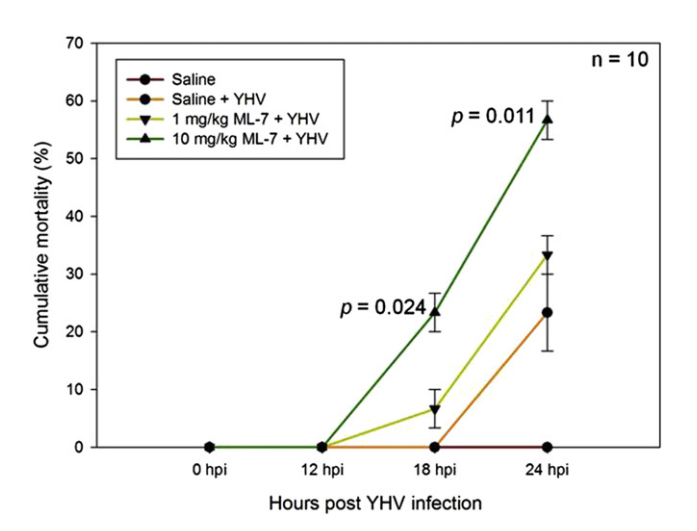


Fig. 7. Comparison of cumulative mortality after challenge with YHV in shrimp treated or not with MRLC inhibitors. The mortality was higher in shrimp treated with 10 mg/kg ML-7 inhibitor than in untreated control shrimp at 18 and 24 h post challenge (p values indicated) (n=10 shrimps in each of 3 replicates from the test and control groups).

activation of MRLC function through phosphorylation might be linked to the host defense mechanism against viral pathogens.

A role for myosin light chain and its partner (myosin) in the hemocyte antiviral defense mechanism has been demonstrated by involvement in regulation of phagocytosis in the kuruma shrimp, *Penaeus* (*Marsupenaeus*) *japonicus* [8,22]. Similarly, our experiments with *P. monodon* have shown that YHV activates *PmMRLC* phosphorylation that is concomitant with cellular actin remodeling to favor the phagocytic process [8,21,22]. These results suggest that phagocytosis may be part of the host anti-YHV mechanism.

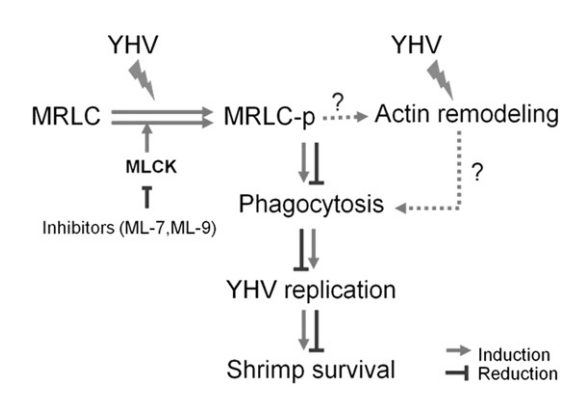


Fig. 8. A diagram of the proposed hemocyte defense mechanism against YHV with respect to *PmMRLC* association. It is proposed that *PmMRLC* activation by YHV results in hemocyte antiviral phagocytosis via regulation of cytoskeletal proteins.

Other studies have also shown that activation of host cell cytoskeletal proteins is essential for viral replication in cells [23]. MRLC phosphorylation leads to myosin activation and influences the function of actin. Actin may affect viral infection in both negative and positive ways. During invasion a virus may use the host cytoskeleton for assistance in intracellular movement and transportation. For example, MRLC function and actin remodeling may be related to the receptor-mediated endocytosis process that has been proposed as the main route for YHV entry and vesicle movement or translocation in host cells [24]. However, in the case of YHV-infected shrimp, we postulate that activation of the cytoskeleton (i.e. MRLC and actin) results in an antiviral defense mechanism to counter hemocyte infection. This proposal was supported by both in vitro and in vivo experiments showing that inhibition of PmMRLC phosphorylation by MLCK inhibitors resulted in higher YHV replication in hemocytes and higher shrimp mortality (see diagram in Fig. 8).

In summary, we demonstrated that hemocyte MRLC is highly phosphorylated in GC exposed to YHV. Inhibition of MRLC phosphorylation resulted in a significant reduction in hemocyte phagocytic activity with enhancement in shrimp mortality and YHV multiplication in GC. Therefore, we hypothesized that activation of MRLC phosphorylation by YHV may enhance hemocyte antiviral phagocytosis that has been suggested to be a major process for antivirus defense in shrimp.

Acknowledgements

This work was supported by the Royal Golden Jubilee Ph.D. program (RGJ-Ph.D to S. Taengchaiyaphum), the Thailand Research Fund (TRF-DBG51) and the National Research University (NRU-MU) grants to C. Krittanai. We thank Mrs. Somjai Wongtripop at Shrimp Genetic Improvement Center, (SGIC, BIOTEC) for shrimp supply. We also deeply thank Miss Atchara Paemanee (Genome Institute, BIOTEC) and Mrs. Nuanwan Pungtanom for technical support, and Professor T.W. Flegel for assistance in editing the manuscript.

References

- Cowley JA, Dimmock CM, Spann KM, Walker PJ. Gill-associated virus of Penaeus monodon prawns: an invertebrate virus with ORF1a and ORF1b genes related to arteri- and coronaviruses. Gen Virol 2000;81:1473–84.
- [2] Sittidilokratna N, Dangtip S, Cowley JA, Walker PJ. RNA transcription analysis and completion of the genome sequence of yellow head nidovirus. Virus Res 2008;136:157–65.
- [3] Lu YTL, Loh PC, Brock JA, Gose RB. Distribution of yellow-head virus in selected tissues and organs of penaeid shrimp *Penaeus vannamei*. Dis Aquat Organ 1995;23:67–70.

- [4] Wang YT, Liu W, Seah JN, Lam CS, Xiang JH, Korzh V, et al. White spot syndrome virus (WSSV) infects specific hemocytes of the shrimp *Penaeus merguiensis*. Dis Aquat Organ 2002;52:249–59.
- [5] Smith RC, Cande WZ, Craig R, Tooth PJ, Scholey JM, Kendrick-Jones J. Regulation of myosin filament assembly by light-chain phosphorylation. Philos Trans R Soc Lond B Biol Sci 1983:302:73—82.
- [6] Tan JL, Ravid S, Spudich JA. Control of nonmuscle myosins by phosphorylation. Annu Rev Biochem 1992;61:721–59.
- [7] Haidari M, Zhang W, Ganjehei L, Ali M, Chen Z. Inhibition of MLC phosphorylation restricts replication of influenza virus — a mechanism of action for anti-influenza agents. PLoS One 2011;6:e21444.
- [8] Han F, Wang Z, Wang X. Characterization of myosin light chain in shrimp hemocytic phagocytosis. Fish Shellfish Immunol 2010;29:875–83.
- [9] van de Braak CB, Botterblom MH, Liu W, Taverne N, van der Knaap WP, Rombout JH. The role of the haematopoietic tissue in haemocyte production and maturation in the black tiger shrimp (*Penaeus monodon*). Fish Shellfish Immunol 2002;12:253–72.
- [10] Soderhall K, Smith VJ. Separation of hemocyte populations of Carcinus maenas and other marine decapods, and prophenoloxidase distribution. Dev Comp Immunol 1983;7:229–39.
- [11] Bradford MM. A rapid and sensitive method for the quantitation of microgram quantities of protein utilizing the principle of protein-dye binding. Anal Biochem 1976:7:248–54.
- [12] Sritunyalucksana K, Gangnonngiw W, Archakunakorn S, Fegan D, Flegel TW. Bacterial clearance rate and a new differential hemocyte staining method to assess immunostimulant activity in shrimp. Dis Aquat Organ 2005;63:89–94.
- [13] Sithigorngul P, Chauychuwong P, Sithigorngul W, Longyant S, Chaivisuthangkura P, Menasveta P. Development of a monoclonal antibody specific to yellow head virus (YHV) from *Penaeus monodon*. Dis Aquat Organ 2000;42:27–34.
- [14] Burgess A, Vigneron S, Brioudes E, Labbe JC, Lorca T, Castro A. Loss of human Greatwall results in G2 arrest and multiple mitotic defects due to deregulation of the cyclin B-Cdc2/PP2A balance. Proc Natl Acad Sci U S A 2010;107:12564–9.
- [15] de Graauw M, Hensbergen P, van de Water B. Phospho-proteomic analysis of cellular signaling. Electrophoresis 2006;27:2676–86.
- [16] Tan CS, Bodenmiller B, Pasculescu A, Jovanovic M, Hengartner MO, Jorgensen C, et al. Comparative analysis reveals conserved protein phosphorylation networks implicated in multiple diseases. Sci Signal 2009;2:ra39.
- [17] Seth RB, Sun L, Chen ZJ. Antiviral innate immunity pathways. Cell Res 2006; 16:141–7.
- [18] Chen WY, Ho KC, Leu JH, Liu KF, Wang HC, Kou GH, et al. WSSV infection activates STAT in shrimp. Dev Comp Immunol 2008;32:1142–50.
- [19] Havanapan PO, Kanlaya R, Bourchookarn A, Krittanai C, Thongboonkerd V. C-terminal hemocyanin from hemocytes of *Penaeus vannamei* interacts with ERK1/2 and undergoes serine phosphorylation. J Proteome Res 2009;8: 2476–83.
- [20] Mansfield PJ, Shayman JA, Boxer LA. Regulation of polymorphonuclear leukocyte phagocytosis by myosin light chain kinase after activation of mitogenactivated protein kinase. Blood 2000;95:2407–12.
- [21] Flannagan RS, Jaumouillé V, Grinstein S. The cell biology of phagocytosis. Annu Rev Pathol Mech Dis 2012;7:61–98.
- [22] Wu W, Zong R, Xu J, Zhang X. Antiviral phagocytosis is regulated by a novel Rab-dependent complex in shrimp *Penaeus japonicus*. J Proteome Res 2008;7: 424–31.
- [23] Dohner K, Sodeik B. The role of the cytoskeleton during viral infection. Curr Top Microbiol Immunol 2005;285:67–108.
- [24] Ongvarrasopone C, Chanasakulniyom M, Sritunyalucksana K, Panyim S. Suppression of PmRab7 by dsRNA inhibits WSSV or YHV infection in shrimp. Marine Biotechnol (New York, NY) 2008;10:374–81.



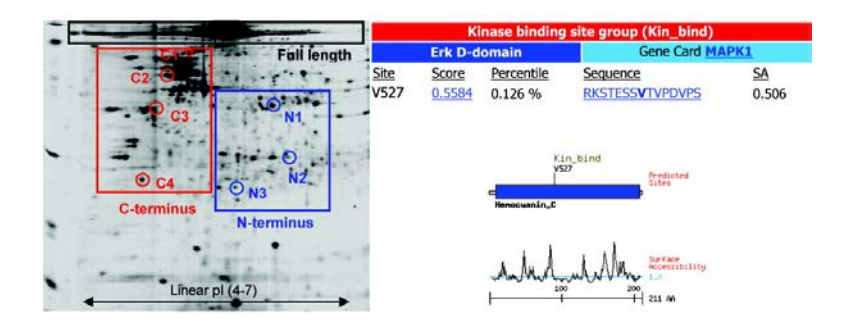
Article

C-Terminal Hemocyanin from Hemocytes of *Penaeus vannamei* Interacts with ERK1/2 and Undergoes Serine Phosphorylation

Phattara-orn Havanapan, Rattiyaporn Kanlaya, Apichai Bourchookarn, Chartchai Krittanai, and Visith Thongboonkerd

J. Proteome Res., Article ASAP • DOI: 10.1021/pr801067e • Publication Date (Web): 13 March 2009

Downloaded from http://pubs.acs.org on April 8, 2009



More About This Article

Additional resources and features associated with this article are available within the HTML version:

- Supporting Information
- Access to high resolution figures
- Links to articles and content related to this article
- Copyright permission to reproduce figures and/or text from this article

View the Full Text HTML



C-Terminal Hemocyanin from Hemocytes of *Penaeus vannamei* Interacts with ERK1/2 and Undergoes Serine Phosphorylation

Phattara-orn Havanapan,^{†,‡} Rattiyaporn Kanlaya,[†] Apichai Bourchookarn,[‡] Chartchai Krittanai,[‡] and Visith Thongboonkerd*,[†]

Medical Proteomics Unit, Office for Research and Development, Faculty of Medicine Siriraj Hospital, Mahidol University, Bangkok, Thailand, and Institute of Molecular Biology and Genetics, Mahidol University, Salaya Campus, Nakhonpathom, Thailand

Received December 13, 2008

To understand molecular immune response of *Penaeus vannamei* during Taura syndrome virus (TSV) infection, expression and functional proteomics studies were performed on hemocyanin, which is a major abundant protein in shrimp hemocytes. Two-dimensional electrophoresis (2-DE) revealed upregulation of several C-terminal fragments of hemocyanin, whereas the N-terminal fragments were down-regulated during TSV infection. 2-D Western blot analysis showed that the C-terminal hemocyanin fragments had more acidic isoelectric points (p/l), whereas the N-terminal fragments had less acidic p/l. Further analysis by NetPhos showed a greater number of serine phosphorylation sites in the C-terminal hemocyanin. Additionally, motif scan using Scansite revealed ERK D-domain, which is required for activation of ERK1/2 effector kinase, as a kinase-binding site at the 527th valine in the C-terminal hemocyanin, whereas neither motif nor functional domain was found in the N-terminus. Co-immunoprecipitation confirmed the interaction between the C-terminal hemocyanin and ERK1/2. 1-D Western blot analysis showed that ERK1/2 was also up-regulated during TSV infection. Our findings demonstrate for the first time that ERK1/2 signaling pathway may play an important role in molecular immune response of *P. vannamei* upon TSV infection through its interaction with the C-terminal hemocyanin.

Keywords: ERK • Hemocyanin • Hemocytes • Host response • Phosphorylation • Proteome • Proteomics

Introduction

Taura syndrome virus (TSV) is an important pathogen in penaeid shrimps. It causes serious morbidity in the infected shrimps with a mortality rate of up to 95% in *P. vannamei*.¹ Shrimp epithelial cells are normally the virus target as viral particles can replicate and accumulate in the cytoplasm of the infected epithelial cells. Electron micrograph of purified TSV illustrates a nonenveloped virion with icosahedral shape and size of approximately 31-32 nm in diameter. 2 TSV has recently been classified into a new genus, namely, "Cricket paralysislike viruses" based on its nucleotide sequences.3 The viral genome contains a positive single-stranded RNA of approximately 10 kb with two distinct open reading frames (ORFs). ORF1 and ORF2 encode for nonstructural and structural proteins, respectively. Separation of TSV structural proteins by SDS-PAGE shows three major bands with molecular masses of 24, 40, and 55 kDa, and one minor band at 58 kDa.³

Recently, an immune response has been demonstrated in shrimp as an antiviral defense mechanism.⁴ However, molecular mechanisms underlying crustacean immune response remains unknown. Hence, elucidation of such molecular mechanisms in the TSV-infected shrimps would be beneficial for prevention of TSV infection and/or reduction of its high mortality rate. One of the potential targets involved in crustacean immunity is hemocyanin,⁵ which is the most abundant protein (~95%) in hemolymph and hemocytes of shrimp that are comparable to blood and blood cells, respectively, in mammals. 6-9 Hemocyanin is a copper-containing protein that plays a major role as an oxygen transporter in crustacean and other arthropods. 10 Its function therefore simulates that of mammalian hemoglobin.11 Extensive characterizations of hemocyanin have demonstrated its other significant roles in defense mechanisms via phenoloxidase activity12-14 and antimicrobial activity through its C-terminal peptide.^{5,12} Additionally, hemocyanin isolated from shrimp hemolymphs has recently been demonstrated to have antiviral activity against a fish virus¹⁵ and also a shrimp virus.¹⁶

Recently, our group performed a preliminary study to evaluate alterations in *Penaeus vannamei* hemocytic proteome during TSV infection.⁸ Differential proteomics analysis by two-dimensional electrophoresis (2-DE) revealed several altered hemocytic proteins upon TSV infection.⁸ Interestingly, we

^{*} To whom correspondence should be addressed. Visith Thongboonkerd, MD, FRCPT, Medical Proteomics Unit, Office for Research and Development, 12th Floor Adulyadejvikrom Building, 2 Prannok Road, Siriraj Hospital, Bangkoknoi, Bangkok 10700, Thailand, Phone/Fax: +66-2-4184793. E-mail: thongboonkerd@dr.com or vthongbo@yahoo.com.

[†] Medical Proteomics Unit, Mahidol University.

[‡] Institute of Molecular Biology and Genetics, Mahidol University.

research articles Havanapan et al.

observed significant changes in levels of several fragments of hemocyanin. Some fragments were up-regulated, whereas some other fragments were down-regulated. Molecular mechanisms underlying these disparate results remained unclear, but might be associated with the altered proteolytic activity to cleave hemocyanin or differential stability of the N-terminus versus the C-terminus upon TSV infection. In the present study, we therefore extended our previous expression proteomics study and then further characterized functional significance of hemocyanin fragments during TSV infection. Functional proteomics revealed interesting findings, which pointed out that the C-terminus of hemocyanin underwent phosphorylation at serine residues and interacted with ERK1/2 via its 527th valine residue localized in the C-terminus. Therefore, ERK1/2 signaling pathway may play an important role in molecular immune response of P. vannamei upon TSV infection through its interaction with the C-terminal hemocyanin.

Materials and Methods

Shrimp Preparation and TSV Injection. Juvenile *P. vannamei* with approximate size of 10-14 cm in length and 17-20 g in weight from local farm were reared in 25-ppt artificial seawater (Mariscience International Co. Ltd.; Bangkok, Thailand) at 25 °C. A total of 12-15 shrimps were cultured in each 40×60 cm² plastic tank. Air was continuously supplied using an electric pump and artificial seawater was changed daily. TSV stock was purified and diluted (1:250) in NTE buffer (200 mM NaCl, 20 mM Tris-HCl, and 20 mM EDTA; pH 7.4). Shrimps were intramuscularly injected with $100~\mu$ L of diluted TSV using 26G-gauge needle through a lateral surface of the fourth abdominal segment. Control shrimps were injected with an equal volume of NTE buffer but without TSV.

Isolation of Hemocytes and Protein Extraction. At 24 h postinfection, each group of shrimps was chilled on ice. Hemolymph was drawn from shrimp abdominal hemocoel using 18G-gauge needle. The sample was mixed with an equal volume of an anticoagulant solution (27 mM sodium citrate, 450 mM NaCl, 115 mM glucose and 10 mM EDTA; pH 7.0) and immediately kept on ice. Hemocytes were harvested by centrifugation at 830g, 4 °C for 15 min. The pellet (packed hemocytes) were washed twice with cold anticoagulant and then homogenized in a lysis buffer (8 M urea, 2 M thiourea, 0.2% (v/v) triton-X, 50 mM DTT, 1 mM PMSF and 1 mM benzamidine). The protein mixture was collected after centrifugation at 12 000 rpm, 4 °C for 15 min. Protein concentration was determined using Bio-Rad Protein Assay (Bio-Rad Laboratories; Hercules, CA).

Two-Dimensional Gel Electrophoresis (2-DE). A pool of hemocyte samples isolated from 3 individual shrimps (within the same group) was resolved in each 2-DE (totally, 4 gels derived from 12 individual shrimps were included in each group). A total of 400 μg of hemocytic protein was loaded onto each IPG strip (nonlinear pH 4-7; 13-cm long) (GE Healthcare; Uppsala, Sweden). Rehydration was done at 50 μ A per strip in the presence of 8 M urea, 2 M thiourea, 4% (v/v) CHAPS, 50 mM DTT, 1 mM benzamidine and 0.5% (v/v) IPG buffer for 12 h. Isoelectric focusing (IEF) was performed at 20 °C in Ettan IPGphor II system (GE Healthcare) using a continuous increase of voltage (up to 8000 V) to reach 50 000 Vh. The strip was then incubated for 15 min in an equilibration buffer (6 M urea, 2% SDS, 30% glycerol, 50 mM Tris-HCl (pH 8.8), 100 mM DTT and 0.002% (w/v) bromophenol blue). The strip was then further equilibrated for 15 min in a similar buffer, which replaced 100 mM DTT with 250 mM of iodoacetamide. The IPG strips were placed onto 12.5% polyacrylamide slab gels and proteins were further separated in a SE600 Ruby electrophoresis set with a constant voltage of 150 V until the tracking dye reached the gel bottom. After the second-dimensional separation, the gel was fixed in a fixative solution containing 50% (v/v) ethanol and 2% (v/v) phosphoric acid, and stained with Coomassie Brilliant Blue-G250 stain, containing 10% (w/v) ammonium sulfate, 2% (v/v) phosphoric acid, and 0.001% (w/v) of Brilliant Blue G (USB Corp.; Cleveland, OH).

Image Analysis. The 2-D gel images were analyzed with MELANIE software (GeneBio; Geneva, Switzerland). Comparative analysis of protein spots was performed by matching corresponding spots across different gels. Each of the matched protein spots was rechecked manually. Intensity volumes of individual spots were normalized to total intensity volume of all spots present in each gel. Statistical analysis was performed to compare normalized intensity volumes of individual spots between control and infected groups. Only differentially expressed proteins with statistical significant were excised and subsequently identified by mass spectrometry. The degree of difference of a protein spot is reported as mean \pm SD of ratio of intensity level of such spot present in individual gels of TSV-infected group versus all gels in control group.

In-Gel Tryptic Digestion. Differentially expressed protein spots were excised from 2-D gels with sterile scalpel. The gel pieces were washed with 50% (v/v) acetonitrile in 25 mM ammonium bicarbonate (pH 8.5) for 15 min twice to remove Coomassie dye. After dehydration with 100% (v/v) acetonitrile for 10 min at room temperature (RT), the gel pieces were vacuum-dried and rehydrated with sequencing-grade modified trypsin (Promega; Madison, WI) in 25 mM ammonium bicarbonate (pH 8.5) at 37 °C overnight. The resulting peptides were then subjected to nanoliquid chromatography coupled with electrospray ionization tandem mass spectrometry (nanoLC-ESI-MS/MS).

NanoLC-ESI-MS/MS. NanoLC-ESI-MS/MS was performed as described previously. Briefly, in-gel tryptic digested samples were injected into an integrated nanoLC-ESI-MS/MS system (Quadrupole/time-of-flight Ultima API, Micromass; Manchester, U.K.). The injected samples were first trapped and desalted isocratically on an LC-Packings PepMap C_{18} μ -Precolumn cartridge (Dionex; Sunnyvale, CA). After dissolving with 0.1% formic acid, the samples were loaded into an analytical C_{18} capillary column connected online to a mass spectrometer. Instrumental operation, data acquisition, and analysis were performed under the full control of MassLynx 4.0 (Micromass). The survey scans were run over the mass range of m/z from 400 to 2000. A maximum of three concurrent MS/MS acquisitions were triggered for 2^+ , 3^+ and 4^+ charged precursor detection at an intensity above the predefined threshold.

The acquired peptide ions obtained from nanoLC-ESI-MS/MS were analyzed with the MASCOT search tool (www.matrixscience.com) using both NCBInr and EST databases. Parameters for the MASCOT search were peptide mass tolerance of 1 Da; MS/MS ion mass tolerance of 1 Da, maximally one missed cleavage; and tryptic digestion. Peptides were assumed as monoisotopic, oxidized at methionine residues and carbamidomethylated at cysteine residues. Only proteins with the significant ions scores (>40) were reported.

Calculation of Theoretical pI, Prediction of Phosphorylation Sites, And Motif/Domain Scan. The calculation of theoretical pI of the C- and N-termini of hemocyanin were

research articles Hemocyanin and ERK1/2

performed using the "ProtParam" tool (http://expasy.org/tools/ protparam.html). To predict the specific phosphorylation sites at Serine, Threonine and Tyrosine residues of the C- and N-termini of hemocyanin, "NetPhos 2.0 Server" (http://www. cbs.dtu.dk/services/NetPhos/) was used. For motif and domain scanning, "Scansite" version 2.0 (http://scansite.mit.edu) was utilized to investigate potential motifs within proteins that are likely to be phosphorylated by specific protein kinases or bound to functional domains.

1-D and 2-D Western Blot Analysis. Proteins were resolved either by SDS-PAGE or 2-DE and transferred onto a polyvinylidene difluoride membrane (Perkin-Elmer; Waltham, MA) by semidry blotting using a Mini Trans-Blot electrophoresis transfer cell (Bio-Rad Laboratories). Membrane was presoaked in absolute methanol and equilibrated in Tris-glycine transfer buffer (39 mM glycine, 0.04% SDS, 10% methanol and 48 mM Tris-HCl). Nonspecific binding was blocked with 5% skim milk in 0.5% TTBS buffer (0.5% Tween, 20 mM Tris-HCl and 150 mM NaCl; pH 7.4). Immunodetection was performed by incubating the blots in one of the following antibodies, including polyclonal rabbit anti-C-terminus hemocyanin (kindly provided by Prof. Chu Fang Lo, National University of Taiwan), anti-N-terminus hemocyanin (kindly provided by Prof. Chu Fang Lo, National University of Taiwan), anti-p-serine (Chemicon; Temecula, CA) and anti-ERK 1/2 (Cell Signaling Technology; Danvers, MA) in 2.5% skim milk/0.5% TTBS at RT for 1 h. After three washes with 0.5% TTBS, the membrane was incubated at RT for 1 h with respective secondary antibody conjugated with horseradish peroxidase (KPL; Gaitherburg, MD) 1:10 000 in 2.5% skim milk/0.5% TTBS. Immunoreactive protein bands or spots were visualized with a chemiluminescence substrate using the ECL Plus Western Blot Detection System (GE Healthcare).

Co-Immunoprecipitation (Co-IP) Assay. Shrimp hemocytes were resuspended in ice-cold RIPA buffer [50 mM Tris-HCl pH 8.0, 150 mM NaCl, 2 mM EDTA, 0.1% SDS, 1% NP-40, 1 mM PMSF] on ice for 30 min. Cell lysate was clarified by a centrifugation at 10 000 rpm for 5 min. Totally, 500 μ g of resolved proteins was incubated with 5 μ g of rabbit polyclonal anti-ERK1/2 antibody (Cell Signaling Technology) at 4 °C for 16 h. The mixture was further incubated with 50 μ L of protein G beads (GE Healthcare) at 4 °C for 4 h. Thereafter, the beads were collected by centrifugation at 2000 rpm for 2 min and washed twice with ice-cold RIPA buffer. Immunoprecipitated proteins were eluted, separated by SDS-PAGE under reducing condition, and subjected to Western blot analyses. Immunoprecipitation with rabbit IgG (Santa Cruz Biotechnology; Santa Cruz, CA) served as an isotype control for Co-IP.

Results

Alterations in C- and N-Terminal Fragments of Hemocyanin from Hemocytes of P. vannamei during TSV Infection. Expression proteomics using 2-DE (totally, 4 gels derived from 12 individual shrimps per group were analyzed) revealed upregulation of the C-terminal hemocyanin fragments (labeled as C1–C4; TSV-infected/control ratios ranged from 1.50 \pm 0.15 to 2.25 \pm 0.26-fold), whereas the N-terminal fragments were down-regulated (labeled as N1-N3; TSV-infected/control ratios were ranged from 0.37 ± 0.19 to 0.53 ± 0.11 -fold) (Figure 1A,B). NanoLC-ESI-MS/MS identified these fragments with the same NCBI Accession number (CAA57880) with MS/MS ions scores of 74–334 and sequence coverage of 2–13%. Figure 2 showed mapping of amino acid sequences of the N-terminus (1st to 230th residues) and C-terminus (438th to 648th residues) of hemocyanin that were used for production of rabbit polyclonal antibodies against these two respective fragments and for subsequent bioinformatic and functional analyses. Note that we used the pI range of 4-7 in the present study because our initial screening using the broader pI range of 3-10 demonstrated that almost all of hemocyte proteins had pI range of 4-7 (data not shown).

C-Terminal Hemocyanin Fragments Underwent Serine **Phosphorylation.** Interestingly, the C-terminal hemocyanin fragments were localized in the more acidic region, whereas the N-terminal fragments were localized in the less acidic region in 2-D gels (Figure 1A,B). Calculation of their theoretical p*I* by the "ProtParam" tool using their sequences illustrated in Figure 2 revealed that the C-terminus had a more acidic pI(approximately 5.16; with 37 negatively charged amino acid residues), whereas the N-terminus had a less acidic pI (approximately 6.04; with 27 negatively charged amino acid residues), consistent to their actual positions in 2-D gels. Moreover, the expression proteomics data were confirmed by 2-D Western blot analysis using specific antibodies against the C- and N-termini of hemocyanin, strengthening our results by 2-DE and p*I* calculation (Figure 1C,D).

These selective locales of the C- and N-termini of hemocyanin drew our attention for further functional analyses of the C- and N-terminal hemocyanin fragments. One of the possibilities for this difference in pI of the C- and N-termini was the process of "post-translational modification (PTM)", and the most likely PTM that caused pI shift was phosphorylation, which might cause a pI shift toward the acidic end (up to >1 $\mathrm{p}I$ unit shift). 17 We thus screened for potential phosphorylation sites in the C-terminal hemocyanin compared to the Nterminus. The "NetPhos 2.0 Server" 18 for prediction of possible phosphorylation sites revealed greater number of phosphoserine (7 residues) in the C-terminus, whereas only 2 phosphoserine residues were predicted in the N-terminus (Figure 3). There were comparable numbers of potential phospho-threonine and phospho-tyrosine residues predicted in the C- and N-termini of hemocyanin (Figure 3).

We then validated our prediction by 1-D Western blot analysis for phospho-serine, C-terminal, and N-terminal hemocyanin. Figure 4 shows that serine phosphorylation was observed only in the C-terminus, not in the N-terminus of hemocyanin. We then hypothesized that serine phosphorylation in the C-terminal hemocyanin fragments might be the key for differential regulation of the C-terminus compared to the Nterminus of hemocyanin.

C-Terminal Hemocyanin Interacted with ERK1/2. To further investigate the differential roles of C- and N-termini of hemocyanin in shrimp hemocytes, "Scansite" (version 2.0) software was employed for motif scan in the C-terminus, compared to the N-terminus of hemocyanin. The scan was performed against all 65 individual motifs and 12 motif groups available in the Scansite, using the "high stringency" criteria indicated in the software. 19 Only ERK docking domain (Ddomain), which is required for activation of ERK1/2 effector kinase, was identified as a kinase-binding site in the C-terminal hemocyanin at 527th valine residue (Figure 5), whereas no individual motif or motif group was identified in the Nterminus (data not shown). This data strongly suggested that ERK interacted with the C-terminal hemocyanin, leading to serine phosphorylation in this terminus.

research articles Havanapan et al.

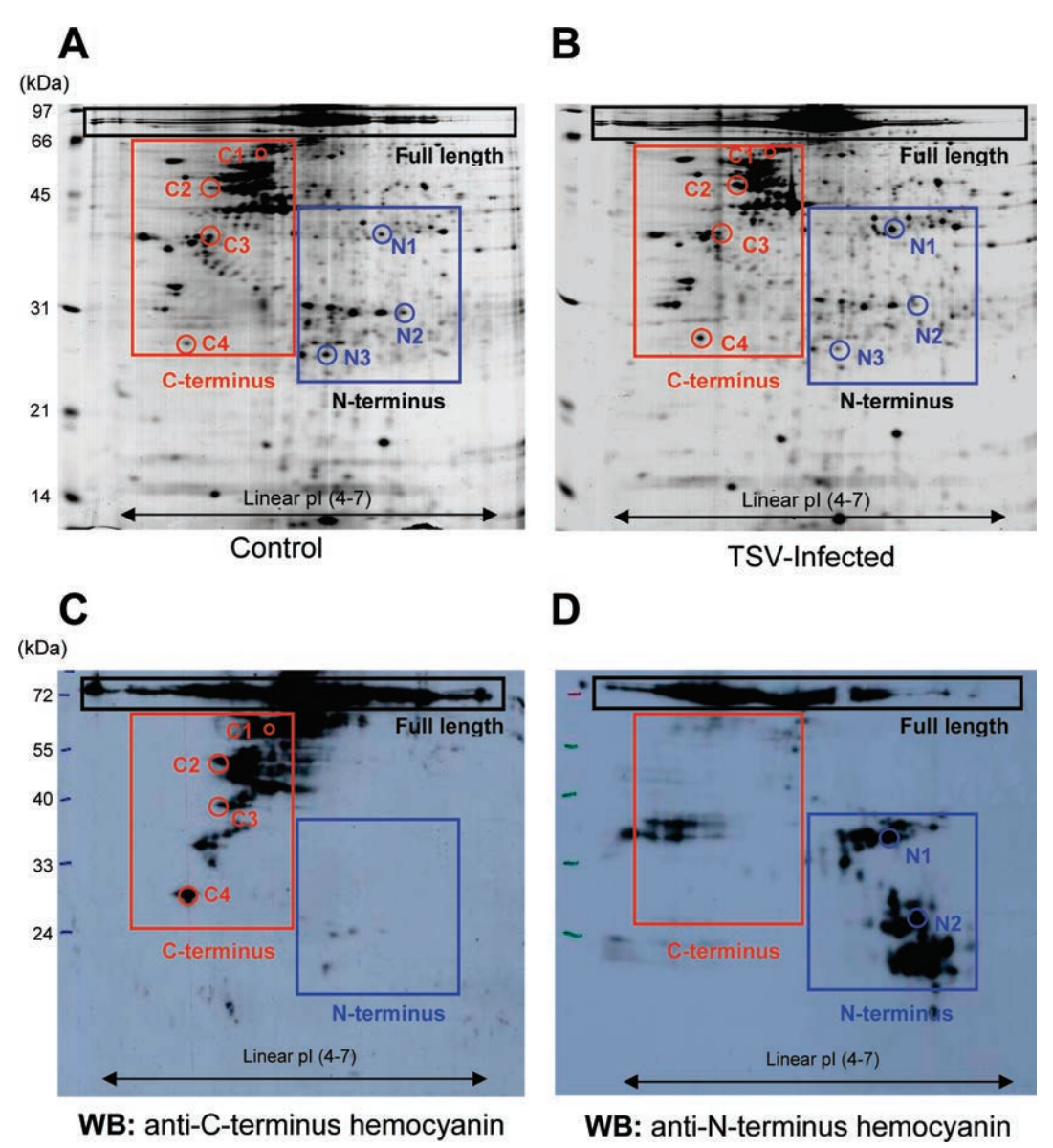


Figure 1. Alterations in C- and N-terminal fragments of hemocyanin from hemocytes of *P. vannamei* during TSV infection. (A) and (B) show proteome maps of altered C- (C1-C4) and N-terminal fragments (N1-N3) of hemocyanin during TSV infection (n = 4 gels derived from 12 individual shrimps for each group; totally, 8 gels were analyzed using Coomassie Brilliant Blue G-250 staining). (C) and (D) show 2-D Western blot analysis of C- and N-terminal hemocyanin fragments, respectively, in the control group. Note that one of the N-terminal fragments (N4) could not be detected by Western blot analysis. Moreover, there were many more fragments of hemocyanin, but their levels were not significantly altered by TSV infection; thus, they were neither labeled nor identified by mass spectrometry.

The motif scan results were confirmed by co-immunoprecipitation (Co-IP) to address potential interaction between the C-terminal hemocyanin and ERK1/2. Figure 6A showed Co-IP using anti-ERK1/2 and the resulting complexed proteins were examined with 1-D Western blot analysis using anti-C-terminal hemocyanin. The results showed that the C-terminus of hemocyanin bound to ERK1/2, whereas the isotype control yielded none of the C-terminal fragments. However, the fulllength, but not C-terminus, hemocyanin could be pulled down from the IgG isotype control sample, suggesting the nonspecific binding of the full-length hemocyanin to protein G bead surfaces. This result was not surprising as hemocyanin is normally sticky and almost always pulled down by Co-IP (similar to albumin in mammalians). Figure 6B illustrated that there were no N-terminal hemocyanin fragments detected in both ERK-1/2 and isotype control immunoprecitated samples.

Western blot analysis for ERK1/2 confirmed the positive ERK1/2 band at the expected size, whereas the isotype control sample showed a faint band of ERK1/2 (Figure 6C). This result again was not unexpected, as the full-length of hemocyanin that was nonspecifically pulled down by the isotype IgG also contained the 527th valine residue (the predicted site of ERK D-domain; see Figure 5); thus, it should be able to bind to ERK1/2 as well. However, the ERK1/2 band in the isotype control sample was not as prominent as the one present in the ERK1/2 Co-IP sample. These data indicate that only the C-terminus, not the N-terminus, of hemocyanin interacts with ERK1/2.

Because the C-terminal hemocyanin fragments were upregulated in hemocytes of *P. vannamei* during TSV infection, we then further hypothesized that ERK1/2 as the interacting protein of the C-terminal hemocyanin should be also upregulated in the TSV-infected hemocytes. 1-D Western blot

research articles Hemocyanin and ERK1/2

Hemocyanin (full length = 648 residues)

1 FQVASADVQQQKDVLYLLNKIYGDIQDGDLLATANSFDPVGNLGSYSDGG

N-terminus (1st_230th aa) 51 AAVQKLVQDLNDGKLLEQKHWFSLFNTRHRNEALMLFDVLIHCKDWASFV 101 GNAAYFRQKMNEGEFVYALYVAVIHSSLAEQVVLPPLYEVTPHLFTNSEV 151 IEEAYRAKQKQTPGKFKSSFTGTKKNPEQRVAYFGEDIGLNTHHVTWHME 201 FPFWWNDAYGHHLDRKGENFFWIHHOLTVRFDAERLSNYLDPVGELQWNK 251 PIVDGFAPHTTYKYGGQFPARPDNVKFEDVDDVARIRDMVIVESRIRDAI 301 AHGYIVDSEGKHIDISNEKGIDILGDIIESSLYSPNVOYYGALHNTAHIV 351 LGRQGDPHGKFDLPPGVLEHFETATRDPSFFRLHKYMDNIFKEHKDNLPP YTKADLEFSGVSVTELAVVGELETYFEDFEYSLINAVDDAEGIPDVEIST C-terminus YVPRLNHKEFTFRIDVENGGAERLATVRIFAWPHKDNNGIEYTFDEGRWN 501 AIELDKFWVSLKGGKTSIERKSTESSVTVPDVPSIHDLFAEAEAGGAGLA 551 KFESATGLPNRFLLPKGNDRGLEFDLVVAVTDGDADSAVPNLHENTEYNH 601 YGSHGVYPDKRPHGYPLDRKVPDERVFEDLPNFKHIQVKVFNHGEHIH

Figure 2. Mapping of sequences of the N-terminus and Cterminus of hemocyanin from hemocytes of P. vannamei that were used for antibody production and for subsequent bioinformatic and functional analyses.

analysis was performed to address this hypothesis. Figure 7 illustrates that ERK1/2 level was also up-regulated in the TSVinfected hemocytes.

Discussion

TSV is one of the most serious pathogens in shrimps. Accumulative mortality rate of TSV-infected shrimps varies from 5% to 95%, which really affects the shrimp industry. Many efforts have been done to eliminate and prevent TSV infection, but this infectious problem remains worldwide due to a limitation of current knowledge to explain molecular immune response in shrimps against TSV infection. Elucidation of such molecular mechanisms in the TSV-infected shrimps may lead to successful prevention of TSV infection and/or reduction of its high mortality rate. To investigate molecular immune response of hemocytes in P. vannamei during TSV infection, we performed a comparative analysis of proteome profiles of mock (uninfected) control and TSV-infected hemocytes. Our expression proteomics study revealed that many fragments but not the full-length of hemocyanin, a major abundant protein in shrimp hemocytes, were altered in response to TSV infection. These protein spots were found at various pI and MW in 2-D gels. Hemocyanin is a protein with MW of approximately 75 kDa and comprises multiple subunits. Hemocyanin is a major component in hemolymphs of arthropods and mollusks.²⁰ Arthropod hemocyanin complex is composed of hexamer or multihexamers formed by similar or identical subunits.²¹ The main function of hemocyanin is oxygen transport. In addition, hemocyanin has been reported as a multifunctional protein involved in several physiological processes, including phenoloxidase activation, 14 antimicrobial mechanisms, 5,15,22 and acts as lectin in specific agglutination. 23,24 Study on differential gene expression in normal shrimps versus white spot syndrome virus (WSSV)-resistant Penaeus japonicus showed that one subunit of hemocyanin protein complex was increased in the infected shrimps.¹⁶ Moreover, hemocyanin could bind to WSSV¹⁵ and high concentrations of hemocyanin could delay WSSV infection in a copper-independent manner.16

Currently, there is a growing number of literatures reporting molecular elucidation of shrimp immune response to viral infection at translational or protein level.^{8,25–27} However, the functional significance of those altered proteins in response to viral infection remains unclear. Previous findings by Destoumieux-Garzon D, et al.⁵ suggested that hemocytes could concomitantly contribute to a release of enzyme(s) responsible for hemocyanin cleavage. Although the mechanism(s) underlying hemocyanin processing remains unknown, it is likely to be enzymatic driven.5 Our expression proteomics study revealed that some fragments of hemocyanin were up-regulated, whereas some other fragments of hemocyanin were downregulated during TSV infection in hemocytes of P. vannamei. The underlying mechanisms of this interesting finding drew our attention to focus on further characterizations and functional significance of hemocyanin fragments in crustacean hemocytes.

We observed that the C-terminal fragments were upregulated, whereas the N-terminal fragments were downregulated. There should be some molecular mechanisms underlying these disparate regulations. Several other studies have reported that both N- and C-termini of hemocyanin are important for an innate immune system in shrimps. The N-terminus is believed to involve in a regulation of hemocyanin activity, whereas the C-terminus has been evidenced for its antiviral activity as the antiviral peptides could be generated from the C-terminal domain.^{5,22} The up-regulation of the C-terminal hemocyanin fragments found in our present study, thus, might be one of the host defense mechanisms against TSV in P. vannamei.

Herein, we describe molecular characterizations of hemocyanin fragments in hemocytes of P. vannamei. The expression proteomics data demonstrated that the up-regulated C-terminal fragments had more acidic pI as compared to the Nterminal fragments, which were down-regulated (Figure 1). The up-regulation of the C-terminus, which had more acidic pI, suggested that phosphorylation might play role for differential regulations between the C- and N-termini. Screening for potential phosphorylation sites (Figure 3) and Western blot analysis of phospho-serine (Figure 4) both confirmed that the C-terminus underwent serine phosphorylation, which explained the more acidic p*I* of the C-terminus (more phosphate groups in the protein molecule cause acidic shift of such protein molecule). ¹⁷ Moreover, motif scan for individual motifs and motif groups revealed an ERK D-domain in the C-terminus, whereas none was observed in the N-terminus (Figure 5). The interaction between C-terminal hemocyanin and ERK1/2 was finally confirmed by Co-IP (Figure 6).

In general, many cellular functions are regulated by phosphorylation of serine, threonine and tyrosine residues in various proteins. Phosphorylation plays important role in regulation of protein-protein interaction of enzymes, 28 protein degradation, and inhibition of enzymes.^{29,30} One of the four mitogenactivated protein kinase (MAPK) signaling pathways is a Raf/ MEK/ERK cascade, which is a highly conserved signal transduction module.³¹ The ERK cascade is activated by various stimuli and participates in regulation of cell proliferation, differentiation, survival, apoptosis, morphological determination, and oncogenic transformation.^{32–35} Surprisingly, little is known about specific roles of two major ERK isoforms, ERK1 and ERK2, which share 85% sequence identity in mammals.³⁶ These two proteins coexpress in all mammalian tissues with a remarkable variation in relative abundance. ERK1/2 signaling has been implicated as the important regulator of cell proliferation. For this reason, several inhibitors of the ERK pathway have been studied and some are now entering clinical trial phase as potential anticancer agents. Recently, study on a white shrimp, Fenneropenaeus indicus, revealed a significant role of ERK1/2

research articles Havanapan et al.

	Serine predictions			
	Pos	Context	Score	Pre
S		v_		
3	5	FQVASADVQ	0.004	
	36	ATANSFDPV	0.005	
=	45	GNLGSYSDG	0.654	*s*
rminus	47	LGSYSDGGA	0.107	
<u></u>	73	KHWFSLFNT	0.154	
N-te	98	KDWASFVGN	0.010	
-	126	AVIHSSLAE	0.006	
_	127	VIHSSLAEQ	0.386	
	148	LFTNSEVIE	0.005	
	168	GKFKSSFTG	0.022	
	169	KFKSSFTGT	0.968	*S*

Threonine predictions				
Pos	Context v	Score	Pred	
33	DLLATANSF	0.026		
77	SLFNTRHRN	0.071		
141	LYEVTPHLF	0.482		
146	PHLFTNSEV	0.136		
162	KQKQTPGKF	0.881	*T*	
171	KSSFTGTKK	0.034		
173	SFTGTKKNP	0.855	*T*	
192	${\tt IGL}{\tt NTHHVT}$	0.650	*T*	
196	THHVTWHME	0.046		
228	HHQLTVR	0.736	*T*	
	^			

Tyr	osine predic	tions	
Pos	Context v	Score	Pred
16	KDVLYLLNK	0.421	
22	LNKIYGDIQ	0.402	
46	NLGSYSDGG	0.660	*Y*
105	GNAAYFRQK	0.069	
117	GEFVYALYV	0.140	
120	VYALYVAVI	0.041	
138	LPPLYEVTP	0.512	*Y*
155	IEEAYRAKQ	0.665	*Y*
183	QRVAYFGED	0.018	
209	WNDAYGHHL	0.762	*Y*
l	^		

Serine predictions				
Pos	Context v	Score	Pred	
12	DVEISTYVP	0.599	*S*	
73	KFWVSLKGG	0.954	*S*	
80	GGKTSIERK	0.984	*S*	
85	IERKSTESS	0.998	*S*	
88	KSTESSVTV	0.522	*S*	
89	STESSVTVP	0.942	*S*	
97	PDVPSIHDL	0.927	*S*	
117	AKFESATGL	0.034		
150	GDADSAVPN	0.294		
166	NHYGSHGVY	0.310		
	^			

Thre	eonine predi	ctions	
Pos	Context v	Score	Pred
13	VEISTYVPR	0.446	
24	HKEFTFRID	0.705	*T*
39	ERLATVRIF	0.893	*T*
56	GIEYTFDEG	0.386	
79	KGGKTSIER	0.633	*T*
86	ERKSTESSV	0.777	*T*
91	ESSVTVPDV	0.114	
119	FESATGLPN	0.019	
144	VVAVTDGDA	0.134	
159	LHENTEYNH	0.203	
	٨		

Tyrosine predictions			
Pos	Context	Score	Pred
	v		
14	EISTYVPRL	0.161	
55	NGIEYTFDE	0.112	
161	ENTEYNHYG	0.933	*Y*
164	EYNHYGSHG	0.751	*Y*
170	SHGVYPDKR	0.574	*Y*
178	RPHGYPLDR	0.026	
	^		

11	Predicted phosphorylation sites			
Hemocyanin fragments	p-serine	p-threonine	p-tyrosine	
N-terminus	2	4	4	
C-terminus	7*	4	3	

Figure 3. Prediction of potential phosphorylation sites in C- and N-terminus of hemocyanin from hemocytes of *P. vannamei.* "NetPhos 2.0 Server" tool¹⁸ was used for prediction of phosphorylation sites at Ser, Thr and Tyr residues in C- and N-termini of hemocyanin. Scores above the threshold of 0.500 were considered as positive predictions and are designated as *S*, *T*, or *Y*. Note that the position (Pos) of potential phosphorylation sites in the C-terminus corresponded to a numerical order of the 211 amino acid residues of the C-terminus submitted to the software, not the actual position (438th to 648th) in the full-length as illustrated in Figure 2.

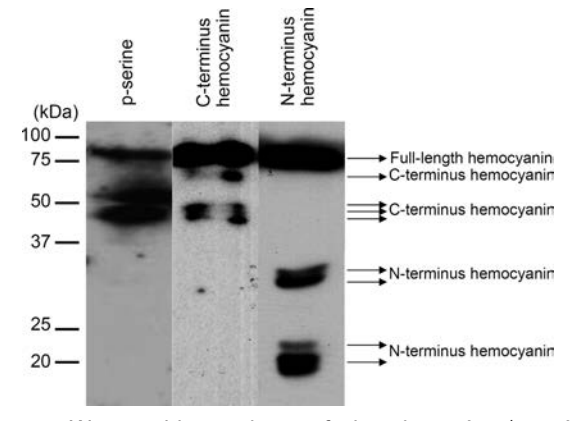


Figure 4. Western blot analyses of phospho-serine (p-serine), C-terminus, and N-terminus of hemocyanin. Immunoreactive bands corresponding to full-length, C-terminus, and N-terminus of hemocyanin are indicated with arrows and legends.

signaling pathway in regulating molt-inhibition hormone expression, which controls the molt cycles.³⁷ Therefore, ERK1/2 plays pivotal roles in biological phenomena not only in mammalians but also in crustaceans. Moreover, ERK kinase

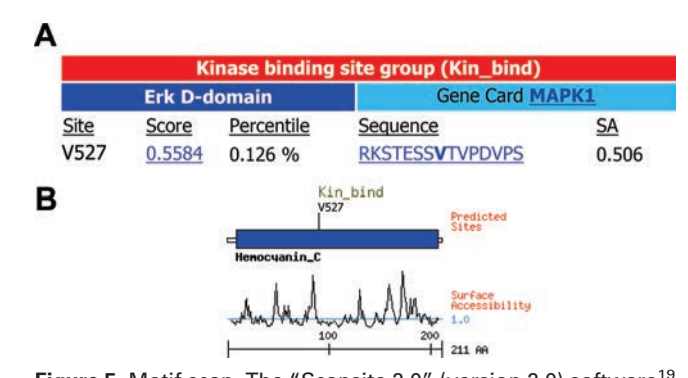


Figure 5. Motif scan. The "Scansite 2.0" (version 2.0) software 19 was utilized to screen for potential motifs or functional domains in the C-terminus of hemocyanin. When the "high stringency" criteria was used, only one kinase-binding site (ERK D-domain) was found in the C-terminus of hemocyanin (A). Predicted site (527th valine residue) in peptide map and the surface accessibility are shown in (B). Note that the surface accessibility shown at the bottom of panel (B) was obtained from only 211 amino acid residues of the C-terminal hemocyanin (corresponded to the 438th to 648th residues of the full-length). Neither a potential motif nor a functional domain was identified in the N-terminus of hemocyanin (data not shown).

research articles Hemocyanin and ERK1/2

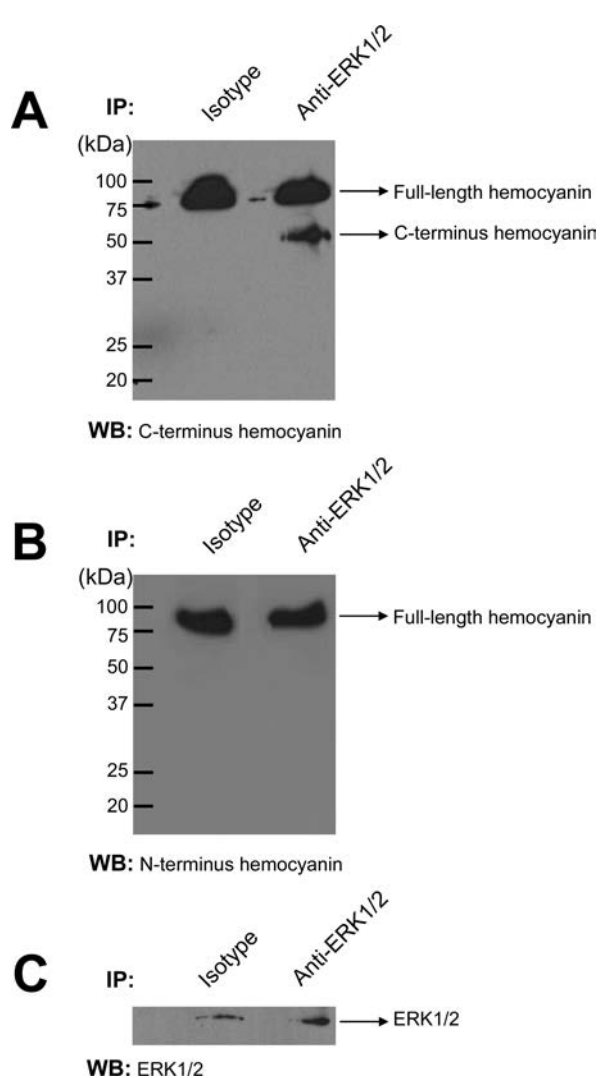


Figure 6. C-terminal hemocyanin bound to ERK1/2 as demonstrated by Co-IP using anti-ERK1/2. The resulting complexed proteins were examined with 1-D Western blot analysis using anti-C-terminal hemocyanin (A), anti-N-terminal hemocyanin (B), and anti-ERK1/2 (C). Rabbit IgG served as the isotype control in a parallel experiment.

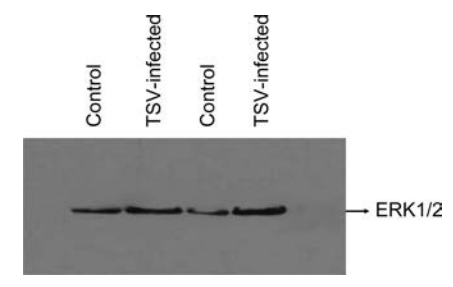


Figure 7. Western blot analysis of ERK1/2 in TSV-infected hemocytes compared to the mock (uninfected) control. Immunoreactive band of ERK1/2 is indicated with arrow and legend.

family has been demonstrated to play an important role in immune response in both vertebrates ^{38,39} and invertebrates. ⁴⁰

In the present study, we screened for any motifs or functional domains in the N- and C-termini of hemocyanin from P. vannamei. A kinase-binding site, ERK D-domain, was uniquely found in the C-terminus. In addition, ERK D-domain could be predicted in hemocyanin from a closely related shrimp Penaeus

monodon or black tiger shrimp (data not shown). Indeed, binding of ERK to protein substrates is mediated by two docking sites, the FXFP motif and the D-domain. The D-domain is required for activation of the ERK1/2 effector kinase.41 Activated ERK1 and ERK2 phosphorylate many substrates in all cellular compartments, including membrane proteins, nuclear substrates, cytoskeleton proteins, and several protein kinases.42 We found that only C-terminal hemocyanin can specifically bind to ERK1/2 by Co-IP assay. Taken together, our findings suggested that the C-terminal hemocyanin served as a kinase substrate for ERK1/2. In addition, ERK1/2 signaling might be involved in host defense mechanisms against virus infection in crustaceans via the C-terminal hemocyanin by targeting at serine residues.

In summary, we identified differential regulations of C- and N-terminal fragments of hemocyanin that might be important for molecular response to TSV infection in P. vannamei. Functional analyses revealed that phospho-serine residues were predominant in the C-terminus, which contained ERK Ddomain that is required for activation of the ERK1/2 effector kinase. The interaction between the C-terminal hemocyanin and ERK1/2 was confirmed by Co-IP. To the best of our knowledge, this is the first study that demonstrates the potential role of ERK signaling pathway in host immune defense of shrimp through its interaction with hemocyanin. Difference between these two (C- versus N-) termini of hemocyanin might be a molecular basis of their differential roles in shrimp innate immunity. Further functional studies on hemocyanin processing involved in the defense mechanism may provide better understanding of shrimp—virus interplay during TSV infection.

Abbreviations: 2-DE, two-dimensional electrophoresis; CHAPS, 3-[(3-cholamidopropyl) dimethyl-amino]-1-propanesulfonate; Co-IP, co-immunoprecipitation; D-domain, dockingdomain; DTT, dithiothreitol; IEF, isoelectric focusing; MS/MS, tandem mass spectrometry; nanoLC-ESI-MS/MS, nano liquid chromatography coupled to electrospray ionization MS/MS; ORF, open reading frame; pI, isoelectric point; PTM, posttranslational modification; TSV, Taura syndrome virus; WSSV, white spot syndrome virus.

Acknowledgment. We are grateful to Prof. Dr. Chu Fang Lo at Institute of Zoology, National Taiwan University, Taipei, Taiwan, ROC for providing polyclonal antibodies against N- and C-terminal hemocyanin. This work was supported by the Royal Golden Jubilee Ph.D. Program, The Thailand Research Fund (TRF), and by the Postdoctoral Fellowship Grant from Mahidol University (to P. Havanapan).

References

- (1) Overstreet, R. M.; Lightner, D. V.; Hasson, K. W.; McIlwain, S.; Lotz, J. M. Susceptibility to taura syndrome virus of some penaeid shrimp species native to the Gulf of Mexico and the southeastern United States. J. Invertebr. Pathol. 1997, 69, 165-176.
- Bonami, J. R.; Hasson, K. W.; Mari, J.; Poulos, B. T.; Lightner, D. V. Taura syndrome of marine penaeid shrimp: characterization of the viral agent. J. Gen. Virol. 1997, 78, 313-319, Pt 2.
- (3) Mari, J.; Poulos, B. T.; Lightner, D. V.; Bonami, J. R. Shrimp Taura syndrome virus: genomic characterization and similarity with members of the genus Cricket paralysis-like viruses. J. Gen. Virol. **2002**, 83, 915-926.
- (4) Robalino, J.; Browdy, C. L.; Prior, S.; Metz, A.; Parnell, P.; Gross, P.; Warr, G. Induction of antiviral immunity by double-stranded RNA in a marine invertebrate. J. Virol. 2004, 78, 10442-10448.
- (5) Destoumieux-Garzon, D.; Saulnier, D.; Garnier, J.; Jouffrey, C.; Bulet, P.; Bachere, E. Crustacean immunity. Antifungal peptides

research articles Havanapan et al.

are generated from the C terminus of shrimp hemocyanin in response to microbial challenge. *J. Biol. Chem.* **2001**, *276*, 47070–47077.

- (6) Muta, T.; Iwanaga, S. The role of hemolymph coagulation in innate immunity. Curr. Opin. Immunol. 1996, 8, 41–47.
- (7) Sellos, D.; Lemoine, S.; Van Wormhoudt, A. Molecular cloning of hemocyanin cDNA from Penaeus vannamei (Crustacea, Decapoda): structure, evolution and physiological aspects. *FEBS Lett.* 1997, 407, 153–158.
- (8) Chongsatja, P. O.; Bourchookarn, A.; Lo, C. F.; Thongboonkerd, V.; Krittanai, C. Proteomic analysis of differentially expressed proteins in Penaeus vannamei hemocytes upon Taura syndrome virus infection. *Proteomics* 2007, 7, 3592–3601.
- (9) Martin, G. G.; Castro, C.; Moy, N.; Rubin, N. N-acetyl-D-glucosamine in crustacean hemocytes; possible functions and usefulness in hemocyte classification. *Invertebr. Biol.* 2003, 122, 265– 270
- (10) Burmester, T. Origin and evolution of arthropod hemocyanins and related proteins. J. Comp. Physiol., B 2002, 172, 95–107.
- (11) van Holde, K. E.; Miller, K. I.; Decker, H. Hemocyanins and invertebrate evolution. J. Biol. Chem. 2001, 276, 15563–15566.
- (12) Lee, S. Y.; Lee, B. L.; Soderhall, K. Processing of an antibacterial peptide from hemocyanin of the freshwater crayfish Pacifastacus leniusculus. J. Biol. Chem. 2003, 278, 7927–7933.
- (13) Nagai, T.; Osaki, T.; Kawabata, S. Functional conversion of hemocyanin to phenoloxidase by horseshoe crab antimicrobial peptides. J. Biol. Chem. 2001, 276, 27166–27170.
- (14) Decker, H.; Rimke, T. Tarantula hemocyanin shows phenoloxidase activity. J. Biol. Chem. 1998, 273, 25889–25892.
- (15) Zhang, X.; Huang, C.; Qin, Q. Antiviral properties of hemocyanin isolated from shrimp Penaeus monodon. *Antiviral Res.* 2004, 61, 93–99.
- (16) Lei, K.; Li, F.; Zhang, M.; Yang, H.; Luo, T.; Xu, X. Difference between hemocyanin subunits from shrimp Penaeus japonicus in anti-WSSV defense. *Dev. Comp. Immunol.* 2008, 32, 808–813.
- (17) Powell, D. W.; Rane, M. J.; Joughin, B. A.; Kalmukova, R.; Hong, J. H.; Tidor, B.; Dean, W. L.; Pierce, W. M.; Klein, J. B.; Yaffe, M. B.; McLeish, K. R. Proteomic identification of 14–3-3zeta as a mitogen-activated protein kinase-activated protein kinase 2 substrate: role in dimer formation and ligand binding. *Mol. Cell. Biol.* 2003, 23, 5376–5387.
- (18) Blom, N.; Gammeltoft, S.; Brunak, S. Sequence and structure-based prediction of eukaryotic protein phosphorylation sites. *J. Mol. Biol.* 1999, 294, 1351–1362.
- (19) Obenauer, J. C.; Cantley, L. C.; Yaffe, M. B. Scansite 2.0: Proteomewide prediction of cell signaling interactions using short sequence motifs. *Nucleic Acids Res.* 2003, 31, 3635–3641.
- (20) Voit, R.; Feldmaier-Fuchs, G. Arthropod hemocyanins. Molecular cloning and sequencing of cDNAs encoding the tarantula hemocyanin subunits a and e. J. Biol. Chem. 1990, 265, 19447–19452.
- (21) Markl, J.; Burmester, T.; Decker, H.; Savel-Niemann, A.; Harris, J. R.; Suling, M.; Naumann, U.; Scheller, K. Quaternary and subunit structure of Calliphora arylphorin as deduced from electron microscopy, electrophoresis, and sequence similarities with arthropod hemocyanin. J. Comp. Physiol., B 1992, 162, 665–680.
- (22) Destoumieux, D.; Bulet, P.; Loew, D.; Van Dorsselaer, A.; Rodriguez, J.; Bachere, E. Penaeidins, a new family of antimicrobial peptides isolated from the shrimp Penaeus vannamei (Decapoda). *J. Biol. Chem.* 1997, 272, 28398–28406.
- (23) Zhang, Y.; Wang, S.; Xu, A.; Chen, J.; Lin, B.; Peng, X. Affinity proteomic approach for identification of an IgA-like protein in Litopenaeus vannamei and study on its agglutination characterization. J. Proteome Res. 2006, 5, 815–821.
- (24) Alpuche, J.; Pereyra, A.; Agundis, C.; Rosas, C.; Pascual, C.; Slomianny, M. C.; Vazquez, L.; Zenteno, E. Purification and

- characterization of a lectin from the white shrimp Litopenaeus setiferus (Crustacea decapoda) hemolymph. *Biochim. Biophys. Acta* **2005**, *1724*, 86–93.
- (25) Bourchookarn, A.; Havanapan, P. O.; Thongboonkerd, V.; Krittanai, C. Proteomic analysis of altered proteins in lymphoid organ of yellow head virus infected Penaeus monodon. *Biochim. Biophys. Acta* 2008, 1784, 504–511.
- (26) Rattanarojpong, T.; Wang, H. C.; Lo, C. F.; Flegel, T. W. Analysis of differently expressed proteins and transcripts in gills of Penaeus vannamei after yellow head virus infection. *Proteomics* 2007, 7, 3809–3814.
- (27) Wang, H. C.; Wang, H. C.; Leu, J. H.; Kou, G. H.; Wang, A. H.; Lo, C. F. Protein expression profiling of the shrimp cellular response to white spot syndrome virus infection. *Dev. Comp. Immunol.* 2007, 31, 672–686.
- (28) Babior, B. M. NADPH oxidase: an update. *Blood* 1999, 93, 1464–1476.
- (29) Cole, P. A.; Shen, K.; Qiao, Y.; Wang, D. Protein tyrosine kinases Src and Csk: a tail's tale. Curr. Opin. Chem. Biol. 2003, 7, 580– 585
- (30) van Weeren, P. C.; de Bruyn, K. M.; Vries-Smits, A. M.; van Lint, J.; Burgering, B. M. Essential role for protein kinase B (PKB) in insulin-induced glycogen synthase kinase 3 inactivation. Characterization of dominant-negative mutant of PKB. J. Biol. Chem. 1998, 273, 13150–13156.
- (31) Galabova-Kovacs, G.; Kolbus, A.; Matzen, D.; Meissl, K.; Piazzolla, D.; Rubiolo, C.; Steinitz, K.; Baccarini, M. ERK and beyond: insights from B-Raf and Raf-1 conditional knockouts. *Cell Cycle* 2006, 5, 1514–1518.
- (32) Yoon, S.; Seger, R. The extracellular signal-regulated kinase: multiple substrates regulate diverse cellular functions. *Growth Factors* **2006**, *24*, 21–44.
- (33) Viala, E.; Pouyssegur, J. Regulation of tumor cell motility by ERK mitogen-activated protein kinases. Ann. N.Y. Acad. Sci. 2004, 1030, 208–218.
- (34) Torii, S.; Nakayama, K.; Yamamoto, T.; Nishida, E. Regulatory mechanisms and function of ERK MAP kinases. *J. Biochem.* 2004, 136, 557–561.
- (35) Seger, R.; Krebs, E. G. The MAPK signaling cascade. FASEB J. 1995, 9, 726–735.
- (36) Boulton, T. G.; Cobb, M. H. Identification of multiple extracellular signal-regulated kinases (ERKs) with antipeptide antibodies. *Cell Regul.* 1991, 2, 357–371.
- (37) Devaraj, H.; Natarajan, A. Molecular mechanisms regulating molting in a crustacean. FEBS J. 2006, 273, 839–846.
- (38) Mathur, R. K.; Awasthi, A.; Wadhone, P.; Ramanamurthy, B.; Saha, B. Reciprocal CD40 signals through p38MAPK and ERK-1/2 induce counteracting immune responses. *Nat. Med.* 2004, 10, 540–544.
- (39) Papoutsopoulou, S.; Symons, A.; Tharmalingham, T.; Belich, M. P.; Kaiser, F.; Kioussis, D.; O'Garra, A.; Tybulewicz, V.; Ley, S. C. ABIN-2 is required for optimal activation of Erk MAP kinase in innate immune responses. *Nat. Immunol.* 2006, 7, 606–615.
- (40) Garcia-Garcia, E.; Prado-Alvarez, M.; Novoa, B.; Figueras, A.; Rosales, C. Immune responses of mussel hemocyte subpopulations are differentially regulated by enzymes of the PI 3-K, PKC, and ERK kinase families. *Dev. Comp. Immunol* 2008, 32, 637–653.
- (41) Fantz, D. A.; Jacobs, D.; Glossip, D.; Kornfeld, K. Docking sites on substrate proteins direct extracellular signal-regulated kinase to phosphorylate specific residues. *J. Biol. Chem.* 2001, 276, 27256– 27265.
- (42) Chen, Z.; Gibson, T. B.; Robinson, F.; Silvestro, L.; Pearson, G.; Xu, B.; Wright, A.; Vanderbilt, C.; Cobb, M. H. MAP kinases. *Chem. Rev.* 2001, 101, 2449–2476.

PR801067E





Mud crab susceptibility to disease from white spot syndrome virus is species-dependent

Somboonna et al.





SHORT REPORT Open Access

Mud crab susceptibility to disease from white spot syndrome virus is species-dependent

Naraporn Somboonna^{1,2,5*}, Seksan Mangkalanan³, Attasit Udompetcharaporn², Chartchai Krittanai³, Kallaya Sritunyalucksana^{1,2}, TW Flegel^{1,2,4}

Abstract

Background: Based on a report for one species (*Scylla serrata*), it is widely believed that mud crabs are relatively resistant to disease caused by white spot syndrome virus (WSSV). We tested this hypothesis by determining the degree of susceptibility in two species of mud crabs, *Scylla olivacea* and *Scylla paramamosain*, both of which were identified by mitochondrial 16 S ribosomal gene analysis. We compared single-dose and serial-dose WSSV challenges on *S. olivacea* and *S. paramamosain*.

Findings: In a preliminary test using *S. olivacea* alone, a dose of 1×10^6 WSSV copies/g gave 100% mortality within 7 days. In a subsequent test, 17 *S. olivacea* and 13 *S. paramamosain* were divided into test and control groups for challenge with WSSV at 5 incremental, biweekly doses starting from 1×10^4 and ending at 5×10^6 copies/g. For 11 *S. olivacea* challenged, 3 specimens died at doses between 1×10^5 and 5×10^5 copies/g and none died for 2 weeks after the subsequent dose $(1 \times 10^6 \text{ copies/g})$ that was lethal within 7 days in the preliminary test. However, after the final challenge on day 56×10^6 copies/g), the remaining 7 of 11 *S. olivacea* (63.64%) died within 2 weeks. There was no mortality in the buffer-injected control crabs. For 9 *S. paramamosain* challenged in the same way, 5 (55.56%) died after challenge doses between 1×10^4 and 5×10^5 copies/g, and none died for 2 weeks after the challenge dose of 1×10^6 copies/g. After the final challenge (5×10^6 copies/g) on day 56, no *S. paramamosain* died during 2 weeks after the challenge, and 2 of 9 WSSV-infected *S. paramamosain* (22.22%) remained alive together with the control crabs until the end of the test on day 106. Viral loads in these survivors were low when compared to those in the moribund crabs.

Conclusions: *S. olivacea* and *S. paramamosain* show wide variation in response to challenge with WSSV. *S. olivacea* and *S. paramamosain* are susceptible to white spot disease, and *S. olivacea* is more susceptible than *S. paramamosain*. Based on our single-challenge and serial challenge results, and on previous published work showing that *S. serrata* is relatively unaffected by WSSV infection, we propose that susceptibility to white spot disease in the genus *Scylla* is species-dependent and may also be dose-history dependent. In practical terms for shrimp farmers, it means that *S. olivacea* and *S. paramamosain* may pose less threat as WSSV carriers than *S. serrata*. For crab farmers, our results suggest that rearing of *S. serrata* would be a better choice than *S. paramamosain* or *S. olivacea* in terms of avoiding losses from seasonal outbreaks of white spot disease.

Hypothesis

White spot syndrome virus (WSSV) is the world's most serious disease threat to all species of cultivated shrimp, and is also known to infect many other crustacean species that can act as carriers [1,2]. Among these carriers,

mud crabs have been considered to be a particularly dangerous threat to shrimp farms because they are generally believed (based on a report for the species *Scylla serrata*) to be highly tolerant to WSSV and remain infected for long periods of time without signs of disease [2-4]. We wished to test this hypothesis by determining the degree of susceptibility and tolerance to WSSV infection in common Thai species of *Scylla* other than *Scylla serrata*. To do so, it was first necessary for us to develop a mitochondrial 16 S rDNA method to

Full list of author information is available at the end of the article



^{*} Correspondence: Naraporn.S@chula.ac.th

¹Shrimp-Virus Interaction Laboratory, National Center for Genetic Engineering and Biotechnology, National Science and Technology Development Agency, Klong Luang, Pathumthani 12120, Thailand

distinguish among 4 *Scylla* species found in Thailand, because species determination by morphology alone remains controversial [5-8].

Scylla species identification by analysis of 16 S rDNA sequences

To develop a species identification method based on mitochondrial 16 S rDNA sequences, reference sequences of S. serrata (GenBank Accession Number AF109318), S. paramamosain (AF109319), S. olivacea (AF109321) and S. tranquebarica (AF109320) were used to design primers for polymerase chain reaction (PCR) analysis and sequencing. The PCR primer 16sar-L (5' cgcctgtttatcaaaaacat 3') was designed by Imai et al. [9], and primer 16sar-R (5' ggtctgaactcagatcacgt 3') was designed in this study. Each PCR reaction consisted of 10×PCR buffer, 0.75 mM MgCl₂, 0.1 mM dNTPs, 0.15 μM of each primer, 2.5 U taq DNA polymerase and 100 ng DNA in a total volume of 100 µl reaction. The thermocycling profile was 2 min at 94°C followed by 30 cycles of 94°C for 1 min, 45°C for 30 sec and 72°C 1.5 min. Sequencing was performed by Macrogen Inc., Seoul, Korea. Each sequence was confirmed manually via electropherogram analysis (BioEdit 7.0.0, Carlsbad, CA) [10].

This method was used with 31 Scylla samples arbitrarily collected from 500 g male mud crabs from Samutprakarn and Samutsongkram provinces, Thailand, during 3 different months in 2008. Since the Ethical Principles and Guidelines for the Use of Animals of the National Research Council of Thailand (1999) apply to vertebrates only and there is no official standard for invertebrates, we adapted its principles to crabs. We also followed the guidelines of the Australian, New South Wales state government for the humane harvesting of fish and crustaceans http://www.dpi.nsw.gov.au/ agriculture/livestock/animal-welfare/general/fish/shellfish with respect to details regarding the transport of the crabs and their laboratory maintenance. With respect to processing the crabs for histological analysis or for killing at the end of an experiment, the salt water/ice slurry method was used as recommended in the Australian guidelines. The amplicon sizes obtained using our 16 S rDNA PCR method were 562 base pairs (bp) for S. olivacea, S. serrata and S. paramamosain and 563 bp for S. tranquebarica. These sequences together with the corresponding regions from GenBank records of Scylla species (above), were compared using MEGA 3.1 software [10,11]. Pairwise distances were calculated by the p-distance model using the program default parameters, including different substitution rates for transitions and transversions and a uniform rate of substitution among sites [12]. Pairwise % nucleotide identities and p-distances indicated a close relationship between S. paramamosain and S. tranquebarica (95.7% nt identity and 0.041 p-distance), whereas S. olivacea and S. serrata showed a relatively lower percent nt identity and the greatest p-distances (90.8% nt identity and 0.086 p-distance) to the other species. Neighbor-joining trees calculated using the Kimura-2-parameter model and assuming constant nucleotide frequencies and rates of substitution among sites [12,13] revealed 4 clusters that clearly corresponded to the 4 species (Figure 1). Bootstrap replicates (= 1,000) were used to determine the percent confidence for each clustering branch. The topology for any branch with a bootstrap value of 95% or higher is considered true clustering [11]. S. tranquebarica was not found in our 31 samples while there were 17 S. olivacea, 13 S. paramamosain and only 1 S. serrata. Since there was only one specimen of S. serrata, it was not included in the ongoing tests with WSSV.

WSSV stock inoculum and virulence confirmation in shrimps

WSSV inoculum was kindly provided by the Shrimp Cultivation Research Center, Charoen Pokphand Group, Thailand. Number of WSSV copies was determined by real-time PCR (qPCR). For quantitation of WSSV stock and WSSV in the samples, DNA (100 ng) were used as the template in a total 20 µl reaction mixture containing 1× QuantiTect SYBR Green PCR Master Mix (Qiagen, the Netherlands) and 300 nM of each primer for qPCR using ABI 7500 SDS machine (Applied Biosystems, Foster City, CA, USA). Primers 229F1 (5' gatggaaacggtaacgaatctgaa 3') and 447R1 (5' cagagcctagtctatcaatcat 3') were designed from the WSSV genome (GenBank Accession No. AF440570) [14]. Each qPCR plate contained standard curve samples, triplicates of each DNA sample, and a no-template control. The thermocycling profile was 95°C for 15 min, followed by 40 cycles of 95° C for 15 s, 55°C for 30 s and 72°C for 45 s [14]. For all experiments, the specificity of the amplified products was verified by analyses of the dissociation curves to verify the melting temperature for each amplicon. The quantity was determined from the standard curve of Ct values and WSSV copy numbers. Results were expressed as mean copy numbers ± standard deviations (SDs) for triplicate samples.

For semi-quantitative estimation of WSSV copy numbers, the IQ2000™WSSV Detection and Prevention System (Farming IntelliGene Technology Corporation, Taipei, Taiwan) was used. Using 100 ng of total DNA as the template, infections could be classified as absent, very light, light, moderate and severe based on 1.5% agarose gel electrophoresis patterns of PCR amplicons, and these were approximately equal to the following respective WSSV copy numbers in the 100 ng template: 0 to <10, 10 to <20, 20 to <200, 200 to <2,000 and 2,000 to <20,000.

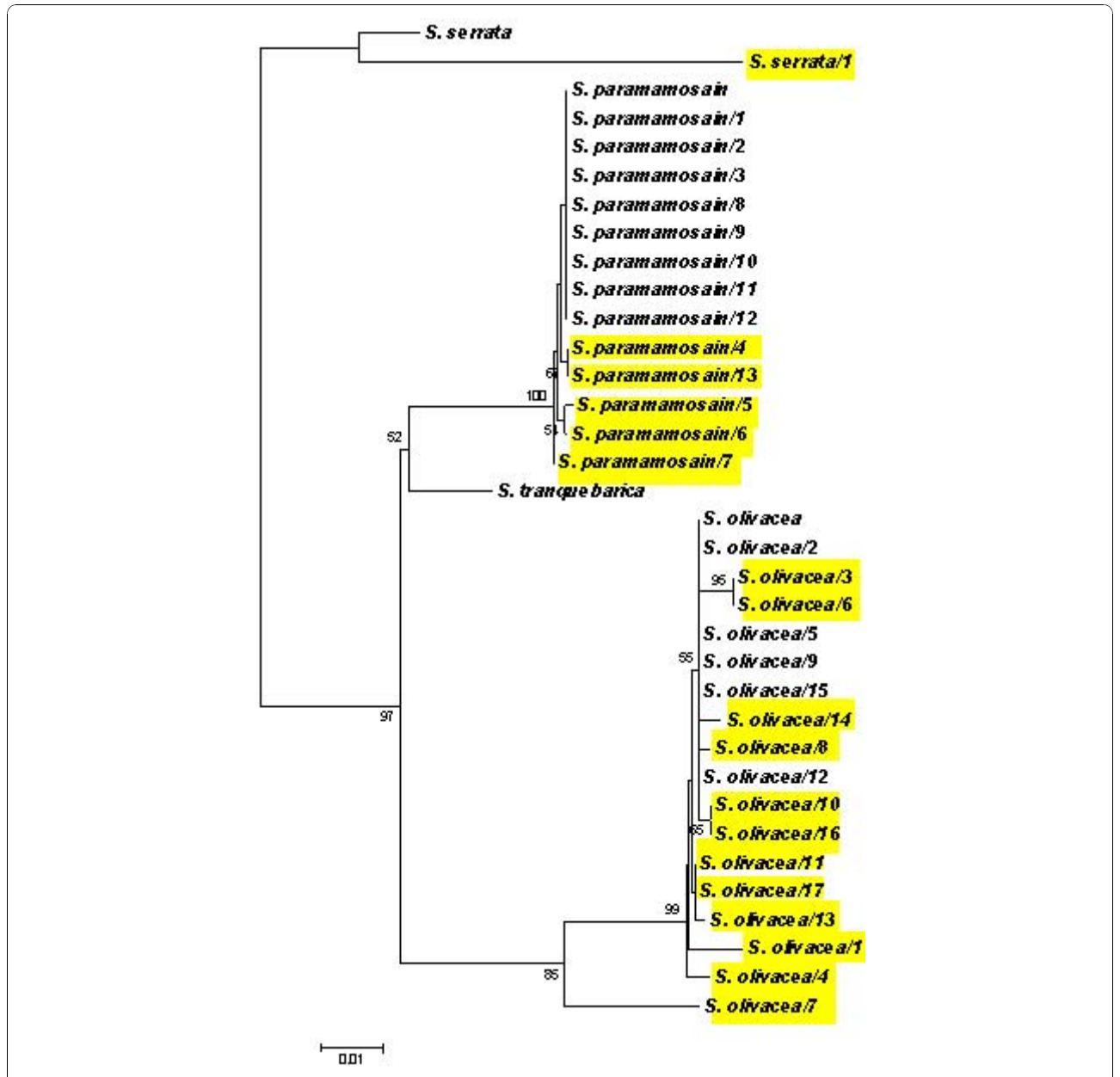


Figure 1 Phylogenetic relationship of 31 representative *Scylla* **specimens from Samutprakarn and Samutsongkram provinces of Thailand.** A neighbor-joining tree was constructed using mitochondrial 16 S rDNA sequences of reference *S. serrata, S. paramamosain, S. tranquebarica* and *S. olivacea,* and 31 recent *Scylla* species collected from Samutprakarn and Samutsongkram provinces of Thailand. Yellow highlights indicate crabs with at least 1 nt difference compared with those of the respective reference species. The value at each node is the percent bootstrap confidence calculated from 1000 bootstrap resamplings. Bootstrap values of 50% and below have been omitted in the figure. Each branch distance corresponds to sequence divergence.

To measure WSSV loads in shrimp, hemolymph was withdrawn from the ventral sinus into a syringe containing anticoagulant I (ACI) (0.45 M NaCl, 0.1 M glucose, 30 mM Na-citrate, 26 mM citric acid, 10 mM EDTA, pH 7.0) [15] in a 1:2 volume-to-volume ratio. DNA was extracted following the manufacturer's protocols using a DNeasy Blood & Tissue Kit (Qiagen, Valencia, California, USA). The DNA concentration and quality were

measured by spectrophotometry at A_{260} and A_{280} , and the amount of WSSV in the samples was determined as described above.

To verify virulence of the WSSV stock, 2 specific pathogen-free (SPF) whiteleg shrimp *P. vannamei* and 6 SPF black tiger shrimp *P. monodon* were injected with 5×10^6 copies/g tissue at the first abdominal segment. Shrimp mortality for *P. vannamei* and *P. monodon* was

50% and 100%, respectively, within 3-4 days after injection and moribund shrimp gave IQ2000 test results for severe WSSV infection levels. Matching qPCR results ranged from 2 \times 10⁴ - 1.3 \times 10⁶ copies/100 ng DNA (data not shown). This was equivalent to approximately 2 \times 10⁴ - 1.3 \times 10⁶ WSSV copies in 33.33 μ l of infected shrimp hemolymph.

These results were similar to those previously published for these and other species of penaeid shrimp that usually show 100% mortality within 5-10 days after injection with similar doses of WSSV [16].

Preliminary, single-dose challenge with Scylla olivacea

Because injection is considered an effective route of WSSV infection in crabs [4], different WSSV copies per gram of crab tissue in a total sterile phosphate buffer saline (PBS) volume of 300 μ l was injected into each crab at the coxa of the right swimming leg using a 26G1 syringe (Nipro Corporation Ltd.). A preliminary single-dose challenge test with 34 male *S. olivacea* was carried out to determine appropriate viral challenge doses for crabs. They were divided into three groups. One group (n = 9) was injected with a single dose of 1 × 10⁵ WSSV copies per g, one group (n = 13) with 1 × 10⁶ WSSV copies per g and one control group (n = 12) with buffer solution.

At the low injection dose (1×10^5) , 4 of 9 (44%) died within 7 days while 5 of 9 (56%) survived for more than 30 days. However, at a higher dose (1×10^6) , 6 of 13 died on day 3 post injection (46% mortality), 4 more died on day 4 (77% cumulative mortality), 2 more on day 5 (92% cumulative mortality) and 1 on day 7 (100% cumulative mortality in 7 days). None of the 12 buffer-injected crabs died over the 30 day experimental period. These results indicated that a single, high dose challenge with the WSSV inoculum was lethal for *S. olivacea* as it was for shrimp. This contrasted markedly with results from a previous report in which *S. serrata* challenged with WSSV showed severe WSSV lesions by histopathological analysis but no mortality [1,3,17].

Serial-dose challenge protocol

Male mud crabs (500 g) were collected from Samutprakarn and Samutsongkram provinces, Thailand, and species was determined by 16 S rDNA analysis as described above. Each crab was free of WSSV, yellow head virus (YHV) and infectious hypodermal and hematopoietic necrosis virus (IHHNV) as determined using standard commercial kits for nested PCR and RT-PCR detection (IQ 2000 detection system, Gene Reach, Taiwan). Individual crabs were cultivated in separate plastic containers at room temperature with aeration [18]. Every 24-30 h, crabs were fed with boiled fish at 10% of their body

weight, and artificial seawater at 28 parts per thousand (ppt) salinity was replaced to the level where the crabs still had some area to come out of the water [1,18].

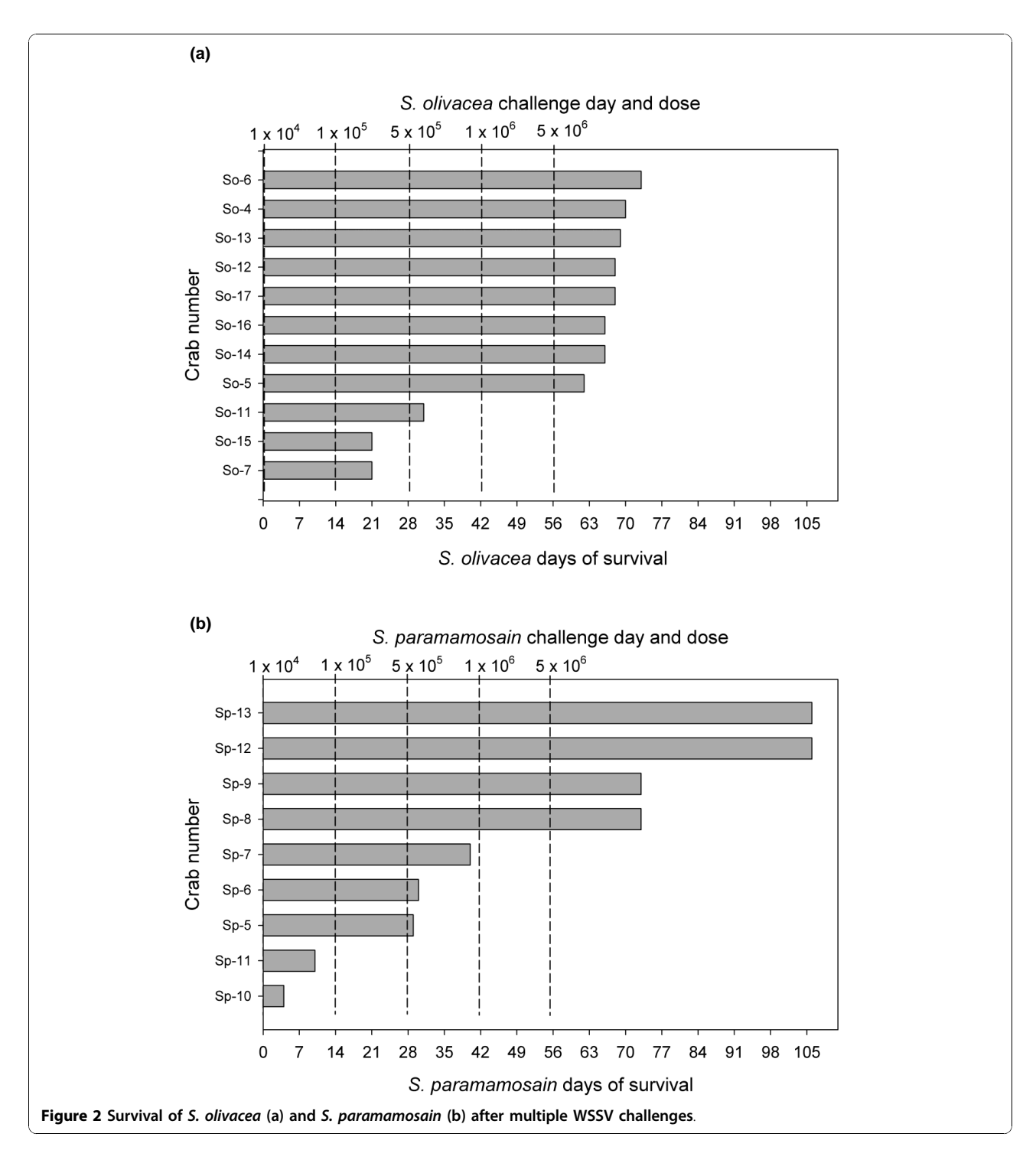
For the challenge tests with each species, 18 crabs were acclimatized for 1-2 weeks after which it was expected that 10-12 each would be used for WSSV challenge and 5-6 each for PBS buffer-injected controls. However, since only 30 (not 36) remained in sufficiently good health for testing at the end of acclimatization (17 S. olivacea and 13 S. paramamosain), they were divided into 20 crabs (11 S. olivacea and 9 S. paramamosain) for challenge with WSSV, and 10 (6 S. olivacea and 4 S. paramamosain) as controls. They were numbered sequentially for each species (So 1 to 17 and Sp 1 to 13) but selected arbitrarily for inclusion in challenge or control groups. WSSV challenge began with 1×10^4 WSSV copies/g at day 0 followed every 14 days by increasing doses of 1×10^5 , 5×10^5 , 1×10^6 and ending with 5×10^6 10⁶ WSSV copies/g at day 56. The crabs were observed for further 50 days after the final challenge dose (a total of 106 days for the whole challenge experiment).

For these tests, all the buffer-injected control crabs were healthy as defined by no appetite loss, no weight loss, reactive swimming and walking legs, and no mortality throughout the experimental period (106 days) plus the period of 4-10 days during which the crabs were acclimatized, screened for specific pathogens and subjected to PCR and sequencing for species identification. None of the controls for either species gave positive results for WSSV using the IQ2000 test kit, qPCR or histological analysis. For the test crabs given multiple challenges with WSSV, there were generally three types of outcomes as follows: (i) moribund at low dose ($< 10^6$ copies/g), (ii) moribund at high dose (5×10^6 copies/g), and (iii) survival at high dose (5×10^6 copies/g).

To quantify WSSV in each crab by qPCR or test kit (see above), hemolymph was withdrawn at the coxa of the right swimming leg using a 26G1" syringe (Nipro Corporation Limited, Bangkok, Thailand) containing the same anticoagulant used for shrimp above. DNA extraction was also carried out in the same manner.

Serial-dose challenge with Scylla olivacea

Of the 11 *S. olivacea* specimens used for the serial-challenges with WSSV (Figure 2a), there was no mortality in 14 days following the initial 1×10^4 challenge dose, while 2 specimens died 7 days following the $2^{\rm nd}$ challenge dose (1×10^5 copies/g) and 1 died 3 days following the third challenge dose (5×10^5 copies/g). Curiously, no mortality occurred during the 2-week period following the dose of 1×10^6 copies/g, despite the fact that the dose was 100% lethal in the preliminary single challenge test with this species. All the remaining 8 crabs died within 7 to 17 days following the $5^{\rm th}$ (highest) challenge



dose $(5\times10^6 \text{ copies/g})$. The longest survival was for one specimen at 73 days after the initial challenge and the mean time to death was 55.9 ± 20.6 days and the Kaplan-Meier survival probability [19] was 0.63 for 63 days and 0 for 70 days. For this species, the majority of the crabs fell into two rough groups, one that showed mortality after a relatively low challenge dose of WSSV

and one that showed mortality only after the highest dose $(5\times10^6 \text{ copies/g})$.

All the challenged *S. olivacea* gave positive reactions for severe WSSV infections using the IQ2000 test kit, except for the 2 crabs that died after the lowest challenge dose of 1×10^5 copies/g. These gave negative results with the kit. Their WSSV copies were also below

the qPCR detection limit. For 8 of the 9 IQ2000 test kit-positive moribund samples, results corresponded to those for qPCR where viral levels ranged from 3.1×10^7 to 3.4×10^9 WSSV copies per 100 ng total DNA (mean 6.5×10^8 copies per 100 ng total DNA). Extracted DNA of 100 ng represented a fresh muscle tissue weight of approximately 0.15 mg, so qPCR results would have to be multiplied by 6.7×10^3 to obtain viral loads per g fresh crab tissue. Curiously, one sample (So6) gave a reaction for severe infection with the test kit but a qPCR result for only 7×10^3 WSSV copies per 100 ng total DNA. Of the 9 specimens that gave results for severe reactions with the kit, 7 were examined histologically and all were positive with typical WSSV lesions (Figure 3) except for So6.

In addition, hemocytes of 2 samples (So5 and So13) were examined by confocal microscopy for the presence of WSSV by immunohistochemistry. Hemolymph was collected in 1:1 vol./vol. of hemolymph fixative (0.45 M NaCl and 4% formalin in sterile distilled water) and then further fixed with 4% paraformaldehyde in PBS, and permeabilized with 0.1% Triton X-100 (Acros Organics, Morris Plains, NJ, USA) for immunofluorescence analysis using a polyclonal antibody raised against WSSV recombinant VP28 (rVP28) envelope protein. Detection was achieved using a secondary antibody labeled with Alexa Fluor 488 (Molecular Probes, Eugene, OR, USA) as previously described [20]. Negative controls included hemocytes from buffer-injected crabs stained with the anti-WSSV polyclonal antibody, hemocytes from infected crabs with no anti-WSSV polyclonal antibody label, and hemocytes from infected crabs that were stained with a polyclonal antibody raised against monodon baculovirus (MBV), which is not known to infect crabs. TO-PRO-3 (Molecular Probes) was used for nucleic acid counterstaining. Immunofluorescentlabeled cells were analyzed by an FV1000 confocal laser scanning microscope (Olympus, Tokyo, Japan). Results showed immunopositive signals in the cytoplasm for the majority of the hemocytes (Figure 4b).

The multiple challenge group at the highest challenge dose also died, gave test kit results for severe WSSV infections and also showed severe histopathology typical of WSSV. More difficult to explain is the mortality of the 2 *S. olivacea* specimens that died after an injection dose of 1 × 10⁵ or fewer WSSV copies per g and gave negative results for WSSV by both test-kit assay and qPCR. We assume that they died as a result of some undetermined complication resulting from the WSSV injection, but not because of WSSV alone and not because of the injection process itself, since none of the control crabs died after buffer injections. Similar examples occurred with *S. paramamosain* (below). Most of the *S. olivacea* specimens were not examined histologically because the few examined gave

consistent results for severe infections by histopathology and qPCR. We cannot explain the disparity between the test-kit result for severe WSSV infection and the qPCR result for a low WSSV load in specimen So6.

In summary, the overall results suggested that S. olivace was generally as susceptible to mortality from WSSV as P. vannamei and P. monodon. However, the fact that approximately 50% of the S. olivacea specimens died within 3 days in the single dose challenge at $1 \times$ 10⁶ copies of WSSV per g but that 7 of 11 (63.64%) survived for 2 weeks after the same dose in the multiple challenge test indicates that a prior infection with WSSV could aid in the ability of the crabs to better survive a subsequent challenge. This is not surprising in the light of the fact that shrimp survivors from WSSV outbreak ponds have been shown to survive a WSSV challenge dose sufficient to kill uninfected shrimp [21,22], and that prior injection of shrimp with inactivated WSSV can result in improved survival upon subsequent challenge [23]. S. olivacea would be a good model for a molecular study on the comparative response of multiple-challenge crabs that survive the WSSV dose $(1 \times 10^6 \text{ copies/g})$ that was sufficient to kill naïve crabs.

Serial-dose challenge with Scylla paramamosain

Of 9 S. paramamosain specimens used for serial WSSV challenges (Figure 2b), 2 specimens died within 2 weeks after the 1st challenge dose (1×104). There was no additional mortality in the 2-week interval after the 2nd challenge dose (1×10^5) , but 2 specimens died within 2 days and 1 specimen within 12 days after the 3rd challenge dose (5×10^5) . As with S. olivacea, no subsequent mortality occurred within two weeks after challenge with a dose of 1×10^6 copies/g. Then, 2 specimens died within 17 days after the 5th and highest challenge dose (5×10⁶), while the two remaining crabs were still alive and active at the end of the experiment on day 106. The mean time to death for those that died was 37.0 ± 27.5 days, and this was not significantly different (p = 0.11) from that for S. olivacea (55.9 \pm 20.6). The Kaplan-Meier survival probability of S. paramamosain for 63 days was 0.44 (0.63 for S. olivacea) but for 70 to 106 days was 0.22 (0 for S. olivacea). Similar to S. olivacea, there was one group of crabs that died after low challenge doses and one (22.22%) that died after the highest challenge dose. Unlike S. olivacea, there was an additional group (22.22%) that did not die, even at the highest challenge dose. In addition, S. paramamosain showed a pattern of proportionally higher mortality at low WSSV doses and proportionally lower mortality at high doses, a pattern that was opposite to that for S. olivacea.

For *S. paramamosain*, the moribund specimens challenged with doses of 5×10^5 or less gave negative

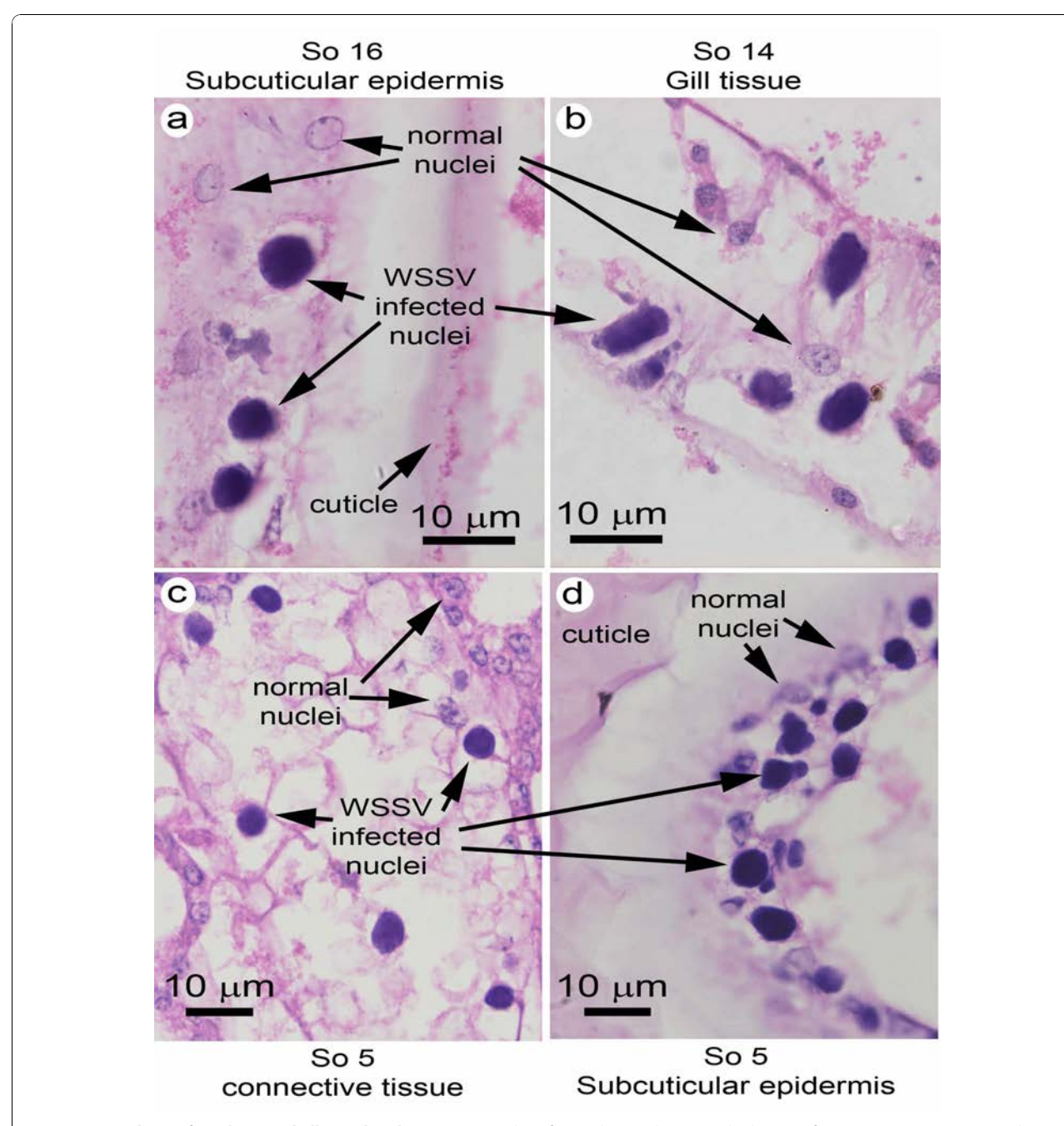


Figure 3 Histology of S. olivacea challenged with WSSV. Examples of typical WSSV lesions at high magnification in various tissues, indicating heavy infections consistent with PCR test kit and real-time PCR results.

reactions for WSSV infections using the IQ2000 test kit, negative qPCR results (i.e., below the detection limit) and negative histopathology for WSSV lesions (Figure 5a). Of the three specimens that died after the challenge dose of 5×10^5 (i.e., Sp5, 6, 7) histological examination revealed the presence of severe lesions by other pathogens that may have been the cause of mortality (Figure 5b-d). In Sp5, there were severe lesions in tubule

epithelial cells of the hepatopancreas that showed parasite nuclei of large and small sizes, resembling those of a microsporidian undergoing spore development [24] (Figure 5b). In Sp6, the hepatopancreas had severe lesions of a different type, this time in the connective tissue cells showing very large, eosinophilic, viral-like, cytoplasmic inclusions and accompanied by hemocytic aggregation (Figure 5c). In Sp7, the connective tissue of

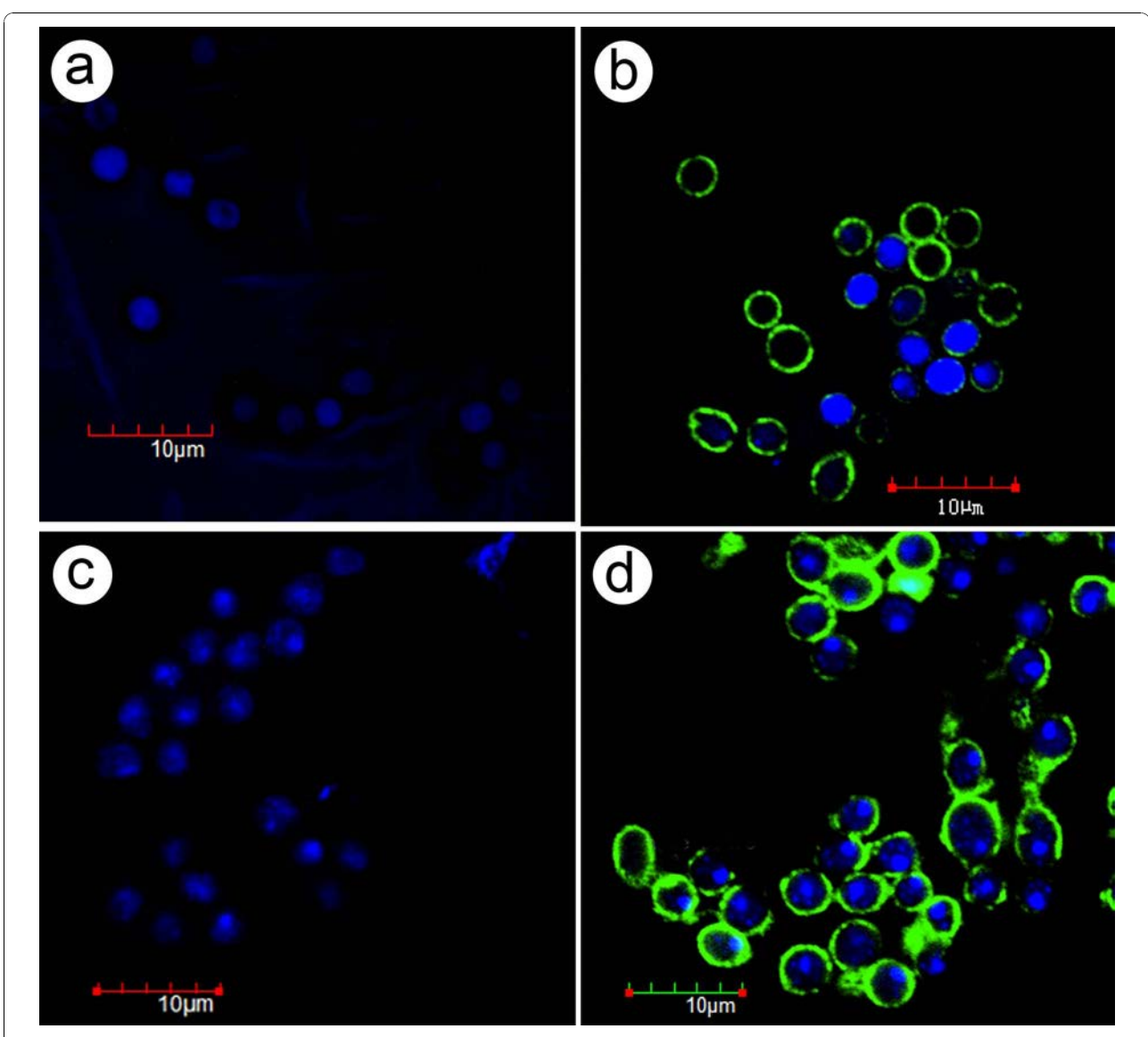


Figure 4 Immunohistochemical analysis of crab hemocytes. (a) Hemocytes of a normal *S. olivacea* specimen showing large (non-condensed) nuclei. (b) Hemocytes of *S. olivacea* (So5 day 59) infected with WSSV showing positive immunofluorescence (green) for WSSV in the cytoplasm. (c) Hemocytes of normal *S. paramamosain* specimen showing large (non-condensed) nuclei. (d) Hemocytes of *S. paramamosain* (Sp12 day 82) showing positive immunofluorescence for WSSV in the cytoplasm and condensed and fragmenting nuclei.

the hepatopancreas, muscle and epidermis showed large numbers of small, magenta, viral-like, cytoplasmic inclusions often adjacent to nuclei (Figure 5d). The severity and number of these lesions were consistent with possible cause of mortality. Hemocytes of these specimens examined by confocal microscopy (as described above) revealed positive immunofluorescence for WSSV in the cytoplasm (Figure 4d).

After the highest challenge dose of 5×10^6 copies per g, the 2 moribund crab specimens gave IQ2000 test kit results for severe WSSV infections and this corresponded to the qPCR results of 1.2×10^9 and 8.9×10^8

WSSV copies per 100 ng total DNA. The 2 remaining crabs that still survived at the end of the experiment (106 days) gave IQ2000 test kit results for a medium infection and a medium-to-severe infection, and the corresponding qPCR results gave 2.9×10^3 and 5.4×10^3 WSSV copies per 100 ng total DNA, respectively. None of these high-dose specimens were examined for WSSV histopathology, but the 2 crabs that survived to the end of the experiment (106 days) showed positive immunofluorescence in the cytoplasm of very few hemocytes on day 59 (data not shown) and most of the hemocytes on day 82 (Figure 4d), which was 26 days after the highest

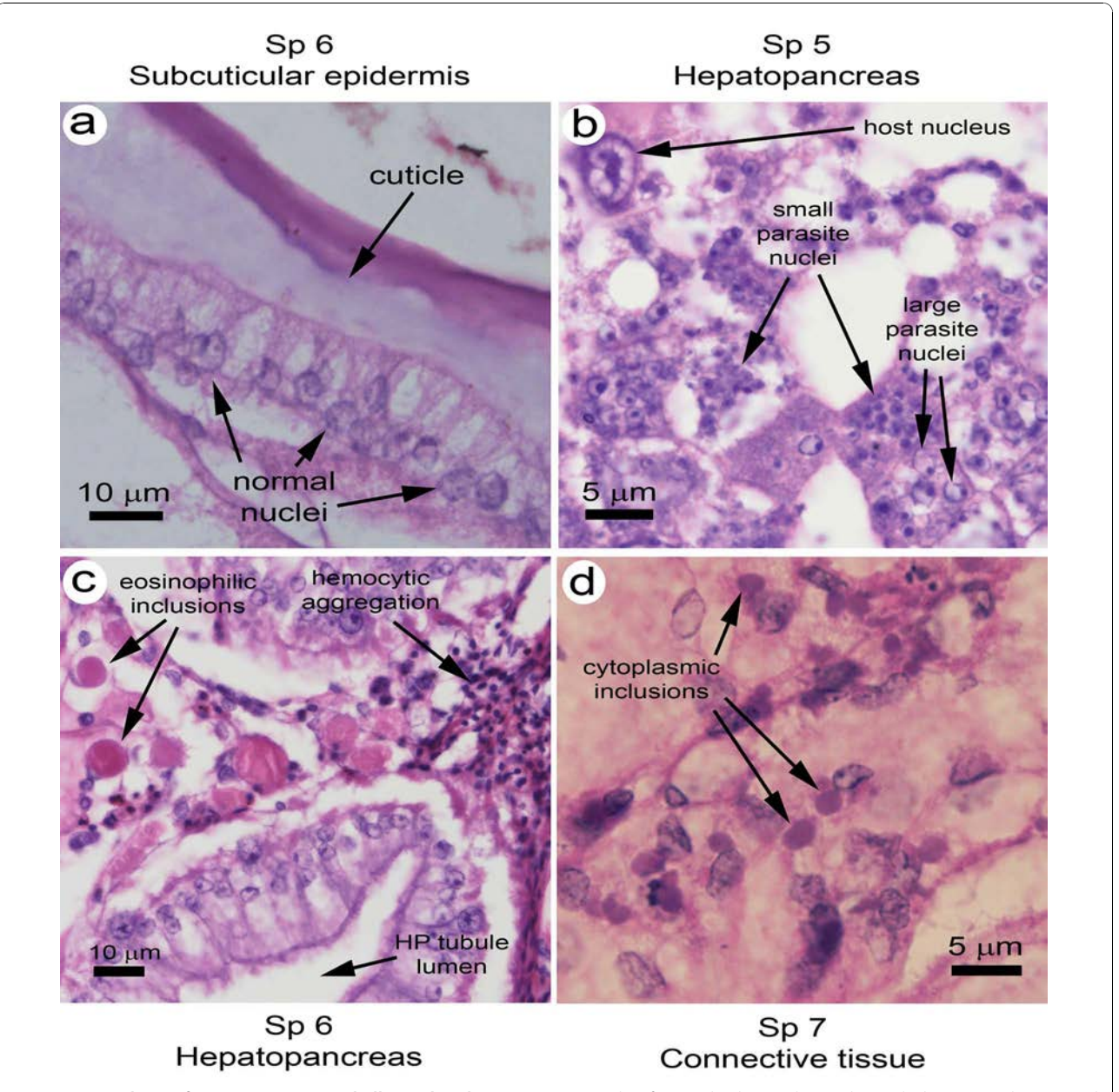


Figure 5 Histology of S. paramamosain challenged with WSSV. (a) Example of normal subcuticular epidermis lacking WSSV lesions and consistent with the negative PCR test kit and real time PCR results. (b) Example of a hepatopancreatic tissue lesion resembling those caused by crustacean microsporidians undergoing spore development. (c) Example of a hepatopancreatic lesion showing large eosinophilic cytoplasmic inclusions of unknown nature and also hematocytic aggregation typical of severe bacterial infections. (d) Example of small cytoplasmic inclusions adjacent to the nuclei of connective tissue cells.

dose challenge on day 56. The nuclei of these hemocytes were condensed and often fragmented possibly indicating apoptosis leading to hemocyte depletion as previously reported for shrimp infected with WSSV [25].

Results for *S. paramamosain* are more difficult to interpret than those for *S. olivacea* because all 5 crabs that died at injection doses lower than 1×10^6 WSSV copies per g gave negative test results for WSSV

infection using both the IQ2000 kit and qPCR. If they had died from WSSV, kit reactions for severe WSSV infections and qPCR results indicating high loads of WSSV would have been expected. Histopathological analysis for 3 of the 5 specimens revealed no WSSV lesions but instead severe lesions from at least 3 unknown pathogens that could have been the cause of their death. As with the 2 similar, low-dose challenge

S. olivacea specimens described above, we assume that these *S. paramamosain* died as a result of some undetermined complication resulting from the WSSV injection, but not because of WSSV alone and not because of the injection process itself, since none of the control crabs died after buffer injections.

Although the S. paramamosain specimens did not show typical WSSV lesions with enlarged basophilic nuclei in normal WSSV-target tissues such as the subcuticular epidermis and gills, they did show immunopositive hemocytes, most with condensed or karyorrhectic nuclei indicative of apoptosis as previously reported for WSSV infections in shrimp [25]. In addition, the two specimens (Sp12 and Sp13 representing 22.22% of the crabs) that survived the highest WSSV challenge dose showed WSSV immunopositive hemocytes after challenge on day 56, and the proportion of positive cells was higher on day 87 than on day 59, indicating that viral replication had occurred in the interim. For these specimens, the PCR test kit results were below the severe level and the WSSV loads by qPCR were low. Furthermore, the immunopositive reaction was in the hemocyte cytoplasm only, while WSSV virions are normally assembled in the nucleus. Using these facts to attempt to explain our results, we speculate that hemocytes may be the prime target for WSSV in S. paramamosain and that the virus may replicate there, but induce apoptosis before mature virions are assembled. The resulting depletion of hemocytes could impair the host ability to combat pre-existing infections or new infections by other pathogens, and that would explain the variety in the histopathology seen in the moribund S. paramamosain we examined. It would also explain why there was no mortality from other infectious agents in the control crabs injected with buffer only. At the same time, it would also suggest that the hemocytes play an important role in the S. paramamosain response to WSSV, and that they normally limit or clear WSSV, except when overwhelmed by a sufficient challenge dose. Thus, S. paramamosain challenged with WSSV may be a good model organism to study the process of WSSV clearance in crabs.

Overall comparison

In summary, the results revealed great individual variation in the response of *S. olivacea* and *S. paramamosain* to WSSV. At the same time, both species are susceptible to white spot disease, in contrast with *S. serrata* that has been reported to show no mortality even in the presence of extensive WSSV lesions. In addition, *S. olivacea* was more susceptible to disease than *S. paramamosain*, since its survival probability at 70 days post-infection was 0 while that for *S. paramamosain* was 0.22. Thus, based on previous published work for *S. serrata* and on

our results, we propose that susceptibility to white spot disease in the genus *Scylla* is species-dependent but may also be dose-history dependent as seen with *S. olivacea*. In practical terms for shrimp farmers, our results show that *S. olivacea* and *S. paramamosain* may be infected with WSSV for periods of several weeks or more and potentially act as carriers during that interval, but that they might pose less threat than *S. serrata* that is apparently unaffected by WSSV infection. For crab farmers, our results suggest that rearing of *S. serrata* would be a better choice than *S. paramamosain* or *S. olivacea* in terms of avoiding losses from seasonal WSSV outbreaks.

Acknowledgements

This work was supported by the National Center for Genetic Engineering and Biotechnology (BIOTEC), Thailand Research Fund (TRF), and Mahidol University.

Author details

¹Shrimp-Virus Interaction Laboratory, National Center for Genetic Engineering and Biotechnology, National Science and Technology Development Agency, Klong Luang, Pathumthani 12120, Thailand. ²Center of Excellence for Shrimp Molecular Biology and Biotechnology, Mahidol University, Rama 6 Road, Bangkok 10400, Thailand. ³Institute of Molecular Biosciences, Mahidol University, Salaya Campus, Nakhonpathom 73170, Thailand. ⁴Department of Biotechnology, Faculty of Science, Mahidol University, Rama 6 Road, Bangkok 10400, Thailand. ⁵Department of Microbiology, Faculty of Science, Chulalongkorn University, Bangkok 10330, Thailand.

Authors' contributions

NS participated in the conception and design of the study, carried out all experimental work, collected and analyzed the data and contributed to writing the manuscript. SM participated in the preliminary *S. olivacea* test. CK participated in the design of the study. KS conceived and participated in the design of the study. TWF did the histopathological analysis of the WSSV-infected crabs and participated in data analysis and manuscript writing. All authors read and approved the final manuscript.

Competing interests

The authors declare that they have no competing interests.

Received: 22 June 2010 Accepted: 20 November 2010 Published: 20 November 2010

References

- Rajendran KV, Vijayan KK, Santiago TC, Krol RM: Experimental host range and histopathology of white spot syndrome virus (WSSV) infection in shrimp, prawns, crabs and lobsters from India. J Fish Dis 1999, 22:183-191.
- Flegel TW: Detection of major penaeid shrimp viruses in Asia, a historical perspective with emphasis on Thailand. Aquaculture 2006, 258:1-33.
- Kanchanaphum P, Wongteerasupaya C, Sitidilokratana N, Boonsaeng V, Panyim S, Tassanakajon A, Withyachumnarnkul B, Flegel TW: Experimental transmission of white spot syndrome virus (WSSV) from crabs to shrimp Penaeus monodon. Dis Aquat Org 1998, 34:1-7.
- Supamattaya K, Hoffmann RW, Boonyaratpalin S, Kanchanaphun P: Experimental transmission of white spot syndrome virus (WSSV) from black tiger shrimp Penaeus monodon to the sand crab Portunus pelagicus, mud crab Scylla serrata and krill Acetes sp. Dis Aquat Org 1998, 32:79-85.
- Estampador EP: Studies on Scylla (Crustacea: Portunidae), 'I. Revision of the genus.". Philipp J Sci 1949, 78:95-108.
- Stephenson W, Campbell B: The Australian Portunids (Crustacea: Portunidae) IV. Remaining genera. Aust J Mar Freshw Res 1960, 11:73-122.
- Overton JL, Macintosh DJ, Thorpe RS: Multivariate analysis of the mud crab Scylla serrata (Brachyura: Portunidae) from four locations in Southeast Asia. Mar Biol 1997, 128:55-62.

- Gopurenko D, Hughes JM: Regional patterns of genetic structure among Australian populations of the mud crab Scylla serrata (Crustacea: Decapoda): evidence from mitochondrial DNA. Mar Freshw Res 2002, 53:849-857.
- Imai H, Cheng J, Hamasaki K, Numachi K: Identification of four mud crab species (genus Scylla) using ITS-1 and 16 S rDNA markers. Aquat Living Resour 2004. 17:31-34.
- Somboonna N, Mead S, Liu J, Dean D: Discovering and differentiating new and emerging clonal populations of Chlamydia trachomatis with a novel shotgun cell culture harvest assay. Emerg Inf Dis 2008, 14:445-453.
- Kumar S, Tamura K, Nei M: MEGA3: Integrated software for molecular evolutionary genetics analysis and sequence alignment. Brief Bioinform 2004, 5:150-163.
- Nei M, Kumar S: Molecular evolution and phylogenetics New York, Oxford University Press: 2000.
- Kimura M: A simple method for estimating evolutionary rates of base substitutions through comparative studies of nucleotide sequences. J Mol Evol 1980. 16:111-120.
- Srisala J, Tacon P, Flegel TW, Sritunyalucksana K: Comparison of white spot syndrome virus PCR-detection methods that use electrophoresis or antibody-mediated lateral flow chromatographic strips to visualize PCR amplicons. J Virol Meth 2008, 153:129-133.
- Söderhäll K, Smith VJ: Separation of the haemocyte populations of Carcinus maenas and other marine decapods, and prophenoloxidase distribution. Dev Comp Immunol 1983, 7:229-239.
- Flegel TW: Special topic review: major viral diseases of the black tiger prawn (*Penaeus monodon*) in Thailand. World J Microbiol Biotech 1997, 13:433-442.
- Flegel TW: Update on viral accommodation, a model for host-viral interaction in shrimp and other arthropods. Dev Comp Immunol 2007, 31:217-231.
- Lin YC, Vaseeharan B, Chen JC: Identification of the extracellular copperzinc superoxide dismutase (ecCuZnSOD) gene of the mud crab Scylla serrata and its expression following beta-glucan and peptidoglycan injections. Mol Immunol 2008, 45:1346-1355.
- Kaplan EL, Meier P: Nonparametric estimation from incomplete observations. J Am Stat Assoc 1958, 53:457-481.
- Sriton A, Kanthong N, Gangnonngiw W, Sriurairatana S, Ubol S, Flegel TW: Persistent expression of shrimp-virus antigens in two insect cell lines challenged with two shrimp viruses. Fish Pathol 2009, 44:86-93.
- Venegas CA, Nonaka L, Mushiake K, Nishizawa T, Muroga K: Quasi-immune response of *Penaeus japonicus* to penaeid rod-shaped DNA virus (PRDV). *Dis Aquat Ora* 2000. 42:83-89.
- Wu JL, Nishioka T, Mori K, Nishizawa T, Muroga K: A time-course study on the resistance of *Penaeus japonicus* induced by artificial infection with white spot syndrome virus. *Fish Shellfish Immunol* 2002, 13:391-403.
- 23. Singh ISB, Manjusha M, Pai SS, Philip R: *Fenneropenaeus indicus* is protected from white spot disease by oral administration of inactivated white spot syndrome virus. *Dis Aquat Org* 2005, **66**:265-270.
- Flegel TW, Pasharawipas T: A proposal for typical eukaryotic meiosis in microsporidians. Can J Microbiol 1995, 41:1-11.
- Wongprasert K, Khanobdee K, Glunukarn S, Meeratana P, Withyachumnarnkul B: Time-course and levels of apoptosis in various tissues of black tiger shrimp *Penaeus monodon* infected with white spot syndrome virus. *Dis Aquat Org* 2003, 55:3-10.

doi:10.1186/1756-0500-3-315

Cite this article as: Somboonna *et al.*: Mud crab susceptibility to disease from white spot syndrome virus is species-dependent. *BMC Research Notes* 2010 **3**:315.

Submit your next manuscript to BioMed Central and take full advantage of:

- Convenient online submission
- Thorough peer review
- No space constraints or color figure charges
- Immediate publication on acceptance
- Inclusion in PubMed, CAS, Scopus and Google Scholar
- Research which is freely available for redistribution

Submit your manuscript at www.biomedcentral.com/submit



BMB Reports

Isoleucine at position 150 of Cyt2Aa toxin from *Bacillus* thuringiensis plays an important role during membrane binding and oligomerization

Wanwarang Pathaichindachote¹, Amporn Rungrod¹, Mongkon Audtho¹, Sumarin Soonsanga¹, Chartchai Krittanai² & Boonhiang Promdonkoy^{1,*}

¹National Center for Genetic Engineering and Biotechnology, National Science and Technology Development Agency, 113 Phahonyothin Road, Khlong Nueng, Khlong Luang, Pathum Thani 12120, ²Institute of Molecular Biosciences, Mahidol University, Salaya Campus, Nakhonpathom 73170, Thailand

Cyt2Aa2 is a mosquito larvicidal and cytolytic toxin produced by Bacillus thuringiensis subsp. darmstadiensis. The toxin becomes inactive when isoleucine at position 150 was replaced by alanine. To investigate the functional role of this position, lle150 was substituted with Leu, Phe, Glu and Lys. All mutant proteins were produced at high level, solubilized in carbonate buffer and yielded protease activated product similar to those of the wild type. Intrinsic fluorescence spectra analysis suggested that these mutants retain similar folding to the wild type. However, mosquito larvicidal and hemolytic activities dramatically decreased for the I150K and were completely abolished for I150A and I150F mutants. Membrane binding and oligomerization assays demonstrated that only I150E and 1150L could bind and form oligomers on lipid membrane similar to that of the wild type. Our results suggest that amino acid at position 150 plays an important role during membrane binding and oligomerization of Cyt2Aa2 toxin. [BMB Reports 2013; 46(3): 175-180]

INTRODUCTION

Bacillus thuringienesis is a rod shape, Gram-positive, soil bacterium that can produce insecticidal crystal proteins specifically toxic to various insect larvae (1). The crystal proteins could be divided into 2 major families, Cry and Cyt toxins, which have different molecular structures and target insects (2). Cyt toxins are synthesized by some strains of *B. thuringiensis* and highly toxic against larvae of dipteran insects such as mosquitoes and

*Corresponding author. Tel: +66-2564-6700; Fax: +66-2564-6707; E-mail: boonhiang@biotec.or.th http://dx.doi.org/10.5483/BMBRep.2013.46.3.100

Received 4 May 2012, Revised 26 June 2012, Accepted 3 September 2012

Keywords: Bacillus thuringiensis, Cyt toxin, Membrane binding, Mutagenesis, Oligomerization

blackflies (1, 3, 4). Toxins in this group are produced in the form of inactive crystalline inclusion or protoxin. Upon ingestion by susceptible larvae, the inclusion is solubilized in alkaline condition of the midgut and proteolytic processed by gut proteases to yield the active toxin (5). Inclusions could be solubilized using alkaline buffer and activated by proteases *in vitro*. In addition, the activated toxin exhibits cytolytic activity against broad range of cells including erythrocytes (5-7).

The mechanism of action of the Cyt toxin is thought to involve a cascade of several events leading to insect death after ingestion. There are two possible models currently proposed for the Cyt toxin action. The pore-forming model suggests that binding of the active toxin to cell membrane induces conformational changes and oligomerization of the toxin molecules which finally leads to osmotic imbalance and cell lysis (8, 9). Alternative model proposes that the toxin may bind to the cell membrane and accumulate until reaching a critical number, and then the toxin complex would perturb cell membrane via a detergent-like mechanism (10, 11). Although the mechanism of Cyt toxin is still a controversy, the site of action of both models is the cell membrane that definitely involves membrane binding, conformational changes and oligomerization processes.

To date, more than 30 Cyt toxins have been identified (2, 12). Amino acid sequence alignment of Cyt toxins showed that they share high homology and therefore are expected to have similar 3D structures. In deed, X-ray crystallographic analyses revealed that structures of the protoxin of Cyt2Aa, Cyt1Aa and the activated Cyt2Ba are highly similar in which the toxin is a single domain protein consisting of two outer layers of α -helix hairpins flanking a core of mixed β -sheets (13-15). Membrane binding motif could not be identified from these structures. However, the motif could be formed during the toxin undergoes conformational changes upon approaching the membrane.

Previous studies showed that substitution at Ile150 in Cyt2Aa toxin with Ala resulted in a total loss of activity although the mutant protein retains similar overall structure, solubility and proteolytic processing similar to the wild type (16). This suggested that amino acid at this position plays important role during in-

toxication either at the step of membrane binding, conformational changes or oligomerization. To investigate the functional role of this position, Ile150 was replaced by Leu, Phe, Glu and Lys. Comparative biochemical and biological studies of mutants to the wild type suggested that Ile150 in Cyt2Aa plays significant role during membrane binding and oligomerization.

MATERIALS AND METHODS

Bacterial strain, plasmid and oligonucleotides

Escherichia coli K12 JM109 was used throughout the experiment. The recombinant plasmid pGEM-Cyt2Aa2 (4), containing full-length cyt2Aa2 gene in the pGEM-Teasy vector (Promega), was used as DNA template. The oligonucleotide primers were obtained from Sigma Proligo Co, Ltd. (Singapore). Primer sequences and additional information are shown in supplement 1.

Site-directed mutagenesis

The basic procedure was based on Stratagene's QuikChangeTM Site-directed mutagenesis. PCR reactions were performed using pGEM-Cyt2Aa2 as a template. Nucleotides encoding Ile at position 150 was substituted with codons for Ala, Glu, Lys, Leu and Phe using appropriate oligonucleotide primers. Position and model structure of each mutant protein was shown in supplement 2. Recombinant plasmids containing mutated genes were transformed into *E. coli* JM109. Transformants were screened by restriction endonuclease and DNA sequences of all mutant genes were verified by automated DNA sequencing (Biodesign, Thailand).

Protein preparation

The culture of *E. coli* harboring mutant plasmid was induced with 0.1 mM IPTG during exponential growth (OD₆₀₀ of the culture about 0.4-0.5). Cells were harvested by centrifugation and toxin inclusions were extracted as described previously (4). The toxin inclusions were solubilized in 50 mM Na₂CO₃ buffer pH 10.5 with 10 mM DTT at 37°C for 1 hour. After centrifugation at 12,000 \times g for 5 min, soluble protoxins in supernatant were collected. For proteolytic activation, the soluble protoxins were incubated with 1% (w/w) proteinase K at 37°C for 1 hour.

Intrinsic fluorescence spectroscopy

Protoxin and processed toxin were purified by size-exclusion chromatography using Superdex200, 10/300 GL column. The overall structure of purified toxin was monitored by spectro-fluorometry. Emission spectra were recorded from 300 to 500 nm using excitation wavelength at 280 nm. Both excitation and emission slits were set at 3.0 nm. Each sample was scanned three times and spectrum from buffer was used as background.

Mosquito larvicidal assay

Mosquito larvicidal activity of mutants was tested against 3rd-instar larvae of *Aedes aegypti* and *Culex quinquefasciatus* in 24-well tissue culture plates. One ml of two-fold serial dilutions

of toxin inclusions was added into 1 ml of distilled water containing 10 larvae in each well. The assay was carried out at room temperature. Mortality was recorded after the larvae were fed with toxin for 24 hours. LC $_{50}$ (50% lethal concentration) were analyzed by Probit analysis (17).

Hemolytic assay

Hemolytic activity of the proteinase K activated toxin was performed against sheep red blood cell suspension. The assay was slightly modified from Promdonkoy and Ellar (8). Ten μg of activated toxins were mixed with 1 ml of 1% red blood cell suspension in PBS buffer pH 7.4. After incubation at room temperature for 1 hour, the mixture was centrifuged at 3,000 \times g for 5 min. Hemoglobin released in the supernatant was measured by spectrophotometer using absorbance at 540 nm. Red blood cells treated with 0.1% Triton-X100 were used as 100% lysis and red blood cells incubated in PBS without toxin were used as blank.

Liposome preparation

Synthetic lipid vesicles or liposomes were prepared from the lipid mixture of egg-yolk phosphatidylcholine (PC), cholesterol and stearylamine in a molar ratio of 4:3:1 in chloroform:methanol $(2:1, \ v/v)$ as described by Thomas and Ellar (18). Liposomes were purged with nitrogen gas and stored at -80°C until required.

Toxin-membrane interaction

To test membrane binding and oligomerization of the toxin, 5 μg of the proteinase K activated toxins were incubated with 200 μg liposomes in 200 μl PBS buffer. Reactions were incubated for 2 hours at room temperature. Liposomes carrying membrane-bound toxin were separated from unbound toxin by centrifugation at 20,000 \times g for 20 min then analyzed on SDS-PAGE.

RESULTS AND DISCUSSION

Production level and structure of mutant proteins

Gene encoding Cyt2Aa2 toxin from B. thuringiensis subsp. darmstadiensis has been previously cloned and expressed in E. coli (4). The toxin is highly produced as inclusion bodies inside the cells. The inclusion could be solubilized in carbonate buffer and the protease processed product exhibits high cytolytic activity (4). Cyt2Aa2 shares identical amino acid sequence with Cyt2Aa1 from B. thuringiensis sp. kyushuensis that its crystal structure has been resolved (19). Therefore, Cyt2Aa2 should have the same 3D structure as Cyt2Aa1. Previous study on Cyt2Aa1 found that substitution at Ile-150 by Ala completely abolished larvicidal and hemolytic activities. However, those activities could be recovered after introducing additional mutations at other sites of the toxin (16). These results emphasized the importance of amino acid at position 150, although it is not know how this amino acid contributes to the toxin action. By modeling Cyt2Aa2 with Cyt2A1 strucuture, the Ile-150 is found to locate in

176 BMB Reports http://bmbreports.org

the αD - $\beta 4$ loop on the outer surface of the molecule (Fig. 1). It may involve with any critical steps in intoxication including membrane binding, oligomerization and conformational changes. In order to further investigate the functional role of Ile-150, this position was substituted with 5 amino acids with different properties (I150A, I150L, I150F, I150K and I150E). All mutants were highly produced and formed inclusion bodies at comparable level to the wild type. Partially purified inclusions of all mutants were found to be soluble in 50 mM Na₂CO₃ pH 10.5 plus 10 mM DTT similar to the wild type. Soluble protoxin of all mutants could be activated by proteinase K and yielded 23-kDa processed product similar to that of the wild type (Fig. 2). Therefore, solubilization and protease activation were not affected by these substitutions. Solubilization and protease activation are critical prerequisite steps for intoxication. Toxin activity is usually lost or severely reduced if mutation affects these important steps. Evidences have been previously reported such as

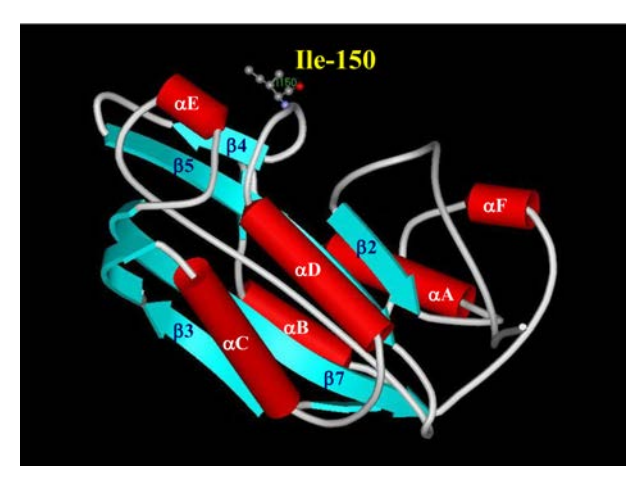


Fig. 1. Model structure of Cyt2Aa2 (wild type). Model was generated based on coordinate of Cyt2Aa1 (PDB accession no. 1CBY). Cyt2Aa1 and Cyt2Aa2 share identical amino acid sequences therefore both toxins should have the same 3D structure.

in Cyt2Aa2-W132F and W154F (20) and some truncated forms of Cyt2Aa2 (21). These mutants were unable to be solubilized in carbonate buffer and showed no larvicidal and hemolytic activities.

Intrinsic fluorescence spectroscopy was performed to monitor structural conformation of the soluble toxin either protoxins or activated toxins in comparison with that of the wild type. If the mutation affects the overall structure of the toxin, emission spectra would be different from the wild type as demonstrated for Cyt2Aa2-L33A mutant (22). Here we found that emission spectra of all mutants (1150A, 1150L, 1150F, 1150K and 1150E) were identical to the wild type (supplement 3). This result indicated that all mutants had adopted similar overall structure to the wild type, suggesting that substitution of Ile150 with Ala, Glu, Lys, Leu and Phe did not affect the overall structure of protoxin and activated toxin.

Larvicidal and hemolytic activities

Mutant protein inclusions were fed to A. aegypti and C. quinquefasciatus larvae to determine their larvicidal activities. It was observed that I150E and I150L mutants were toxic to A. aegypti and C. quinquefasciatus larvae whereas I150A and I150F mutants were not toxic to both types of larvae. The mutant I150K showed very low toxicity to C. quinquefasciatus larvae and inactive against A. aegypti (Table 1). An agreement with larvicidal activity results was also observed from hemolytic assay against sheep red blood cells. Hemolytic activity of I150E and I150L mutants was comparable to the wild type, The I150K mutant showed dramatic reduction in hemolytic activity while I150A and I150F mutants were completely lost their hemolytic activity even when tested at very high dose up to 250 μg/ml (Table 1). Results from both assays clearly showed substitution of Ile150 with Leu and Glu had no effect on protein toxicity, whereas substitution with Ala, Phe, and Lys severely affect protein toxicity.

Loss of toxicity of I150A, I150F, and I150K mutants did not result from inability of the inclusions to be solubilized and activated in the larvae gut since *in vitro* solubilization and protease processing by proteinase K demonstrated that these mutants



Fig. 2. Solubility and proteinase K activation of Cyt2Aa2 wild type (WT) and its mutants. Inclusion bodies (I) were solubilized in 50 mM Na₂CO₃ buffer pH 10.5 plus 10 mM DTT at 37°C for 1 hour. Soluble fraction (S) was separated from insoluble materials or pellet (P) by centrifugation. Soluble proteins were activated by 1% (w/w) proteinase K at 37°C for 1 hour (A). All samples were subjected to SDS-PAGE and Coomassie blue stain. Protein standard markers were shown alongside in kDa.

http://bmbreports.org BMB Reports 177

Table 1. Biological activities of Cyt2Aa2 wild type and its mutants

Destric	Mosquito larvicidal activity; LC ₅₀ (ng/ml)		Hemolytic activity	
Protein -	A. aegypti	C. quinquefasciatus	(% hemoglobin release ± SD	
Wild type	286 (261-314)	313 (271-363)	100 ± 0	
I150A	Non toxic	Non toxic	No lysis	
1150F	Non toxic	Non toxic	No lysis	
I150K	Non toxic	47,507 (27,121-118, 283)	5 ± 2	
1150E	562 (503-628)	359 (315-408)	94 ± 6	
1150L	707 (635-789)	377 (329-431)	96 + 5	

Hemolytic activity of Cyt2Aa mutant toxins against sheep red blood cells was measured after 1 hour incubation of 10 µg of activated toxin with 1 ml of 1% sheep red blood cells in PBS pH 7.4. Mosquito larvicidal activity of mutant toxins against *A. aegypti* and *C. quinquefasciatus* larvae were recorded after feeding the toxin for 24 hours. Three independent experiments were performed and figures in parentheses indicate fiducial limits at 95% confidence.

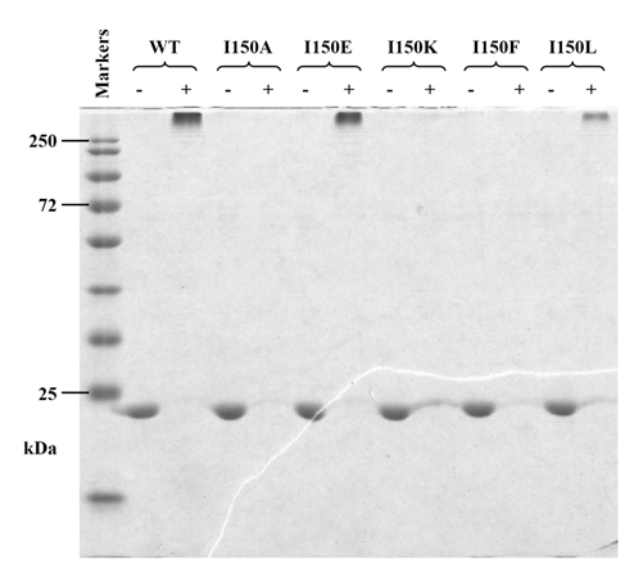


Fig. 3. Membrane binding and oligomerization of the toxin. Proteinase K activated toxins; Cyt2Aa2 wild-type (WT), I150A, I150E, I150K, I150F and I150L, were incubated with (+) or without (-) liposomes at room temperature for 2 hours. Unbound toxins were removed by centrifugation and the membrane-bound toxins were analyzed on SDS-PAGE.

were readily solubilized and yielded similar activated product to that of the wild type (Fig. 2). Moreover, intrinsic fluorescence spectroscopy suggested that these mutants retained similar overall structure to the wild type. Therefore, failure to exhibit larvicidal activity of I150A, I150F, and I150K mutants could due to inability of the processed toxin to bind the target cell membrane, oligomerization and insertion into the membrane.

Membrane binding and oligomerization

Since amino acid replacements at position I150 did not affect overall structure, crystal formation, solubility and protease proc-

essing, the role of Ile150 is possibly involved in membrane binding and perturbation during toxin function. Membrane interaction experiment was performed to validate the effect of alteration at Ile150 on toxin binding to the membrane and oligomerization. Previous reports demonstrated that activated Cyt toxins can bind and form oligomers on the synthetic membrane prepared from pure lipid without a specific receptor (11, 23, 24). To access membrane binding and oligomerization ability of Cyt2Aa2 mutants, activated toxins were incubated with liposomes. Unbound toxin in supernatant was removed after centrifugation and the membrane-bound toxin was analyzed by SDS-PAGE. If the toxin can bind and form oligomers on the membrane, a ladder pattern of protein bands could be observed on SDS-PAGE as shown in Fig. 3. Results demonstrated that 1150E and 1150L mutant toxins could bind and form oligomers on lipid membrane similar to that of the wild type toxin. A ladder pattern was detected at very low amount for the less active mutant 1150K. The inactive 1150A and 1150F mutants were unable to bind and develop oligomers on the lipid membrane.

Results from membrane binding and oligomer formation are consistent with mosquito-larvicidal and hemolytic assays. This suggests that amino acid at position 150 is a critical residue for membrane binding and oligomerization. Substitutions with smaller side chain (I150A) or larger side chain (I150F) resulted in a total loss of biological activities whereas substitutions by a highly conserved amino acid (I150L) or a negatively charged side chain (I150E) preserved the toxin activity. However, substitution by a positive charged amino acid (1150K) significantly reduced toxin activity. This suggests that an appropriate size of the amino acid at this position is required and hydrophobic or negatively charged amino acid is more favorable. Replacement of a highly hydrophobic (isoleucine) by a smaller and less hydrophobic (alanine) or substitution with aromatic residue (phenylalanine) that has intermediate polarity could affect hydrophobic interaction between the toxin and lipid membrane. Substitution by a negatively charged residue (I150E) might enable the mutant toxin to make interaction to stearylamine in liposomes and to

178 BMB Reports http://bmbreports.org

phosphatidylethanolamine that is generally found in red blood cell and mosquito larval gut cell membranes. This interaction is severely interrupted if a positively charged amino acid is introduced into this position (I150K). X-ray structures of the protoxin (13) and protease activated form (14) showed that amino acid at this position is located in the αD - $\beta 4$ loop and sticking out to the environment. It is expected that this residue plays essential role during membrane binding and oligomer formation. However, Ile-150 is not a single position responsible for membrane binding and oligomerization. Reversion mutagenesis of an inactive mutant Cyt2Aa1-I150A has shown that activity could be recovered by introducing additional mutation at other positions (16). Amino acids in αA and αC were reported to involve with membrane binding and oligomerization (7, 25). These amino acids contribute to some extend and function co-operatively.

Acknowledgements

This work was supported by the Thailand Research Fund (TRF), the National Center for Genetic Engineering and Biotechnology, National Science and Technology Development Agency (NSTDA), and the Institute of Molecular Biosciences, Mahidol University, Thailand.

REFERENCES

- Schnepf, E., Crickmore, N., Van, R. J., Lereclus, D., Baum, J., Feitelson, J., Zeigler, D. R. and Dean, D. H. (1998) Bacillus thuringiensis and its pesticidal crystal proteins. Microbiol. Mol. Biol. Rev. 62, 775-806.
- Crickmore, N., Zeigler, D. R., Feitelson, J., Schnepf, E., Van, R. J., Lereclus, D., Baum, J. and Dean, D. H. (1998) Revision of the nomenclature for the *Bacillus thuringiensis* pesticidal crystal proteins. *Microbiol. Mol. Biol. Rev.* 62, 807-813.
- 3. Thiery, I., Delecluse, A., Tamayo, M. C. and Orduz, S. (1997) Identification of a gene for Cyt1A-like hemolysin from *Bacillus thuringiensis* subsp. *medellin* and expression in a crystal-negative *B. thuringiensis* strain. *Appl. Environ. Microbiol.* **63**, 468-473.
- Promdonkoy, B., Chewawiwat, N., Tanapongpipat, S., Luxananil, P. and Panyim, S. (2003) Cloning and characterization of a cytolytic and mosquito larvicidal delta-endotoxin from *Bacillus thuringiensis* subsp. *darmstadiensis*. *Curr. Microbiol.* 46, 94-98.
- Koni, P. A. and Ellar, D. J. (1994) Biochemical characterization of *Bacillus thuringiensis* cytolytic delta-endotoxins. *Microbiology* 140 (Pt 8), 1869-1880.
- Knowles, B. H., White, P. J., Nicholls, C. N. and Ellar, D. J. (1992) A broad-spectrum cytolytic toxin from *Bacillus thuringiensis* var. kyushuensis. Proc. Biol. Sci. 248, 1-7.
- Promdonkoy, B., Rungrod, A., Promdonkoy, P., Pathaichindachote, W., Krittanai, C. and Panyim, S. (2008) Amino acid substitutions in alphaA and alphaC of Cyt2Aa2 alter hemolytic activity and mosquito-larvicidal specificity. J. Biotechnol. 133, 287-293.
- 8. Promdonkoy, B. and Ellar, D. J. (2003) Investigation of the pore-forming mechanism of a cytolytic delta-endotoxin

- from Bacillus thuringiensis. Biochem. J. 374, 255-259.
- Knowles, B. H., Blatt, M. R., Tester, M., Horsnell, J. M., Carroll, J., Menestrina, G. and Ellar, D. J. (1989) A cytolytic delta-endotoxin from *Bacillus thuringiensis* var. *israelensis* forms cation-selective channels in planar lipid bilayers. *FEBS Lett.* 244, 259-262.
- Butko, P. (2003) Cytolytic toxin Cyt1A and its mechanism of membrane damage: data and hypotheses. *Appl. Environ. Microbiol.* 69, 2415-2422.
- Manceva, S. D., Pusztai-Carey, M., Russo, P. S. and Butko, P. (2005) A detergent-like mechanism of action of the cytolytic toxin Cyt1A from *Bacillus thuringiensis* var. israelensis. Biochemistry 44, 589-597.
- Guerchicoff, A., Delecluse, A. and Rubinstein, C. P. (2001) The *Bacillus thuringiensis* cyt genes for hemolytic endotoxins constitute a gene family. *Appl. Environ. Microbiol.* 67, 1090-1096.
- Li, J., Koni, P. A. and Ellar, D. J. (1996) Structure of the mosquitocidal delta-endotoxin CytB from *Bacillus thur*ingiensis sp. kyushuensis and implications for membrane pore formation. J. Mol. Biol. 257, 129-152.
- Cohen, S., Dym, O., Albeck, S., Ben-Dov, E., Cahan, R., Firer, M. and Zaritsky, A. (2008) High-resolution crystal structure of activated Cyt2Ba monomer from *Bacillus thur*ingiensis subsp. israelensis. J. Mol. Biol. 380, 820-827.
- Cohen, S., Albeck, S., Ben-Dov, E., Cahan, R., Firer, M., Zaritsky, A. and Dym, O. (2011) Cyt1Aa toxin: crystal structure reveals implications for its membrane-perforating function. J. Mol. Biol. 413, 804-814.
- Promdonkoy, B. and Ellar, D. J. (2005) Structure-function relationships of a membrane pore forming toxin revealed by reversion mutagenesis. *Mol. Membr. Biol.* 22, 327-337.
- 17. Finney, D. (1971) Probit Analysis, Cambridge University Press, London, UK.
- Thomas, W. E. and Ellar, D. J. (1983) Mechanism of action of *Bacillus thuringiensis* var israelensis insecticidal delta-endotoxin. FEBS Lett. 154, 362-368.
- Koni, P. A. and Ellar, D. J. (1993) Cloning and characterization of a novel *Bacillus thuringiensis* cytolytic delta-endotoxin. *J. Mol. Biol.* 229, 319-327.
- Promdonkoy, B., Pathaichindachote, W., Krittanai, C., Audtho, M., Chewawiwat, N. and Panyim, S. (2004) Trp132, Trp154, and Trp157 are essential for folding and activity of a Cyt toxin from Bacillus thuringiensis. Biochem. Biophys. Res. Commun. 317, 744-748.
- 21. Thammachat, S., Pathaichindachote, W., Krittanai, C. and Promdonkoy, B. (2008) Amino acids at N- and C-termini are required for the efficient production and folding of a cytolytic delta-endotoxin from *Bacillus thuringiensis*. *BMB Rep.* **41**, 820-825.
- Thammachat, S., Pungtanom, N., Kidsanguan, S., Pathaichindachote, W., Promdonkoy, B. and Krittanai, C. (2010)
 Amino acid substitution on Beta1 and alphaF of Cyt2Aa2
 affects molecular interaction of protoxin. BMB Rep. 43,
 427-431.
- Gazit, E., Burshtein, N., Ellar, D. J., Sawyer, T. and Shai, Y. (1997) Bacillus thuringiensis cytolytic toxin associates specifically with its synthetic helices A and C in the membrane bound state. Implications for the assembly of oligomeric transmembrane pores. Biochemistry 36, 15546-

http://bmbreports.org BMB Reports 179

Functional role of Ile150 in Cyt2Aa toxin Wanwarang Pathaichindachote, et al.

15554.

- 24. Promdonkoy, B. and Ellar, D. J. (2000) Membrane pore architecture of a cytolytic toxin from *Bacillus thuringiensis*. *Biochem. J.* **350(Pt 1)**, 275-282.
- 25. Gazit, E. and Shai, Y. (1993) Structural characterization,

membrane interaction, and specific assembly within phospholipid membranes of hydrophobic segments from *Bacillus thuringiensis* var. *israelensis* cytolytic toxin. *Biochemistry* **32**, 12363-12371.

180 BMB *Reports* http://bmbreports.org

BMB reports

Amino acid substitution on $\beta1$ and αF of Cyt2Aa2 affects molecular interaction of protoxin

Siriya Thammachat¹, Nuanwan Pungtanom¹, Somruathai Kidsanguan¹, Wanwarang Pathaichindachote², Boonhiang Promdonkoy² & Chartchai Krittanai^{1,*}

¹Institute of Molecular Biosciences, Mahidol University, Salaya Campus, Phuttamonthon 4 Road, Salaya, Nakhon Pathom 73170, Thailand, ²National Center for Genetic Engineering and Biotechnology, National Science and Technology Development Agency, 113 Phaholyothin Road, Klong 1, Klong Luang, Pathum Thani 12120, Thailand

Cyt2Aa2 is a mosquito-larvicidal protein produced as a 29 kDa crystalline protoxin from Bacillus thuringiensis subsp. darmstadiensis. To become an active toxin, proteolytic processing is required to remove amino acids from its N- and C-termini. This study aims to investigate the functional role of amino acid residues on the N-terminal β1 and C-terminal αF of Cyt2Aa2 protoxin. Mutant protoxins were constructed, characterized and compared to the wild type Cyt2Aa2. Protein expression data and SDS-PAGE analysis revealed that substitution at leucine-33 (L33) of $\beta 1$ has a critical effect on dimer formation and structural stability against proteases. In addition, amino acids N230 and I233-F237 around the C-terminus aF demonstrated a crucial role in protecting the protoxin from proteolytic digestion. These results suggested that $\beta 1$ and αF on the Nand C-terminal ends of Cyt2Aa2 protoxin play an important role in the molecular interaction and in maintaining the structural stability of the protoxin. [BMB reports 2010; 43(6): 427-431]

INTRODUCTION

Cyt2Aa2 is a crystal delta-endotoxin produced during a sporulation stage of a Gram-positive, spore-forming bacterium *Bacillus thuringiensis* subsp. *darmstadiensis* (1, 2). This protein family is recognized as a promising bio-insecticide with a large number of applications. It is highly toxic to the larvae of dipteran insects such as blackflies and mosquitoes (3, 4), the latter of which are a major insect vector for the dengue virus which causes dengue hemorrhagic fever, a serious disease in tropical countries.

The Cyt toxin family shows a broad range of activity *in vitro*. However, *in vivo* it is specifically toxic to dipteran larvae (4-7). Based on amino acid sequence similarity, the toxins can be

*Corresponding author. Tel: 66-2-441-9003 ext. 1410; Fax: 66-2-441-1013; E-mail: stckt@mahidol.ac.th

Received 25 November 2009, Accepted 18 March 2010

Keywords: Bacillus thuringiensis, Cytolytic toxin, Mutagenesis, Protein folding, Toxicity

divided into two classes: Cyt1 and Cyt2. They share 39% and 70% amino acid sequence identity and similarity, respectively (8-11). Expression of Cyt1 toxin requires P20 helper protein, while Cyt2 toxin can be expressed by itself. An X-ray crystal structure of Cyt2 revealed a single domain in α/β architecture. The structural folding is composed of six α -helices and seven β-sheets (12). Even though Cyt2 is produced as a crystal protein in Bacillus thuringiensis, it can be cloned and expressed in E. coli as a protein inclusion (10). These crystal and inclusion proteins are solubilized in an alkaline condition of the larval midgut. Proteolytic digestion by insect gut proteases is generally required for a 29 kDa protoxin to become a 23-25 kDa active toxin. For example, a 259-residue Cyt2Aa2 undergoes proteolytic processing by proteinase K to remove N- and C-terminal fragments at the cleavage sites after serine 37 and serine 228 to become an active form (10, 12, 13). This active molecule then binds to the brush border membrane, resulting in cell lysis (1). Its mode of action is thought to act as either a detergent-like or a pore-forming toxin. In a detergent-like model, the activated toxins are locally aggregated on the surface of lipid bilayers causing membrane disruption, releasing protein and lipid complexes (14, 15). In the pore-forming model, the activated toxins are inserted into the lipid bilayers, forming an oligomeric assembly and generating transmembrane pores. The leakage through these pores then leads to a colloidal osmotic imbalance, lysing the target cells (16).

Since Cyt toxin does not require the N- and C-terminal fragments for its activity (9, 13), this study aims to investigate the significance of its terminal ends - especially the N-terminal $\beta 1$ and C-terminal αF on the production and structural folding of the protoxin. Selected mutations of amino acids on N- and C-terminals were introduced using site-directed mutagenesis. The mutant toxins were expressed in *E. coli* and characterized for their biochemical properties, structural conformation, molecular interactions and biological activities.

http://bmbreports.org BMB reports 427

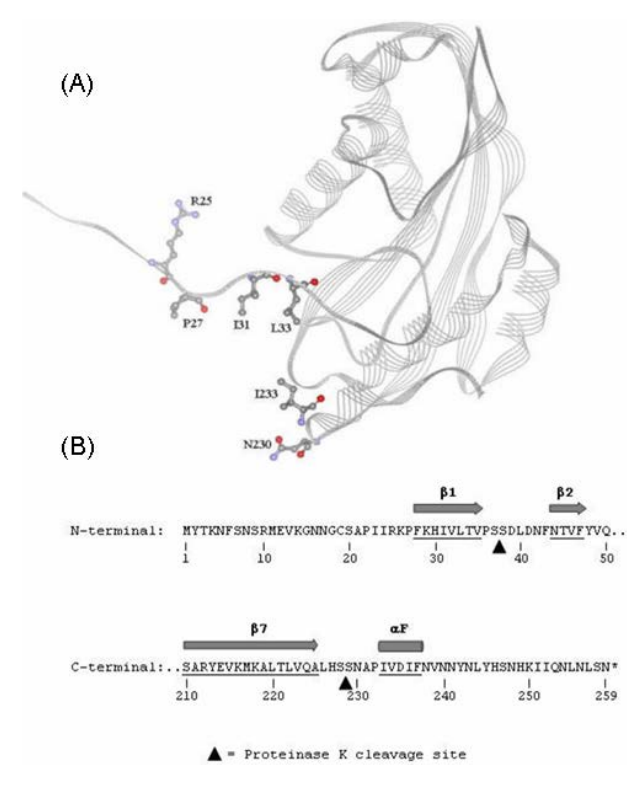


Fig. 1. Mutated residues of Cyt2Aa2: R25, P27, I31, L33 are located around β -1 sheet on N terminus, while N230 and I233 are in α -F helix on C-terminus of Cyt2Aa2 (A). The cleavage site of proteinase K digestion are located after serine 37 and serine 228 (B).

RESULTS AND DISCUSSION

Mutational effect of selected amino acids on toxin production and folding

Based on the crystal structure of Cyt2 toxin, site-directed mutagenesis was designed for alanine substitution on the targeted amino acid residues: R25, P27, I31 and L33, located on N-terminus $\beta 1$ (R25-L33) (12); and N230 and I233, located on C-terminus αF (N230-I233) (Fig. 1). According to their structural folding, the N- and C-terminal fragments are removed via proteolytic processing at cleavage sites at serine 37 and serine 228, yielding the 23-25 kDa active toxin. However the amino acid residues located in these removed fragments are suggested to be important, and may be involved in intermolecular interactions between the protoxins (12).

We have successfully constructed these mutant toxins in an *E. coli* system and confirmed the correct gene sequences by automated DNA sequencing. The constructed mutants were: R25A, P27A, I31A, L33A, N230A, I233A and I233stop (with an introduced stop codon). After IPTG induction, all the prepared cell lysates from each mutant were verified for Cyt2Aa2 expression by SDS-PAGE analysis. The mutants - R25A, P27A,

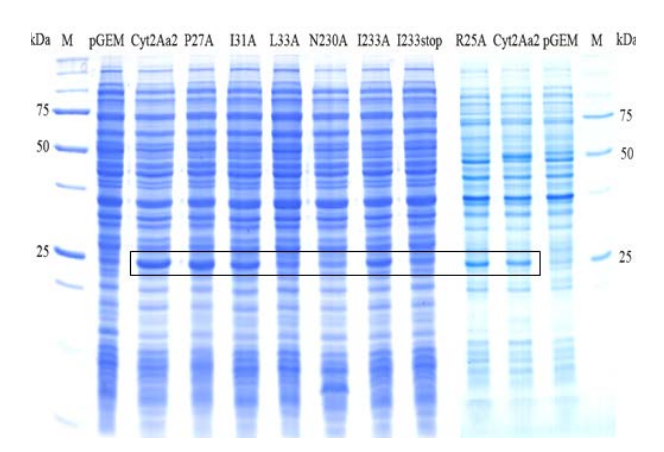


Fig. 2. Expression of mutants and Cyt2Aa2 are analyzed by SDS-PAGE. The toxins were cloned into pGEM-T Easy and expressed under *lac* promoter. The rectangle represents the position of Cyt2Aa2 protein.

I31A, I233A and wild type - showed a high expression level of protoxin products, while the expression of L33A, N230A and I233stop were found to be slightly lower (Fig. 2). This differential expression could be due to the perturbation of substituted amino acids on structural folding and molecular stability of these mutants. Such a mutation and production of truncated protein, leading to structural alteration, can be found in many other proteins, for example in mutated cytochrome cbb3 oxidase (19) and Cry4Ba toxins (20).

Biochemical characterization of toxin solubility revealed that R25A, P27A and I31A were well soluble in carbonate buffer pH 9.5, similar to the wild type. However L33A, N230A, I233A and I233stop showed lower solubility. The reduced solubility also leads to a lower yield of active toxin after proteinase K processing (data not shown).

In routine SDS-PAGE analysis of Cyt2Aa2, two protein bands corresponding to monomeric and dimeric protoxins are generally detected and confirmed by Western blot at 25 and 50 kDa, respectively. In addition, the 50 kDa dimeric band disappears when the toxin is treated in conditions with reducing agents. In this work, we prepared an equal amount of each expressed inclusion protein in carbonate buffer with and without DTT, and loaded on SDS-PAGE. The wild type and other mutants (P27A, I31A and I233A, without DTT) were found to be present as dimers and monomers. Under DTT treatment, their dimeric forms disappeared as expected (Fig. 3). In contrast, we did not detect the dimeric form of L33A, N230A, and I233stop mutants in conditions without DTT. Their monomers were also found to be unstable, and were present as a very faint band. Destabilization of these mutants, especially on the dimeric form, could be due to the loss of inter- and intramolecular interaction by substitution of these residues.

This result was found to be in good agreement with the construction of the N- and C-terminal truncated toxins Cyt\(\Delta \N 26, \)

428 BMB reports http://bmbreports.org

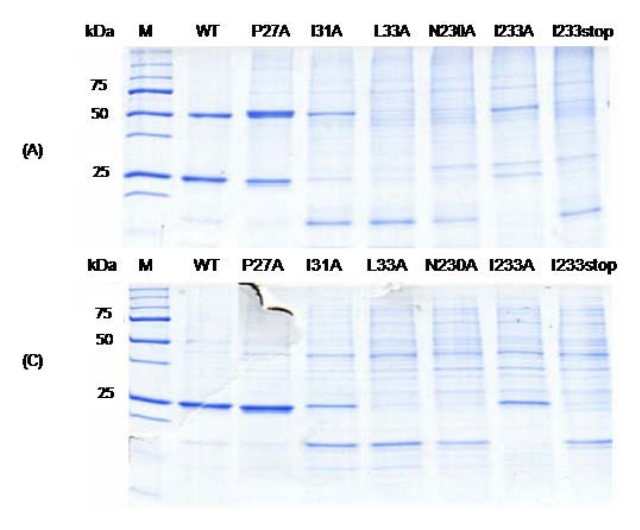


Fig. 3. Coomassie blue stained SDS-PAGE of inclusion protoxins solubilized in 50 mM $Na_2CO_3/NaHCO_3$ pH 9.5 at $37^{\circ}C$ for 1.5 h without DTT and heating (A), compared with conditions with DTT and heating (B).

CytΔN33 and CytΔC31 (21), indicating the critical roles of amino acids located on N- and C-termini in the initial step of protein folding, and in maintaining structural integrity and molecular interaction (21).

L33 is critical for β1 in controlling appropriate conformation From SDS-PAGE analysis, the L33A mutant toxin was expressed at a lower level, but it can be solubilized and processed by proteinase K. A very low yield of Cyt2Aa2 resulted from proteinase K processing. Moreover, the intrinsic fluorescence spectrum of L33A demonstrated a red shift emission, suggesting that L33A has adopted a different conformation compared to that of the wild type (Fig. 4). This amino acid substitution on β1 could lead to a significant perturbation of toxin folding, causing conformational variation and multiple populations of protoxins in solution (12). As a consequence, the misfolded or partially unfolded L33A protoxin was observed to be more sensitive to proteinase K digestion than the native wild type. This finding is in good agreement with a recent report on production of a truncated toxin, lacking $\beta 1$ (21). The product of this truncated mutant cannot be detected, and it was suggested that the β1-sheet of Cyt2Aa2 may be involved in nucleation and protein folding. Consequently, residual L33 on the β1-sheet is recognized as a critical residue for protein conformation and structural folding.

Role of αF and the loop residues between $\beta 7$ and αF

From our previous study (21), a C-terminal truncation protein (N238stop) showed comparable expression and characteristics to the wild type. However when the S229stop mutant was constructed to include a truncation of amino acids in αF and

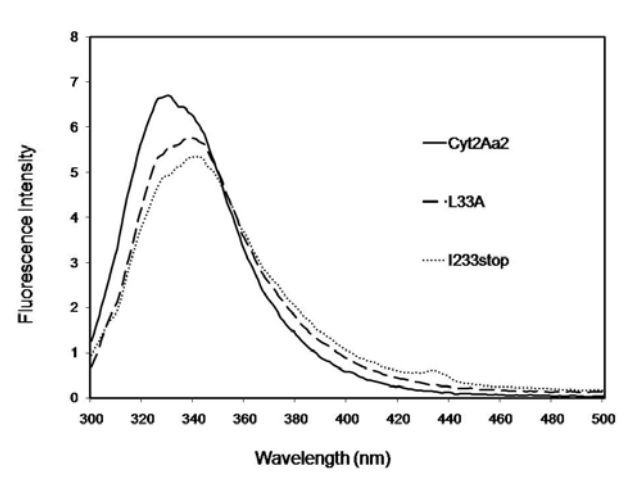


Fig. 4. Intrinsic fluorescence spectra of selected mutants are compared with Cyt2Aa2 wild type. Solubilized protoxins in Na_2CO_3 buffer were excited at 280 nm and emission spectra were scanned from 300 to 500 nm.

the loop between $\beta 7$ and αF regions, a significantly low amount of protein expression was observed (21). Further characterization of this mutant by intrinsic fluorescence also showed unfolded conformation different from the wild type.

In this work, a truncation of αF in the I233stop mutant also showed a lower yield of protein, reduced toxin solubility, and non-native toxin conformation (Fig. 4). The critical role of amino acid residues in αF for protoxin folding and stability was confirmed by N230A and I233A mutants. These mutants produced low amounts of protoxins, and the expressed protoxins showed reduced solubility and high sensitivity to proteinase K digestion.

According to the crystal structure of Cyt2 protoxin, the residues N230 and I233 are located on αF and on the connecting loop to $\beta 7$ of the C-terminal end (12). Thus, they may be involved in intermolecular contacts between αF of dimeric protoxins. Analysis of their bond lengths and bond angles suggested possible interactions between N230 and I233 of one protoxin and A231 and V234 of another protoxin molecule through hydrogen bonding. Replacement of N230 and I233 may perturb interactions that help maintain the proper conformation of αF for dimer formation.

Biological activity

Biological activity of these mutant toxins was investigated using *Aedes aegypti* mosquito larvae and sheep red blood cells for *in vivo* and *in vitro* activity assays, respectively (supplemental material). As expected, larvicidal and hemolytic activities of L33A, N230A and I233stop were found to be much lower than that of the wild type. Reduced toxicity of these toxins may be due to a decrease in protoxin solubility and incorrect conformation. Since these toxins were found to be highly sensitive to proteolytic digestion, they may exist in the non-native

http://bmbreports.org

conformation, becoming more susceptible to protease digestion. Moreover, the truncated C-terminal protoxin 1233stop may exist in monomeric rather than dimeric form, causing the toxin to be more sensitive to gut proteases, resulting in loss of active toxin. In addition, the mutation at these positions may change the conformation of Cyt2Aa2 protoxin, resulting in exposing extra proteolytic cleavage sites.

In conclusion, we have demonstrated that the amino acids on $\beta 1$ and αF of the terminal fragments of Cyt2Aa2 protoxin play a crucial role in protein expression, solubilization, folding and stability. The L33 residue located in the β 1-sheet of the N-terminus may be an important residue in controlling the β1-sheet in the right conformation and protoxin dimerization. The substitution of L33 with alanine residue may affect the protein structure and inclusion formation. On the other hand, amino acids at the C-terminal part of Cyt2Aa2 which are in the loop (β 7 and α -F), and α -F helix are responsible for dimer contacts and maintaining correct protein folding. The alanine substitutions or truncation of this part may destroy the interaction between the two monomers, resulting in misfolded structure of protein. Therefore β 1-sheet, loop (β 7 and α -F), and α -F of Cyt2Aa2 are essential for protein folding, production, dimerization, solubilization, and proteinase K activation.

MATERIALS AND METHODS

Site-directed mutagenesis

In vitro site-directed mutagenesis using a PCR-based method (QuikChangeTM) was carried out to construct mutant toxins. Mutagenic primers were designed using Vector NTI software. The pGEM-T_{Easy} plasmid vector containing the *Cyt2Aa2* gene (10) was amplified with appropriate primers using high-fidelity *Pfu* DNA polymerase in the PCR reaction. The restriction enzymes were used to screen for mutants. The nucleotide sequences for all mutants were then confirmed by automated DNA sequencing (Macrogen Inc., Korea).

Protein expression, solubilization and activation

E. coli cells harboring wild type and mutant plasmids were cultured at 37°C in LB broth containing 100 μg/ml ampicillin. When OD₆₀₀ of the culture reached 0.3-0.4, protein expressions were induced by adding 0.1 mM IPTG. After 5 h, *E. coli* cells expressing protein were collected by centrifugation and lysed by French pressure cell to obtain inclusion toxin. Partially purified inclusions were solubilized in 50 mM Na₂CO₃/NaHCO₃ pH 9.5 at 37°C for 1.5 h. Concentrations of solubilized protoxins were determined by the Bradford method (17) using a Bio-Rad protein assay kit and bovine serum albumin (BSA) as a standard curve. In case that proteolytic processing was required, solubilized protoxins were added with 1% (w/w) proteinase K enzyme, and incubated at 37°C for 1 h.

Mosquito larvicidal activity assay

Inclusion toxin was diluted with distilled water as a two-fold

serial dilution in 1 ml (containing 500 to 0.25 μ g of toxin/ml). The 2nd instar *Aedes aegypti* larvae (10 larvae/well) in 1 ml water were fed with 1 ml of diluted inclusions in each well. Mortality of mosquito larvae was recorded after 24 h, and LC₅₀ (50% lethal concentration) was determined using a Probit program (18).

Hemolytic activity assay

Sheep red blood cells (RBC) were collected by centrifugation at 3,000 rpm, 4°C for 5 min, and then washed twice with PBS buffer (pH 7.4) to make a 2% RBC preparation (4, 10). Toxin samples (500 μ g/ml) were diluted in twofold serial dilutions with PBS buffer (100 μ l/well). A 100 μ l sample of 2% sheep RBC was mixed and incubated with the diluted toxin at room temperature. The end-point of hemolysis was monitored and recorded after 24 h.

Intrinsic fluorescence spectrometry

A 400 μ l fixed volume of 10-40 μ g/ml of purified toxin in carbonate buffer was added into a quartz cuvette and analyzed by a Jasco FP-6300 spectrofluorometer. An intrinsic excitation wavelength was set at 280 nm and the emission spectra were scanned from 300 to 550 nm. Excitation and emission slit widths were 2.5 nm. The fluorescence emission spectra of protein samples were recorded, and the baseline spectrum subtracted from the carbonate buffer.

Acknowledgements

This work was supported by the Thailand Research Fund (TRF), the National Center for Genetic Engineering and Biotechnology, and the Thailand Center of Excellence for Physics (Integrated Physics Cluster). We also would like to thank K. Pootanakit for his contribution in critical reading of the manuscript, and a scholarship received from the Royal Golden Jubilee Ph.D. Program (to S. Thammachat).

REFERENCES

- Schnepf, E., Crickmore, N., Van Rie, J., Lereclus, D., Baum, J., Feitelson, J., Zeigler, D. R. and Dean, D. H. (1998) *Bacillus thuringiensis* and its pesticidal crystal proteins. *Microbiol. Mol. Biol. Rev.* 62, 775-806.
- Drobniewski, F. A. and Ellar, D. J. (1989) Purification and properties of a 28-kilodalton hemolytic and mosquitocidal protein toxin of *Bacillus thuringiensis* subsp. *darmstadien*sis 73-E10-2. J. Bacteriol. 171, 3060-3067.
- 3. Thomas, W. E. and Ellar, D. J. (1983) *Bacillus thuringiensis* var. *israelensis* crystal delta-endotoxin: effects on insect and mammalian cells *in vitro* and *in vivo*. *J. Cell Sci.* **60**, 181-197
- Thomas, W. E. and Ellar, D. J. (1983) Mechanism of action of *Bacillus thuringiensis* var. *israelensis* insecticidal delta-endotoxin. *FEBS Lett.* 154, 362-368.
- Knowles, B. H., Blatt, M. R., Tester, M., Horsnell, J. M., Carroll, J., Menestrina, G. and Ellar, D. J. (1989) A cytolytic delta-endotoxin from *Bacillus thuringiensis* var. isra-

430 BMB reports http://bmbreports.org

- elensis forms cation-selective channels in planar lipid bilayers. FEBS Lett. 244, 259-262.
- Yu, Y. M., Ohba, M. and Gill, S. S. (1991) Characterization of mosquitocidal activity of *Bacillus thuringiensis* subsp. *fukuokaensis* crystal proteins. *Appl. Environ. Microbiol.* 57, 1075-1081.
- Gazit, E., Burshtein, N., Ellar, D. J., Sawyer, T. and Shai, Y. (1997) Bacillus thuringiensis cytolytic toxin associates specifically with its synthetic helices A and C in the membrane bound state - Implications for the assembly of oligomeric transmembrane pores. Biochemistry 36, 15546-15554.
- Koni, P. A. and Ellar, D. J. (1993) Cloning and characterization of a novel *Bacillus thuringiensis* cytolytic delta-endotoxin. *J. Mol. Biol.* 229, 319-327.
- 9. Koni, P. A. and Ellar, D. J. (1994) Biochemical characterization of *Bacillus thuringiensis* cytolytic delta-endotoxins. *Microbiology* **140** (Pt 8), 1869-1880.
- Promdonkoy, B., Chewawiwat, N., Tanapongpipat, S., Luxananil, P. and Panyim, S. (2003) Cloning and characterization of a cytolytic and mosquito larvicidal delta-endotoxin from *Bacillus thuringiensis* subsp. *darmstadiensis*. *Curr. Microbiol.* 46, 94-98.
- Cohen, S., Cahan, R., Ben-Dov, E., Nisnevitch, M., Zaritsky, A. and Firer, M. A. (2007) Specific targeting to murine myeloma cells of Cyt1Aa toxin from *Bacillus thur*ingiensis subspecies israelensis. J. Biol. Chem. 282, 28301-28308
- Li, J., Koni, P. A. and Ellar, D. J. (1996) Structure of the mosquitocidal delta-endotoxin CytB from *Bacillus thur*ingiensis sp. kyushuensis and implications for membrane pore formation. *J. Mol. Biol.* 257, 129-152.
- 13. Cohen, S., Dym, O., Albeck, S., Ben-Dov, E., Cahan, R., Firer, M. and Zaritsky, A. (2008) High-resolution crystal

- structure of activated Cyt2Ba monomer from *Bacillus thuringiensis* subsp. *israelensis*. *J. Mol. Biol.* **380**, 820-827.
- Manceva, S. D., Pusztai-Carey, M., Russo, P. S. and Butko, P. (2005) A detergent-like mechanism of action of the cytolytic toxin Cyt1A from *Bacillus thuringiensis* var. israelensis. Biochemistry 44, 589-597.
- Butko, P. (2003) Cytolytic toxin Cyt1A and its mechanism of membrane damage: data and hypotheses. *Appl. En*viron. *Microbiol.* 69, 2415-2422.
- Promdonkoy, B. and Ellar, D. J. (2003) Investigation of the pore-forming mechanism of a cytolytic delta-endotoxin from *Bacillus thuringiensis*. *Biochem. J.* 374, 255-259.
- Bradford, M. M. (1976) A rapid and sensitive method for the quantitation of microgram quantities of protein utilizing the principle of protein-dye binding. *Anal. Biochem.* 72, 248-254.
- Finney, D. (1971) Probit Analysis, pp.1-333, Cambridge University Press, London, UK.
- Ozturk, M., Gurel, E., Watmough, N. J. and Mandaci, S. (2007) Site-directed mutagenesis of five conserved residues of subunit i of the cytochrome cbb3 oxidase in Rhodobacter capsulatus. J. Biochem. Mol. Biol. 40, 697-707.
- Chayaratanasin, P., Moonsom, S., Sakdee, S., Chaisri, U., Katzenmeier, G. and Angsuthanasombat, C. (2007) High level of soluble expression in *Escherichia coli* and characterisation of the cloned *Bacillus thuringiensis* Cry4Ba domain III fragment. *J. Biochem. Mol. Biol.* 40, 58-64.
- 21. Thammachat, S., Pathaichindachote, W., Krittanai, C. and Promdonkoy, B. (2008) Amino acids at N- and C-termini are required for the efficient production and folding of a cytolytic delta-endotoxin from *Bacillus thuringiensis*. *BMB*. *Rep.* **41**, 820-825.

http://bmbreports.org BMB reports 431

Provided for non-commercial research and education use. Not for reproduction, distribution or commercial use.



This article appeared in a journal published by Elsevier. The attached copy is furnished to the author for internal non-commercial research and education use, including for instruction at the authors institution and sharing with colleagues.

Other uses, including reproduction and distribution, or selling or licensing copies, or posting to personal, institutional or third party websites are prohibited.

In most cases authors are permitted to post their version of the article (e.g. in Word or Tex form) to their personal website or institutional repository. Authors requiring further information regarding Elsevier's archiving and manuscript policies are encouraged to visit:

http://www.elsevier.com/copyright

Author's personal copy

Journal of Biotechnology 141 (2009) 137-141



Contents lists available at ScienceDirect

Journal of Biotechnology

journal homepage: www.elsevier.com/locate/jbiotec



Investigation of the unfolding pathway of *Bacillus thuringiensis* Cyt2Aa2 toxin reveals an unfolding intermediate

Anchanee Sangcharoen^a, Weerachon Tepanant^a, Somruathai Kidsanguan^a, Boonhiang Promdonkoy^b, Chartchai Krittanai^{a,*}

- a Institute of Molecular Biology and Genetics, Mahidol University, Salaya Campus, Putthamonthon 4 Road, Salaya, Nakhonpathom 73170, Thailand
- ^b National Center for Genetic Engineering and Biotechnology (BIOTEC), National Science and Technology Development Agency,
- 113 Phahonyothin Road, Klong 1, Klong Luang, Pathumthani 12120, Thailand

ARTICLE INFO

Article history: Received 1 November 2008 Received in revised form 4 March 2009 Accepted 16 March 2009

Keywords: Cyt2Aa2 Bacillus thuringiensis Protein unfolding Molten globule Intrinsic fluorescence Circular dichroism

ABSTRACT

Cyt2Aa2 is a cytolytic toxin from Bacillus thuringiensis subsp. darmstadiensis. Its active form has a lethal activity against specific mosquito larvae. We characterized an unfolding pathway of Cyt2Aa2 using a guanidinium hydrochloride denaturation. The results revealed three-state transition with a detectable intermediate in a condition with 3–4 M of GuHCl. The conformational free energies for native and intermediate state unfolding were 5.82 ± 0.47 and 16.85 ± 1.47 kcal/mol, respectively. Kinetic analysis suggested that the activation energy of both transitions was around 23–25 kcal/mol, with a rate-limiting step in the second transition. These results have established an energy profile of the Cyt2Aa2 toxin in various conformations involved in the unfolding/refolding pathway. Further characterization of the intermediate state by dye-binding assay, intrinsic fluorescence, and circular dichroism spectroscopy demonstrated characteristics of a molten globule state. This revealed intermediate could play an active role in the structural folding and biological activity of the toxin.

© 2009 Elsevier B.V. All rights reserved.

1. Introduction

Bacillus thuringiensis is a spore-forming, Gram-positive soil bacterium which produces parasporal proteins during sporulation (Nickerson et al., 1975). The produced endotoxins can be solubilized in alkaline pH, and become insecticidal after proteolysis by insect gut proteases (Murphy et al., 1976; Bulla et al., 1977; Andrews et al., 1985; Armstrong et al., 1985). The binding of an active toxin on the brush border membrane of a susceptible insect could result in the formation of ion channels or pores, leading to osmotic imbalance, cell swelling and osmotic lysis (Hofte and Whiteley, 1989; Schnepf et al., 1998).

The cytolytic toxin Cyt2Aa2 is produced by *B. thuringiensis* subsp. *darmstadiensis* (Promdonkoy et al., 2003). This toxin is synthesized as a 29-kDa protoxin and then proteolytically processed into a 25-kDa active form. Its toxicity is found against *Stegomyia* and *Culex* sp. mosquito larvae (Galjart et al., 1987). The X-ray structure of Cyt2 toxin contains a single domain of α/β architecture comprising six α -helices and seven β -sheets (Li et al., 1996). Cyt toxin can bind and form pores in a synthetic lipid membrane without the requirement of a receptor (Thomas and Ellar, 1983). The precise mechanism

of action for Cyt toxin is still unclear, and may be based on either pore-forming (Promdonkoy and Ellar, 2000, 2003) or detergent-like model (Butko, 2003). To study the details of membrane interaction, stable conformational states of the toxin should be identified and characterized. The present study aims to analyze the conformational states of Cyt2Aa2 toxin using a chemically induced unfolding experiment. The identified conformational states and calculated transitional free energy between each state in the unfolding pathway could help reveal an energy map of the toxin. In addition, the stable intermediate state can also be characterized further to provide a clue to its possible involvement in the structural folding and biological function of Cyt2Aa2 toxin.

2. Materials and methods

2.1. Protein expression and purification

Cyt2Aa2 protein was expressed at $37\,^{\circ}\text{C}$ in *Escherichia coli* strain JM 109 (Promdonkoy et al., 2003) in the presence of 0.1 mM IPTG. The culture media was LB broth containing $100-\mu\text{g/ml}$ ampicillin. The cell culture was disrupted using a French pressure cell. The harvested inclusion protein was solubilized in $50\,\text{mM}$ carbonate buffer (pH 10.0). The soluble toxin was then chromatographically purified using a Superdex-200 HR10/30 size-exclusion column (Amersham). Protein concentration was determined based

^{*} Corresponding author. Tel.: +662 800 3624x1410; fax: +662 441 9906. E-mail address: stckt@mahidol.ac.th (C. Krittanai).

on Bradford dye-binding assay and far-UV absorption (Waddell, 1956).

2.2. Circular dichroism spectroscopy

CD spectra were obtained by a Jasco J-715 spectropolarimeter, purged with oxygen-free nitrogen (Jasco, Japan). The instrument was calibrated daily with 1.0 mg/ml (+)-10-camphorsulphonic acid (CSA), yielding an intensity ratio between 192 and 290 nm greater than 2.0. A sample of 0.4–0.6 mg/ml was loaded into a cylindrical quartz cuvette of 0.02-cm path length (Hellma, USA) and analyzed from 190 to 260 nm. Scanning was set at a rate of 20 nm/min, with 1.0-s response time, 50-millidegree sensitivity and four accumulations. All spectra were subtracted by baseline spectra of buffers containing an appropriate concentration of GuHCl.

2.3. Intrinsic fluorescence spectroscopy

Emission spectra were monitored from 300 to 500 nm on Jasco FP-6300 and Perkin Elmer LS-50B spectrofluorometers, based on an excitation of intrinsic fluorescence from aromatic side chains at 280 nm. Samples containing 20–40 μ g/ml of protein were analyzed in a rectangular quartz cuvette of 0.5-cm path length. Scanning rate was 50 nm/min. At least three repetitive scans were obtained and averaged.

2.4. Steady-state unfolding

A series of GuHCl stock from 0 to 6.0 M was freshly prepared and used to unfold the protein at 4 °C. The purified toxin was incubated overnight in various concentrations of GuHCl, and then monitored for conformational state by fluorescence spectroscopy. An accurate concentration of GuHCl in each individual condition was confirmed by a refractive index, as described by Nozaki (1972). An unfolding curve of the toxin was constructed from a fluorescence intensity ratio between 330 and 350 nm ($F_{330/350}$). The observed spectral intensity ($I_{\rm obs}$) was fitted by the three-state equation:

$$I_{\text{obs}} = \frac{I_{\text{N}} + I_{\text{I}} \left(\exp \left(m_{\text{NI}}[C] - m_{\text{NI}}[C]^{\text{NI}} \cdot 50\% \right) / RT \right) + I_{\text{U}} \left\{ \left(\exp \left(m_{\text{NI}}[C] - m_{\text{NI}}[C]^{\text{NI}} \cdot 50\% \right) / RT \right) \times \left(\exp \left(m_{\text{IU}}[C] - m_{\text{IU}}[C]^{\text{IU}} \cdot 50\% \right) / RT \right) \right\}}{1 + \left(\exp \left(m_{\text{NI}}[C] - m_{\text{NI}}[C]^{\text{NI}} \cdot 50\% \right) / RT \right) + \left\{ \left(\exp \left(m_{\text{NI}}[C] - m_{\text{NI}}[C]^{\text{NI}} \cdot 50\% \right) / RT \right) \times \left(\exp \left(m_{\text{IU}}[C] - m_{\text{IU}}[C]^{\text{IU}} \cdot 50\% \right) / RT \right) \right\}}$$

$$I_N = \alpha_N + \beta_N[C]$$
, $I_I = \alpha_I + \beta_I[C]$, and $I_U = \alpha_U + \beta_U[C]$

where $I_{\rm N}$, $I_{\rm I}$ and $I_{\rm U}$ are the intensity for N, I and U states; α and β are Y-intercepts and slopes of these states; and [C] is the GuHCl concentration. The transitional midpoint [C]^{50%} and unfolding free energy of the protein in the absence of denaturant $\Delta G_{\rm w}^{\rm o} = m$ [C]^{50%} at 25 °C were obtained by curve fitting (Ibarra-Molero and Sanchez-Ruiz, 1996).

2.5. Kinetic unfolding

The toxin $(20-40~\mu g/ml)$ was mixed with various concentrations of GuHCl. The fluorescence spectra decay was recorded at 340 nm over a time course from 2000 to 5000 s, using an excitation wavelength of 280 nm. The bandwidths of excitation and emission were 5 nm. The fluorescence decay spectra were subtracted by baseline spectra obtained in the first 50 s. Each curve was then fitted to the first order single exponential equation (using the SigmaPlot 6.0 software suite):

$$I_t = I_{\alpha} + \Delta I \exp^{(-k_{\text{obs}})t}$$

where I_t is the signal intensity at a given time, I_{α} is the signal intensity at the plateau, I_0 is the initial intensity, ΔI is the difference of I_{α} and I_0 , $k_{\rm obs}$ is the kinetic rate constant (which is denaturant

dependent), and t is time. The $\ln k_{\rm obs}$ was plotted against the GuHCl concentration and fitted with the linear equation

$$\ln k_{\rm obs} = m[{\rm GuHCl}] + \ln k_{\rm w}$$

where $\ln k_{\rm W}$ is the natural log of the kinetic rate constant in water, m is the slope, and [GuHCl] is the concentration of GuHCl. The $k_{\rm W}$ value was used for the activation energy calculation

$$k_{\rm W} = \left(\frac{k_{\rm B}T}{h}\right) \exp^{(-E_{\rm ac,w})/RT}$$

where $k_{\rm B}$ is Boltzmann's constant (1.3807 \times 10⁻²³ J/K), h is Planck's constant (6.6261 \times 10⁻³⁴ m² kg/s), T is absolute temperature (K), R is the gas constant (1.987 cal/mol K) and $E_{\rm ac,w}$ is the activation energy.

2.6. ANS binding assay

1-Anilino-8-naphthalene-sulfonate (ANS) was applied to determine the conformational state of an unfolding intermediate. Cyt2Aa2 protoxin (30 $\mu g/ml$) was incubated in various concentrations of GuHCl for 16–18 h. ANS was then added to a final concentration of 100 μM , mixed and incubated for 5 min in the dark. The samples were scanned for emission spectra from 420 to 600 nm at an excitation wavelength of 350 nm. Slit width for excitation and emission spectra was 5 nm. The spectra of blank solution (without protein) were recorded for subtraction. Intensity changes at a particular wavelength (465 nm) versus GuHCl concentrations were documented.

3. Results and discussion

3.1. Steady-state unfolding and transitional free energy analysis

We employed intrinsic fluorescence spectroscopy to monitor for conformational states of Cyt2Aa2 in various GuHCl concentrations. The toxin in an initial condition of carbonate buffer gave a fluorescence emission spectrum with λ_{max} around 330 nm. When the

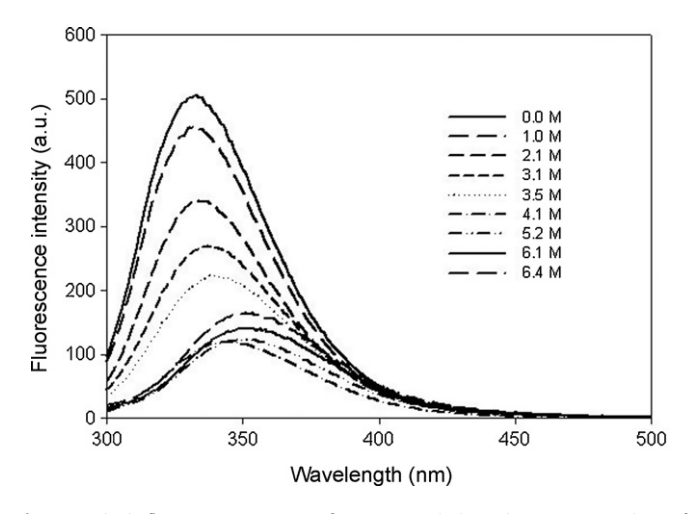


Fig. 1. Intrinsic fluorescence spectra of Cyt2Aa2 toxin in various concentrations of guanidinium hydrochloride. Purified toxin of 20– $40\,\mu g/ml$ was incubated overnight in 0.0– $6.4\,M$ GuHCl. The emission spectra were obtained from 300 to 500 nm, with an excitation at $280\,nm$.

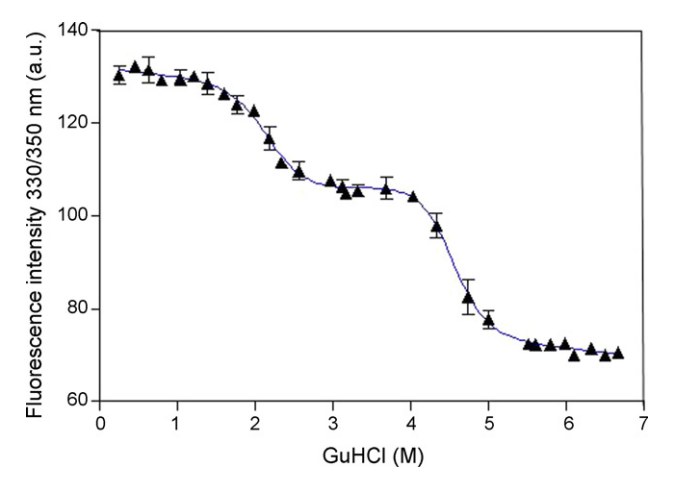


Fig. 2. An unfolding curve of Cyt2Aa2 toxin derived from a plot of the fluorescence intensity ratio for native (N) and unfolded (U) states between 330 and 350 nm, respectively. The three-state transition model was demonstrated to be a function of the denaturant.

intensity and a red shift of λ_{max} toward 350 nm (Fig. 1). The shifting of λ_{max} to a longer wavelength was similar to other reported unfolding proteins such as concanavalin A, methanol dehydrogenase, and glycyl-tRNA synthetase, indicating a conformational change of tryptophan residues from an apolar to a polar environment (Wang et al., 2000; Dignam et al., 2001; Chatterjee and Mandal, 2003). With a series of intensity ratio between 330 and 350 nm representing native and unfolded conformations, an unfolding curve was then established as a function of the denaturant (Fig. 2). The resulting curve demonstrated a well-defined feature corresponding to a three-state transitional model. These three revealed conformational states could be assumed to represent the native (N), intermediate (I) and unfolded states (U). This suggests that GuHCl could bind and help stabilize intermediate and unfolded conformations of the toxin. The steady-state conformations for N, I and U can be obtained at approximately 0-2, 3-4 and 6-7 M of GuHCl, respectively. Based on the three-state model equation, a curve fitting was performed which yielded values for denaturant concentration at a half unfolding ($[\mbox{GuHCl}]^{50\%})$ and transitional slope (*m*). These data were then used to determine the conformational free energy of protein in a denaturant-free condition ($\Delta G_{\rm w}$). After a number of independent repeats, we could report a conformational free energy of the native state at 5.82 ± 0.47 kcal/mol, while the free energy of the intermediate against the fully unfolded state was 16.85 ± 1.47 kcal/mol. The reverse process of these conformational changes was also analyzed by a refolding experiment. Interestingly, the derived refolding curve and free energy values were found to be very similar to those obtained from the unfolding study. These results confirmed that the two investigated pathways are simply a reversal process of the same route and existing conformations. When considering the completed transition, starting from native to unfolded state, the summation of conformational free energy found for Cyt2Aa2 toxin was 22.67 ± 1.94 kcal/mol. This total unfolding free energy was comparable to the stabilizing energy of other native proteins with a similar molecular weight, as reported in the database (Gromiha et al., 1999), such as 25kDa glutathione S-transferase, 21-kDa γD crystallin, and 28-kDa β-lactamase (Vanhove et al., 1997; Hornby et al., 2000; Flaugh et al., 2005). These proteins undergo a three-state unfolding involving 12–27 kcal/mol of free energy. Moreover, the total unfolding free energy for Cyt2Aa2 toxin was also found to be similar to the previously reported data from the two-state unfolding of B. thuringiensis Cry4Ba toxin (Krittanai et al., 2003).

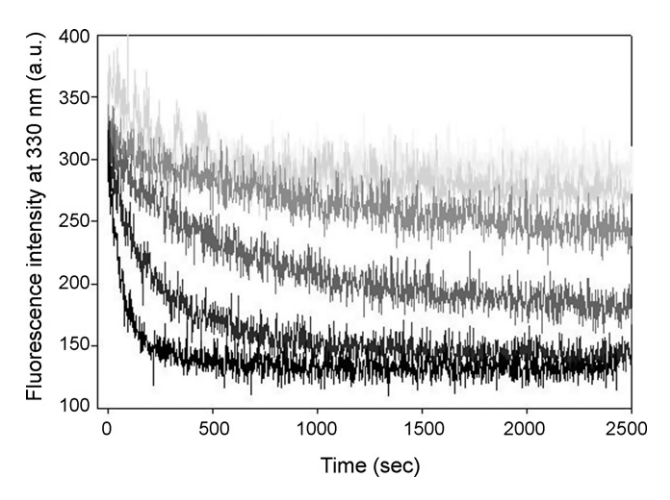


Fig. 3. Exponential decay of the fluorescence intensity at 330 nm from a rapid mixing of Cyt2Aa2 with various concentration of GuHCl. The faster (darker color) and slower (lighter color) decays were observed when using higher and lower concentrations of GuHCl, respectively.

3.2. Kinetics of unfolding and activation energy analysis

In order to investigate the kinetics among these identified conformational states, a rapid mixing of purified toxin in carbonate buffer with various GuHCl concentrations was performed. During the mixing, intensity changes of fluorescence emission spectra were monitored over a period of time, as shown in Fig. 3. The emission intensity corresponding to the native state at 330 nm was found to decrease obviously and rapidly after the addition of a denaturant. In addition, a more significant change of 330-nm intensity was repeatedly obtained when using a higher concentration of GuHCl. Based on the first order of single exponential equation, we were able to obtain an apparent rate constant (k_{obs}) for each denaturant condition. A linear plot between $\ln k_{\rm obs}$ and GuHCl concentrations provided rate constants in a denaturantfree condition $(k_{\rm W})$ of 3.62×10^{-6} and $5.83 \times 10^{-10} \, {\rm s}^{-1}$ for the first and second transitions. Then the activation energy $(E_{ac,w})$ for these two transitions was finally obtained: 23.10 ± 0.28 and 24.89 ± 0.10 kcal/mol, respectively. Despite the activation energy for both transitions being very similar, the rate constant of the second transition was much slower than that of the first one. Thus this transition from an intermediate to an unfolded state could be identified as a rate-limiting step of the unfolding pathway.

3.3. Construction of an energy map

The combined data from steady-state and kinetic analyses can provide necessary information for the construction of a conformational energy map of the unfolding toxin. Conformational free energy (ΔG_{w}) of the three conformational states together with the activation energy $(E_{\mathrm{ac},w})$ of both transitions were mapped along the pathway progression, as shown in Fig. 4. This energy map displays an unfolding pathway starting from a lower-energy native state, and proceeding to higher-energy intermediate and unfolded states, respectively. The transition between each conformational state involves thermodynamic free energy around 5 and 16 kcal/mol, and activation energy around 23-24 kcal/mol. This energy map for the Cyt toxin family was experimentally established for the first time in this study. It could provide relative energy characteristics for the study of protein structure and stability, and could be used as a reference for structural engineering of the mutant toxins.

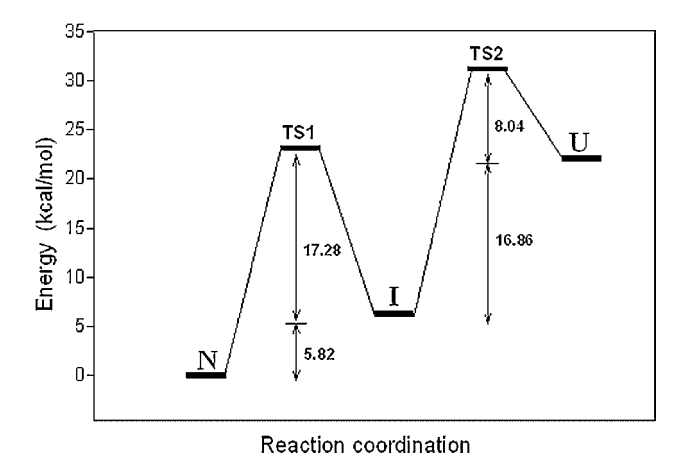


Fig. 4. The energetic map of Cyt2Aa2 unfolding/refolding, showing the relative energy levels for native (N), intermediate (I) and unfolded (U) states. The activation energy was also labeled for each conformational transition.

3.4. Characterization of intermediate state

ANS binding assay was applied to probe for an exposure of the protein hydrophobic core upon a conformational change. When fluorescent dye binds to the toxin, its emission spectrum is experimentally established with a λ_{max} of 465 nm. When this assay was performed for each denaturing condition, the results showed the maximal intensity of binding when the toxin was in 3.0-3.5 M GuHCl. It is apparent that the adopted intermediate state in this denaturing condition has a relaxed structure, and extensively exposes its hydrophobic core to the environment. We also analyzed the secondary structure of the toxin using circular dichroism spectroscopy. The CD spectra obtained for the native, intermediate and unfolded states are shown in Fig. 5. Interestingly, while the CD spectrum for the unfolded state indicated a significant loss of protein secondary structure, the spectra for the intermediate and native states were found to be very similar. This result suggested that the same secondary structure element is maintained in both native and intermediate states. In addition, our intrinsic fluorescence data for the intermediate state showed a red shift of λ_{max} toward 340 nm, indicating a detectable loss of the toxin's tertiary structure. Taking these data together, we were able to demonstrate that the intermediate state was present as a loose folding of the native-like secondary structure and the exposed hydrophobic core. Thus, this stable intermediate can be characterized molten globule state.

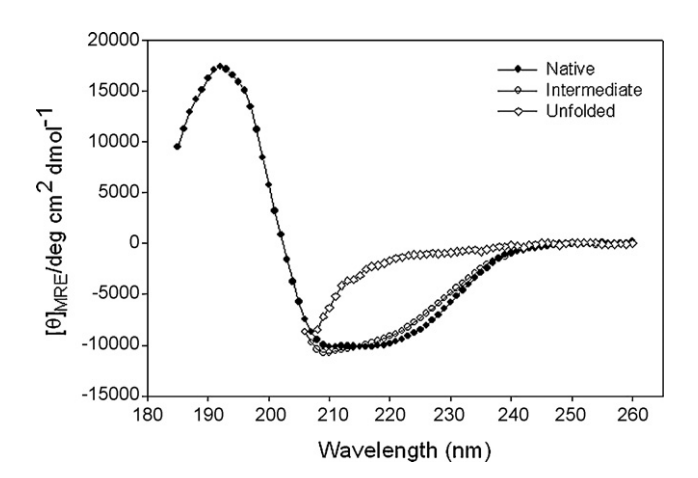


Fig. 5. Circular dichroism spectra of Cyt2Aa2 toxin in the native, intermediate and unfolded states. Purified toxin of 0.3 mg/ml was applied, and the spectra expressed in $[\theta]_{MRE}/\deg cm^2 dmol^{-1}$.

Several reports on the protein folding pathway (Goldberg et al., 1990; Ptitsyn et al., 1990; Sugawara et al., 1991) involve a molten globule state formation. Moreover, the molten globule states for diphtheria toxin (Chenal et al., 2002), anthrax protective antigen (Gupta et al., 2003) and colicins (Zakharov and Cramer, 1997) had been shown to be responsible for their functions in protein-lipid membrane interactions. For B. thuringiensis toxin, a molten globule has been proposed for Cyt1A toxin in the presence of liposome vesicles, using differential scanning calorimetry and CD spectroscopy (Butko et al., 1997). The toxin binds and releases the dye from lipid membrane vesicles at low pH (Butko et al., 1996, 1997). It has been proposed that the molten globule structure binds to the lipid membrane independent from the net charge of the membrane. The importance of a molten globule for biological functions could also be inferred for Cyt2Aa2. Our data directly suggest a presence of molten globule in its unfolding and refolding pathway. When the native and intermediate states of the toxin are related in terms of mechanism of action, it is clear that the native conformation is required for the production of toxin, providing a stable form of protease resistance. However when the toxin undergoes a proteolytic activation and conformational change, a formation of molten globule could then be required for an active role in toxin and membrane interaction. Future investigation of the functional role and interacting mechanism of the intermediate revealed in this work could help provide a basic understanding of the toxin structure as well as a better mechanism model to be used for the application of Cyt2A toxin.

Acknowledgements

This work was supported by the Thailand Research Fund (TRF) and the Thailand Center of Excellence for Physics (Integrated Physics Cluster). Graduate Scholarships from the Commission on Higher Education Staff Development program to A.S. and the Thailand Graduate Institute of Science and Technology (TGIST) to W.T were gratefully acknowledged.

References

Andrews, R.E., Bibilos, M.M., Bulla, L.A., 1985. Protease activation of the entomocidal protoxin of *Bacillus thuringiensis* subsp. *kurstaki*. Appl. Environ. Microb. 50, 737–742.

Armstrong, J.L., Rohrmann, G.F., Beaudreau, G.S., 1985. Delta endotoxin of *Bacillus thuringiensis* subsp. *israelensis*. J. Bacteriol. 161, 39–46.

Bulla, L.A., Kramer, K.J., Davidson, L.I., 1977. Characterization of the entomocidal parasporal crystal of *Bacillus thuringiensis*. J. Bacteriol. 130, 375–383.

Butko, P., Huang, F., Pusztai-Carey, M., Surewicz, W.K., 1996. Membrane permeabilization induced by cytolytic delta-endotoxin CytA from *Bacillus thuringiensis* var. *israelensis*. Biochemistry 35, 11355–11360.

Butko, P., Huang, F., Pusztai-Carey, M., Surewicz, W.K., 1997. Interaction of the δ-endotoxin CytA from *Bacillus thuringiensis* var. *israelensis* with lipid membranes. Biochemistry 36, 12862–12868.

Butko, P., 2003. Čytolytic toxin Cyt1A and its mechanism of membrane damage: data and hypotheses. Appl. Environ. Microb. 69, 2415–2422.

Chatterjee, A., Mandal, D.K., 2003. Denaturant-induced equilibrium unfolding of concanavalin A is expressed by a three-state mechanism and provides an estimate of its protein stability. Biochim. Biophys. Acta 1648, 174–183.

Chenal, A., Savarin, P., Nizard, P., Gillet, D., Forge, V., 2002. Membrane protein insertion regulated by bringing electrostatic and hydrophobic interaction into play: A case study with the translocation domain of diphtheria toxin. J. Biol. Chem. 277, 43425–43432.

Dignam, J.D., Qu, X., Chaires, J.B., 2001. Equilibrium unfolding of *Bombyx mori* glycyltRNA synthetase. J. Biol. Chem. 276, 4028–4037.

Flaugh, S.L., Kosinski-Collins, M.S., King, J., 2005. Contributions of hydrophobic domain interface interactions to the folding and stability of human gamma D-crystallin. Protein Sci. 14, 569–581.

Galjart, N.J., Sivasubramanian, N., Federici, B.A., 1987. A plasmid location, cloning, and sequence analysis of the gene encoding a 27 3-kilodalton cytolytic protein from *Bacillus thuringiensis* subsp. morrisoni (PG-14). Curr. Microbiol. 16, 171–177.

Goldberg, M.E., Semisotnov, G.V., Friguet, B., Kuwajima, K., Ptitsyn, O.B., Sugai, S., 1990. An early immunoreactive folding intermediate of the tryptophan synthease beta 2 subunit is a 'molten globule'. FEBS Lett. 263, 51–56.

Gromiha, M.M., An, J., Kono, H., Oobatake, M., Uedaira, H., Sarai, A., 1999. ProTherm: thermodynamic database for proteins and mutants. Nucleic Acids Res. 27, 286–288.

- Gupta, P.K., Kurupati, R.K., Chandra, H., Gaur, R., Tandon, V., Singh, Y., Maital, K., 2003. Acidic induced unfolding of anthrax protective antigen. Biochem. Biophys. Res. Commun. 311, 229-232.
- Hofte, H., Whiteley, H.R., 1989. Insecticidal crystal proteins of *Bacillus thuringiensis*. Microbiol. Mol. Biol. Rev. 53, 242–255.
- Hornby, J.A., Luo, J.K., Stevens, J.M., Wallace, L.A., Kaplan, W., Armstrong, R.N., Dirr, H.W., 2000. Equilibrium folding of dimeric class mu glutathione transferases involves a stable monomeric intermediate. Biochemistry 39, 12336-12344.
- Ibarra-Molero, B., Sanchez-Ruiz, J.M., 1996. A model-independent, nonlinear extrapolation procedure for the characterization of protein folding energetics from solvent-denaturation data. Biochemistry 35, 14689-14702.
- Krittanai, C., Bourchookarn, A., Pathaichindachote, W., Panyim, S., 2003. Mutation of the hydrophobic residue on Helix 5 of the Bacillus thuringiensis Cry4B affects structural stability. Protein Peptide Lett. 10, 361-368.
- Li, J., Koni, P.A., Ellar, D.J., 1996. Structure of the mosquitocidal δ-endotoxin CytB from Bacillus thuringiensis sp. kyushuensis and implication for membrane pore formation. J. Mol. Biol. 257, 129-152.
- Murphy, D.W., Sohi, S.S., Fast, P.G., 1976. *Bacillus thuringiensis* enzyme-digested delta endotoxin: effect on cultured insect cells. Science 194, 954–956.
- Nickerson, K.W., De Pinto, J., Bulla, L.A., 1975. Lipid metabolism during bacterial growth, sporulation, and germination: kinetics of fatty acid and macromolecular synthesis during spore germination and outgrowth of Bacillus thuringiensis. J. Bacteriol. 121, 227-233.
- Nozaki, Y., 1972. A preparation of guanidine hydrochloride. Methods Enzymol. 26,
- Promdonkoy, B., Ellar, D.J., 2000. Membrane pore architecture of a cytolytic toxin from Bacillus thuringiensis. Biochem. J. 350, 275-282.
- Promdonkoy, B., Chewawiwat, N., Tanapongpipat, S., Luxananil, P., Panyim, S., 2003. Cloning and characterization of a cytolytic and mosquito larvicidal deltaendotoxin from Bacillus thuringiensis subsp darmstadiensis. Curr. Microbiol. 46,

- Promdonkoy, B., Ellar, D.J., 2003. Investigation of the pore-forming mechanism of a cytolytic delta-endotoxin from Bacillus thuringiensis. Biochem. J. 374 (Pt 1),
- Ptitsyn, O.B., Pain, R.H., Semisotnov, G.V., Zerovnik, E., Razgulyaev, O.I., 1990. Evidence for a molten globule state as a general intermediate in protein folding evidence for a molten globule state as a general intermediate in protein folding. FEBS Lett. 262, 20-24.
- Schnepf, E., Crickmore, N., Van Rie, J., Lereclus, D., Baum, J., Feitelson, J., Zeigler, D.R., Dean, D.H., 1998. Bacillus thuringiensis and its pesticidal crystal proteins. Microbiol. Mol. Biol. Rev. 62, 775-806.
- Sugawara, T., Kuwajima, K., Sugai, S., 1991. Folding of staphylococcal nuclease A studied by equilibrium and kinetic circular dichroism spectra. Biochemistry 30,
- Thomas, W.E., Ellar, D.J., 1983. Bacillus thuringiensis var israelensis crystal deltaendotoxin: effects on insect and mammalian cells in vitro and in vivo. J. Cell Sci. 60, 181-197.
- Vanhove, M., Guillaume, G., Ledent, P., Richards, J.H., Pain, R.H., Frere, J.M., 1997. Kinetic and thermodynamic consequences of the removal of the Cvs-77-Cvs-123 disulphide bond for the folding of TEM-1 beta-lactamase. Biochem. J. 321,
- Waddell, W.J., 1956. A simple ultraviolet spectrophotometric method for the deter-
- mination of protein. J. Lab. Clin. Med. 48, 311–314.
 Wang, G.F., Cao, Z.F., Zhou, H.M., Zhao, Y.F., 2000. Comparison of inactivation and unfolding of methanol dehydrogenase during denaturation in guanidine hydrochloride and urea. Int. J. Biochem. Cell Biol. 32,
- Zakharov, S.D., Cramer, W.A., 1997. Insertion intermediates of poreforming colicins in membrane two-dimension space. Biochemistry 36, 12862-12868.